Acoustic Standing Wave Manipulation of Particles and Cells in Microfluidic Chips

Lenshof, Andreas

2009

Acoustic standing wave manipulation of particles and cells in microfluidic chips

Andreas Lenshof

LUND UNIVERSITY

Doctoral Thesis

Department of Electrical Measurements and
Industrial Electrical Engineering and Automation
Lund University

Organization LUND UNIVERSITY Department of Electrical Measurements and Industrial Electrical Engineering and Automation Box 118, 221 00 Lund, Sweden	**Document name** DOCTORAL DISSERTATION
	Date of issue January 30, 2009
Author: Andreas Lenshof	**Sponsoring organization** The Swedish Research Council

Title: Acoustic standing wave manipulation of particles and cells in microfluidic chips

Abstract

The rise of MEMS and μTAS techniques has created a whole new family of microfluidic devices for a wide range of chemical and biomedical analyses to be performed on small Lab-on-a-chip platforms. The operations often include small samples of particle or cell suspensions on which separation, mixing, trapping or sorting is performed. External fields and forces are used for these operations, and this thesis is specifically focused the development of ultrasonic standing wave technology and the use of acoustic force fields to perform bioanalytical unit operations.

The combination of acoustic standing waves and the laminar flow in microfluidics has proven to be well suited for performing particle and cell separation. The fundamental acoustic separator used in this thesis consists of a microfluidic flow channel with a three way flow splitter (trifurcation) in the end of the channel. An acoustic standing wave field is applied to the main flow channel by attaching the transducer underneath the chip. The acoustic standing wave is however obtained perpendicular to the axial propagation of the wave field and the direction of the flow. The half wavelength resonance affects rigid particles or cells driving them into the acoustic pressure node while liquid spheres having other density and compressibility properties may move to the pressure antinode. This enables acoustic separation of different particle types. Blood has proven to be very suitable for acoustic cell manipulation. An application where lipid particles can be removed acoustically from shed blood from open heart surgery is demonstrated. An application for acoustic plasmapheresis is also shown where high quality blood plasma is generated. Different separator designs, device material, and the influence of the separation channel cross-section design are also investigated.

Key words

Microsystem technology, microfluidics, lab on a chip, particle handling, cell handling, ultrasound, separation, acoustic particle manipulation, standing waves

Classification system and/or index terms:

Supplementary bibliographical information **ISRN LUTEDX/TEEM - - 1089 – SE, Report 1/09**		**Language** English
ISSN and key title: 0346-6221		**ISBN: 978-91-628-7678-4**
Recipient´s notes	**Number of pages: 146**	**Price**
	Security classification	

To my parents

The most exciting phrase to hear in science, the one that heralds new discoveries, is not 'Eureka!' but 'That's funny...'
- Isaac Asimov

Cover illustration
A photograph illustrating separation of particles with different acoustic contrast factor, in this case blood cells and coffee cream.

Public Defence
January, 2009, 10.15 in E:1406, E-huset, Lund Institute of Technology, Lund, Sweden

Advisors
Professor Thomas Laurell and Dr Johan Nilsson
Department of Electrical Measurements and Industrial Electrical Engineering and Automation, Lund University, Lund, Sweden

Faculty Opponent
Dr Nicole Pamme
Department of Chemistry, University of Hull, Hull, United kingdom

Board of Examination
Dr Martin Wiklund
Department of Biomedical and X-Ray Physics, Royal Institute of Technology, Sweden
Professor Gunilla Westergren-Thorson
Department Office of Experimental Medical Science, Lund University, Sweden
Yvonne Mårtensson
Cella Vision AB, Lund, Sweden
Deputy member: Professor Per-Olof Larsson
Department of Chemistry, Division of Pure and Applied Biochemistry, Lund University, Sweden

ISBN 978-91-628-7678-4
Report 01/09
ISSN 0346-6221
ISRN LUTEDX/TEEM - - 1089 – SE
Printed in December 2008 by Tryckeriet i E-huset, Lund, Sweden

LIST OF PUBLICATIONS

This thesis is based on the following papers, which will be referred to in the text by their Roman numerals. The papers are appended at the end of the thesis.

I **Acoustic Control of Suspended Particles in Micro Fluidic Chips**
Nilsson A., Petersson F., Jönsson H. and Laurell T.
*Lab on a Chip, 2004, **4**, 131-135*

II **Separation of lipids from blood utilizing ultrasonic standing waves in microfluidic channels**
Petersson F., Nilsson A., Holm C., Jönsson H. and Laurell T.
*Analyst, 2004, **129**, 938 – 943*

III **Particle separation using ultrasound can radically reduce the embolic load to the brain after cardiac surgery**
Jönsson H., Holm C., Nilsson A., Petersson F. and Laurell T.
*Annals of Thoracic Surgery, 2004, **78**:1572-1578*

IV **Acoustic resonances in straight microchannels: Beyond the 1D-approximation**
Hagsäter S.M., Lenshof A., Skafte-Pedersen P., Kutter J.P., Laurell T., Bruus. H.
*Lab on a Chip, 2008, **8**, 1178-1184*

V **Acoustophoresis in wet-etched glass chips**
Evander M., Lenshof A., Laurell T., Nilsson J.
*Analytical Chemistry, 2008, **80**, 5178-5185*

VI **Acoustic whole blood plasmapheresis chip employed for PSA microarray diagnostics**
Lenshof A., Tajudin A.A., Järås K., Swärd-Nilsson A-M., Åberg L., Marko-Varga, G., Malm J., Lilja H., Laurell T.
Manuscript

Papers not included in this thesis:

VII **Continuous separation of lipid particles from erythrocytes by means of laminar flow and acoustic standing wave forces**
Petersson F., Nilsson A., Holm C., Jönsson H. and Laurell T.
*Lab on a Chip, 2004, **5**, 20-22*

VIII **Carrier medium exchange through ultrasonic particle switching in microfluidic channels**
Petersson F., Nilsson A., Jönsson H. and Laurell T.
Analytical Chemistry, 2005, 77, 1216-1221

IX **Particle separation using ultrasound can be used with human shed mediastinal blood**
Jönsson H., Nilsson A., Petersson F., Allers M. and Laurell T.
*Perfusion UK, 2005, **20**: 39-43*

X **Chip integrated strategies for acoustic separation and manipulation of cells and particles**
Laurell T., Petersson F., Nilsson A.
*Chemical Society Reviews, 2007, **36**, 492-506*

THE AUTHOR'S CONTRIBUTIONS TO THE PAPERS

I	Large part of planning, experimental work, evaluation, and writing
II	Part of planning, large part of experimental work and evaluation, part of writing
III	Part of planning, large part of experimental work and evaluation, part of writing
IV	Part of planning, large part of experimental work and evaluation, part of writing
V	Large part of planning, experimental work, evaluation and writing
VI	Major part of planning, experimental work, evaluation and writing

ABBREVIATIONS

DEP	Dielectrophoresis
DRIE	Deep Reactive Ion Etching
FACS	Fluorescent Activated Cell Sorting
FFF	Field Flow Fractionation
KOH	Potassium hydroxide
MEMS	Micro Electro Mechanical Systems
MST	Micro System Technology
nDEP	Negative Dielectrophoresis
PSA	Prostate Specific Antigen
pDEP	Positive Dielectrophoresis
PIV	Particle Image Velocimetry
PRF	Primary Radiation Force
PZT	Lead Zirconate Titanate
RBC	Red Blood Cells
SPLITT	Split Flow Thin Fractionation
SRF	Secondary Radiation Force
WBC	White Blood Cells
USW	Ultrasonic Standing Waves
μTAS	Micro Total Analysis Systems

CONTENTS

1 INTRODUCTION

Humanity has always been fascinated by tiny things. After the invention of the microscope in 1674 by Leeuwenhoek it has been clear that there are a lot of things which cannot be seen by the human eye that influence our everyday presence. By looking at nature from a microscopic point of view, manmade structures in that size range would have been pure science fiction a hundred years ago. The desire to construct microscopic devices and machines has really been concluded well by Richard P. Feynman [1] in the visionary talk *There´s plenty of room at the bottom* from 1959 in which he laid a miniaturization aspect on many things from computers to biological systems.

What once begun with the miniaturization of electronics in terms of the first semiconductor transistor and the integrated circuit is now about to happen in the microfluidic domain. The concept of a micro total analysis system (μTAS) was presented in the early 1990´s [2], but the success similar to microelectronics where you can find it commercially in every home or laboratory is yet to come [3]. The vision of a lab-on-a-chip device is to use very small sample volumes, for instance a drop of blood, perform a bioanalytical step on the sample and receive a readout. Many of the actions performed in such systems include the manipulation of samples of cells or particles by means of separation, mixing or positioning. Multiple techniques have been invented for this purpose and some use the plain geometry of the microfluidic channels, such as posts, weirs, pinches and meshes, while other systems rely on externally applied forces. Examples of such external forces are electrical, magnetical or optical forces. This thesis, however, has the focus on the possibility of using acoustic forces for manipulating cells and particles.

Particles and cells exposed to an acoustic field will be affected by an acoustic radiation force. The movement of particles in a standing wave field was shown already in 1874 where Kundt performed his famous standing wave experiment with a closed pipe containing cork dust [4]. The experiment was very visual showing how the cork particles were moved into the pressure nodes of the standing wave. Although the experiment was performed in a macroscale tube with audible sound, transforming the principle into a microscopic domain is certainly possible and also includes some attractive features.

By using fluidic channels of micrometer size, the wavelength of the sound decreases which is equivalent to an increase of the frequency of the standing wave. This is attractive since the acoustic force acting on the particles is frequency dependent and increases with the increasing frequency. Another positive feature is the presence of laminar flows in microfluidic channels. This provides very suitable conditions for separating fluid streams or sorting particles from each other using flow splitters.

The aim of the work in this thesis has been to develop and utilize the combined power of acoustically driven separation and microfluidics. Contributions to the field of particle and cell manipulation and separation have been done as well as some

investigations of how the acoustic force affects particle suspensions in the separation channel.

The summary of this thesis gives a brief overview of the tools and provides background information to the field of particle manipulation. Chapter 2 gives an introduction to silicon microfabrication, which is essential as the particle manipulation chips used in this thesis are made of silicon. Chapter 3 gives a brief overview of microfluidics where the fluidic effects relevant for this thesis are covered. Chapter 4 gives a more detailed insight to acoustics and acoustic forces, which are the main tools for manipulation of particles and cells presented herein. Chapter 5 comprises a brief summary of the field of particle and cell manipulation and the many different techniques available. It also includes an extended part of acoustic techniques, many of which are results of the work from our research group in Lund. Since much of the work in this thesis is based on applications of blood, a short summary of blood and its constituents is presented in Chapter 6.

2 MICROFABRICATION

2.1 Silicon as a MEMS material

The silicon micro fabrication methods originate from the integrated circuit (IC) industry which evolved in the early 1960´s. This development was driven by the need for improved electronic functionality and the introduction of planar technology on silicon was a major breakthrough as also reflected by the Nobel Prize in Physics awarded to Jack Kilby in 2000. Silicon as a material is not only a semiconductor which is suitable for IC´s as Petersen pointed out in 1982 [5] in his famous paper where he described silicon as a material from a mechanical point of view. The vast ways of processing silicon in combination with the crystalline structure and the degrees of anisotropicity that follows create a dynamic platform for a large amount of different sensors and devices that can be used in a large variety of applications.

Below is a short description of the basic silicon microfabrication steps which are used for fabrication of microstructures. The number on the left side of each processing step indicates chapter numbers in this thesis where the corresponding information of each step can be found.

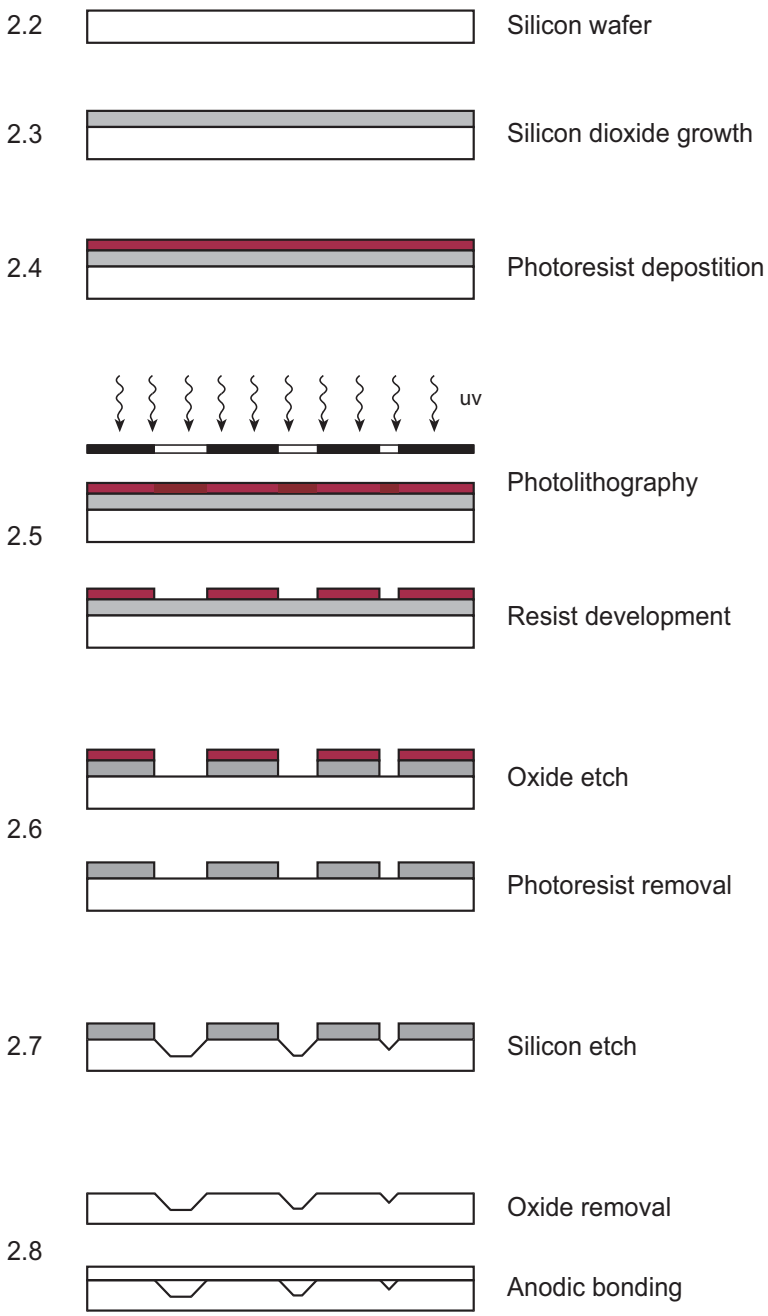

Figure 2.1. The basic process steps for fabricating silicon devices. The numbers on the left side of the schematic indicates chapter numbers in this thesis where the corresponding information can be found.

2.2 Crystal planes and Miller indices

The basic microstructure starting material is the planar silicon wafer. Monocrystalline silicon is grown from a melt using the Czochralski technique [6]. A monocrystalline seed is dipped in a polycrystalline silicon melt and slowly pulled up in a rotary motion. As the silicon cools down the silicon atoms will be arranged in a diamond lattice structure, according to the orientation of the monocrystalline seed. The obtained rod of crystalline silicon is the diced up into wafers. In order to keep track of the crystal orientation of the silicon wafers, Miller indices are used, figure 2.2 and the specific wafer cuts are marked by two flat zones polished at the wafer perimeter accordingly. Since different crystal planes etch unequally fast with different etch solution, the Miller indices denotes how to align the photomask in order to get the desired structure.

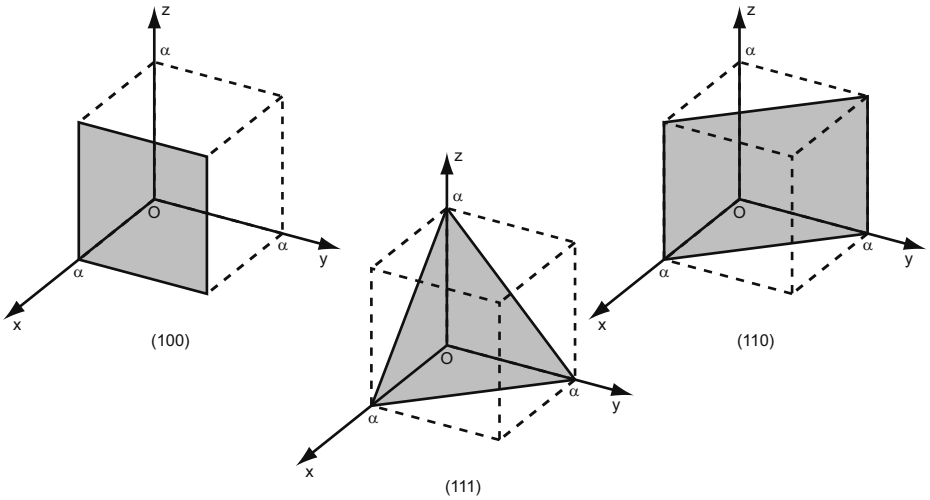

Figure 2.2. Miller indices of some basic planes in a cubic crystal.

When making acoustic separators in (100)-silicon the mask with the separation channels is usually turned 45° in relation to the primary flat of the wafer, such that a rectangular cross-section is achieved with KOH etching, figure 2.3. Unless the rotation is made, the cross-section of the separation channel will be of trapezoidal shape, or in form of a pyramid if the etch is allowed to self terminate.

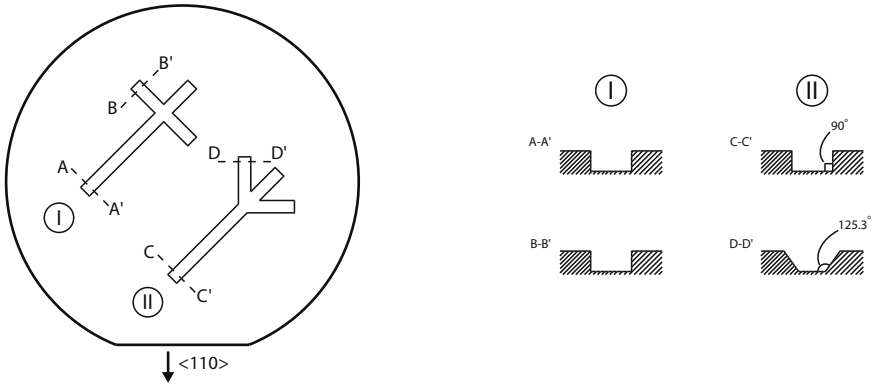

Figure 2.3. Example of silicon structure orientation in (100)-silicon in order to get vertical channel walls.

2.3 Wafer protection layers

To be able to etch patterns in the silicon wafer, it needs to be protected from the etchant, regardless if chemical wet etch or plasma dry etch is to be used. Silicon dioxide (SiO_2) or silicon nitride (Si_3N_4) is mostly used. Silicon dioxide is easy to make since silicon reacts with oxygen spontaneously forming native oxide, however this oxide layer is extremely thin. Thermal oxidation, where oxygen or water vapour reacts with the silicon in a high temperature furnace (~1000°C), is required to receive thicker dioxide layers which is more sustainable to etching solutions or ion bombardment. Silicon nitride is usually deposited by LPCVD (Low Pressure Chemical Vapour Deposition). The nitride deposition process uses gases which are highly toxic and explosive, which puts higher requirements on the equipment and the use of nitride less desirable.

2.4 Photoresists

A photoresist is a light sensitive polymer which is suitable for pattern transfer on a surface. The composition of a photoresist is a photosensitive polymer, a base resin and an organic solvent. The photoresist is usually spin coated onto the wafer, where the rotational speed of the spinner and the viscosity of the resist decide the layer thickness. The resist is then soft baked; a heating process (~80°C for ~25min) where solvent is removed through vaporization in order to make the resist easier to handle and be less sticky. There are some resists in spray form available too.

There are basically two types of photoresists – positive and negative. For the positive photoresist, the exposed regions become more soluble than the surrounding resist as the uv-light break up the polymer chains, and the resulting pattern is thus an image of the pattern on the photomask. For negative resist, the uv-exposed regions are less soluble than the surroundings as the polymer chains exposed are cross-linked. The pattern formed in the resist is the reverse of the pattern on the mask.

2.5 Masking and lithography

The desired pattern or structure is usually drawn using a CAD-software. In order to transfer that pattern to the silicon wafer, a chromium covered glass mask is used. The computer drawn pattern is transferred to the photoresist covered glass mask using software guided laser. The photoresist is then developed and the exposed chromium etched. The result is a see-through pattern printed chromium glass mask. The mask can be used repeatedly for many pattern transfers to the silicon wafers.

There are basically two optical exposure methods: contact printing and proximity printing [Sze, 1985]. In contact printing, as the name suggest, the wafer with the photoresist is in contact with the glass mask. This gives a higher spatial resolution (~1μm) but also a risk of contaminating and damaging the mask which could result in poor results the next time the same mask is used. With proximity printing, there will be a small gap of 10 – 50 μm between the mask and the wafer. This will prevent the mask from getting fouled but instead lower the resolution to 2-5 μm because of optical diffraction from the pattern edges of the photomask.

For increased spatial resolution there are software guided laser systems which can be used to transfer patterns directly onto the wafer. The resolution will be very high, but the exposure time of one wafer is quite high. If multiple wafers are to be processed with the same pattern, this way of exposure is too time consuming in order to be effective.

After lithography and development of the patterned image, it is important to "hard bake" the wafer in order to harden the photoresist by vaporizing the last of the solvent. This is done in an oven at 120°C for ~30 minutes.

2.6 Oxide etching

The silicon dioxide etch is done using a buffered hydrofluoric acid (HF) mixture. The buffer has an altered pH to make the etchant less aggressive towards the photoresist. If nitride is used, the etching of the exposed nitride will be done by plasma etching.

2.7 Etching

Etching is the process where bulk material is removed either by chemical reactions or by mechanical abration. The chemical etchants are a bit more refined since it is possible to utilize the crystal structure of monocrystalline silicon. Different etchants etch at different rates in different directions making complex structures possible to fabricate. In dry etching, or reactive ion etching, the combination of bombardment of the wafer surface with chemically reactive ions provides means to control the degree of anisotropy by the directionality of the impinging ions. Finally milling of the wafer surface by controlling the trajectory of a high energy ion beam, i.e. ion beam milling, is possible offering in very high spatial resolution at the expense of long processing times. Williams et al. presented a very extensive guide on etch rates for every

possible substrate, technique and solutions [7, 8]. The wet etching and the chemical reactive ion etching techniques will be briefly discussed below.

2.7.1 Wet-etching

Using chemical wet etching, two different etch profiles are possible to achieve – isotropic or anisotropic profile.

Isotropic means that the substrate is etched at equal etch rate in all directions. This results in structures which have a semi circular cross section if proper agitation of the etchant is used, figure 2.4A. It is important to agitate the solution in order for a continuous etch reaction to take place since diffusion alone is not fast enough to get fresh ions to the bottom of the deep structure. If proper agitation of the etch solution is not used, the result will be a shallow structure with circular walls and an almost flat bottom, figure 2.4B. The most common etchant for isotropic etching is HNA, which is comprised of HF, HNO_3 and acetic acid (CH_3OOH).

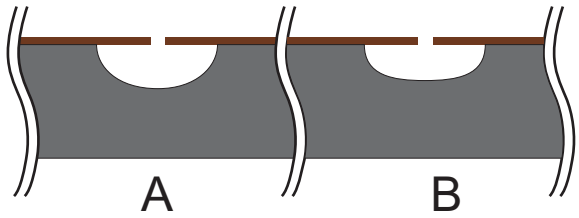

Figure 2.4. Isotropic etch profiles. A) is achieved by etching with agitation of the etch solution while B) is obtained without agitation.

Anisotropic etching is a selective process where some crystal planes are dissolved faster than others. By creative masking of the wafer, precise structures with perfect wall smoothness can be achieved. KOH (potassium hydroxide), EDP (ethylene diamine, pyrocatechol and water) and TMAH ($(CH_3)_4NOH$) are common anisotropic etchants. KOH is the most widely used since it is easy to use, fast etching and much less hazardous than the other etchants. It etches SiO_2 quite slowly but for deep structures and longer etch times, Si_3N_4 is preferable as masking material. EDP is favourable if deep structures are to be etched since it is not as aggressive to the masking material as KOH. It is also advantageous if a dopant dependable etching is to be performed since it is exhibiting near zero etch rates on silicon which has been doped with boron. EDP is, however, toxic and degradable the in contact with oxygen. TMAH is an organic solution, i.e. it does not contain any metal ions, which makes it suitable for making IC components. Nor is it toxic but reacts with the CO_2 in the air so air exposure should be limited.

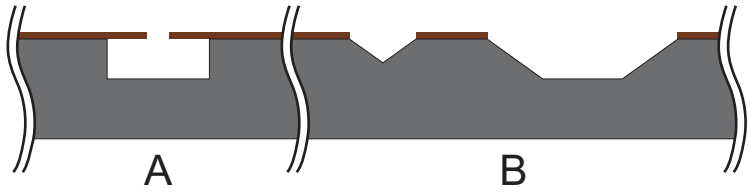

Figure 2.5. Anisotropic etch profiles. Depending on the crystal orientation different etch shapes can be obtained.

2.7.2 Dry etching

Reactive ion etching (RIE) is the use of plasma to etch silicon. An oscillating electric field ionizes the gas in the etch chamber creating a reactive ion plasma. The ions drift towards the wafer where they react chemically with the silicon. A sputtering effect can also occur where some material can be knocked out because of kinetic energy transfer. Since the ion bombardment is mostly vertical, the etch profile is very anisotropic. A modification of the RIE is DRIE (Deep Reactive Ion Etching) where the etch cycle is interrupted by a deposition cycle where a chemically inert passivation layer is introduced. The new layer will protect against the ion bombardment but will eventually be sputtered away at the bottom of the structure, but not at the side walls. This prevents lateral etching and cycling of the procedure creates deep structures with very high anisotropicity.

2.8 Bonding

Anodic bonding [9] is an excellent way of sealing silicon channels with a glass lid. The electrostatic bond effectively eliminates all the pitfalls related with glue and microstructures where capillary effects often cause glue to end up in locations where it arrests the microstructure function. The procedure is quite simple, heat up the silicon and the glass to about 500°C on a hot plate and then apply 1000V through the combined parts with the anodic side on the glass. The voltage will create a charge displacement between the silicon and glass lid and create an electrostatic bond which is very strong. It is important, however, that the glass has a thermal expansion coefficient that is close to silicon otherwise either the glass or the silicon is likely to break when they cool down due to internal stresses. Borofloat glass is the most commonly used glass with anodic bonding. Before the bonding, it is very important to ensure that the glass and silicon substrate are clean. Clean the glass lid with ethanol to remove any fingerprints or dust particles and blow it dry. Removing the silicondioxide is one of the best ways of getting the silicon substrate clean. It will also assure the smoothness of the surface as no oxide residue from masking or silicon dust after dicing the chip is left on the structure.

There is also the silicon fusion bonding where two silicon wafers are bonded together [9]. If the bonding is to be successful it is of paramount importance that the wafers are clean, smooth and flat. Any roughness or dust particle will create voids where the bonding will not succeed. The bonding can be done on wafers with or without a thin layer of thermal oxide or native oxide. Bonding of wafers without thermal oxide is

only recommended if they have not been processed since any structure on the wafer will almost certainly leave a void since the thermal oxide acts as “sticking layer”. The bonding of structures with thermal oxide is recommended for prefabricated wafers. Silicon wafers bond to each other naturally at room temperature. This bond is however not very strong. Instead the wafers are surface activated with either plasma treatment or a chemical process, for instance RCA1. These processes leave the wafer with a native oxide layer with a high density of OH groups at the surface which result in a hydrogen bond when put together. The hydrogen bond is sufficiently strong to hold the wafers fixed before they are moved into a furnace for annealing to make the bond permanent.

3 MICROFLUIDICS

Microfluidics [3, 10] is the science and technology of systems that process or manipulate small amounts of fluids in channels with dimensions of tenths to hundreds of micrometers. The volume of processed fluids is in the range of microliters (10^{-6} l) to femtoliters (10^{-15} l). The use of microfluidics in biology, chemistry and medicine has several attractive features such as small volumes of samples and reagents, little waste production and short reaction and analysis times [11]. The number of microfluidic applications has spawned a vast amount of inventive designs for introducing [12, 13], mixing [14, 15], pumping [16] and storing fluids in channels. Although much is similar in macrofluidic and microfluidic systems, the scaling relations also cause some fundamental differentiations like flow turbulence – or the lack of it in the microfluidic domain [17].

The field of microfluidics is too large to be covered in detail. Instead this chapter focuses on the principles and theories relevant to the work presented in this thesis. These are, for example, the laminar flow and forces exerted on particles in a flow.

Several of the microfluidic systems involve flow channels of various designs. In contrast to macrofluidic systems where pipes of circular cross-sections are common, microfluidic channels may have cross-sections like the trapezoid shaped anisotropically etched silicon channel or the semi-circular isotropic etch profile. The calculation of the flow through a channel with arbitrary cross-section might be very difficult and as a approximation, the hydraulic diameter can be used. The flow in a channel with an arbitrary cross-section is thus approximated with the flow in a circular channel with the diameter equivalent to the hydraulic diameter. The hydraulic diameter is defined as:

$$D_h = \frac{4A}{P_{wet}} \qquad \text{Eq. 3.1}$$

where A is the cross section area and P_{wet} is the wetted perimeter. The hydraulic diameter can not only be used to assess flows through channels completely filled but also channels which are half-filled. In that case, the wetting parameter refers to the part of the channel which is in direct contact with the fluid and the area refers to the area through which the flow is occurring. In case of a completely filled channel, the wetting perimeter is of course the circumference and the area the cross-section of the channel.

Using the hydraulic diameter it is possible to calculate the Reynolds number, which is a good predictor for estimating turbulent or laminar flow in the channel. On larger scales fluids mix convectively, like milk swirled into coffee, which reflect the fact that macroscopic fluid often is more affected by inertia than viscosity. In microfluidic systems fluids do not mix convectively. When two fluid streams come

together in a micro channel they flow in parallel (figure 3.1) and the only mixing that occurs is diffusion of molecules between the fluid layers.

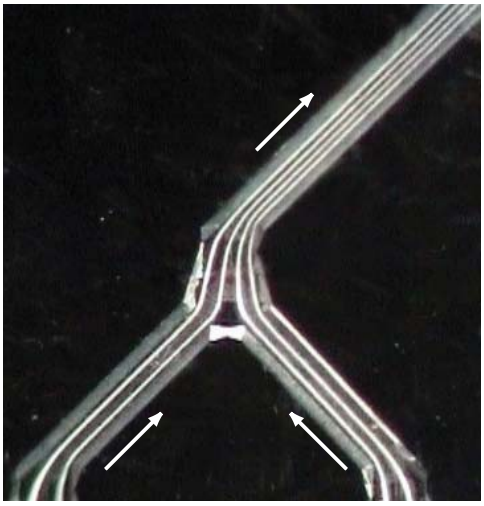

Figure 3.1. Example of laminar flow. Two double particle bands, previously focused by an ultrasonic standing wave, flow in parallel as they are united in a y-shaped channel junction.

The dimensionless Reynolds number is defined by [18]

$$\mathrm{Re} = \frac{\rho D_h u}{\eta} \qquad \text{Eq. 3.2}$$

where D_h is the hydraulic diameter, u is the characteristic velocity in the channel, ρ is the density of the fluid and η is the dynamic viscosity of the fluid. The transitional Reynolds number, i.e. the region in which laminar flow turns to turbulent, is found to be in the range of 1000 – 2500. The exact number of which the transition will occur depends on many parameters such as the channel shape, aspect ratio and the surface roughness. A typical microfluidic channel used for USW separation with 350µm x 125µm cross-section and a flow rate of 100µl/min is calculated to have a Reynolds number of about 7, which needless to say is very well within the laminar region.

Diffusion, as mentioned earlier, is the net transport of molecules from a high concentration region to a region of lower concentration by random molecular motion. In many microfluidic systems diffusion is the only way of mixing fluids because of the obvious absence of turbulence. Diffusion is a very slow process, but as microfluidics deals with small volumes and short diffusion distances, it is still of major importance. The time it takes for a molecule to travel a distance d is given by

$$\tau = \frac{d^2}{2D_{diff}}$$ Eq. 3.3

The diffusion coefficient D_{diff}, derived by Einstein [19] is defined as

$$D_{diff} = \frac{RT}{f N_A}$$ Eq. 3.4

where R is the gas constant, T is the absolute temperature, N_A is the Avogadro number (N_A=6.02x10^{23}) and f is the friction factor which is proportional to the viscosity η. The diffusion coefficient is a fluid property and fluids containing large molecules such as hemoglobin have lower diffusion coefficient than those containing small molecules.

The distance that two laminated fluids must travel before mixing by diffusion is complete is also of importance. The Péclet number (Pe) is a dimensionless number which shows how diffusion relates to convective mixing [20]. The Péclet number is defined as

$$Pe = \frac{u \cdot d}{D_{diff}}$$ Eq. 3.5

where u is the flow velocity and d is the width of the channel. The higher the Péclet number, the more the influence of the flow dominates over molecular diffusion. Newtonian fluids, that is fluids in which the shear stress is linearly proportional to the velocity gradient in the direction of shear, have a parabolic flow profile in laminar flow. This means that the fluid flows faster in the center of the flow channel and slower at the walls because of fluid friction. Channels with small dimensions will encounter a larger pressure in the channel the longer the channel or smaller the channel gets, making it more difficult for a fluid to pass through. The Darcy-Weisbach equation [21] defines the pressure drop in a channel of the length L

$$\Delta p = \frac{f_D \rho L u^2}{2D_h}$$ Eq.3.6

The factor f_D is Darcy's friction factor and can be simplified for laminar flows as

$$f_D = \frac{16}{\mathrm{Re}}$$ Eq.3.7

Suspended particles in a fluid will experience a lot of forces. Besides gravity and buoyant forces, there are also forces induced when travelling with a flow. Any

particle with the diameter D_p that travels with the velocity u in a fluid with the viscosity μ will experience a drag force which acts in the opposite direction of the velocity of the particle. The drag force is sometimes called fluid resistance and is given by Stoke´s law:

$$F = 3\pi\mu D_p u \qquad \text{Eq. 3.8}$$

Stoke´s law is only valid on spherical particles which are not disturbed by other particles and only at very low Reynolds numbers, Re < 1.

4 ACOUSTICS

4.1 Sound and travelling waves

Sound is the transmission of vibrations through gas, liquid or solid matter. The vibration is transmitted as local particle displacement or particle oscillation. However, it is important to remember that it is the wave that travels from the source, not the particles. The soundwaves propagate through longitudinal waves by compression and rarefaction of the medium parallel to the direction of motion of the wave [22]. There are also oscillations perpendicular to the direction of motion of the wave, known as the transversal wave. A travelling wave can be expressed as:

$$y(x,t) = A\sin(\omega t \pm kx) \qquad \text{Eq. 4.1}$$

where $\omega = 2\pi/T$ and $k = 2\pi/\lambda$. T is the time for a full period and λ is the wavelength. The wave can also be represented in terms of pressure, which is achieved by derivation of the displacement wave which gives equation 4.3.

$$p = -\frac{1}{\beta}\frac{\partial y}{\partial x} \qquad \text{Eq. 4.2}$$

$$p(x,t) = p_0\cos(\omega t \pm kx) \qquad \text{Eq. 4.3}$$

$$p_0 = \frac{Ak}{\beta} \qquad \text{Eq. 4.4}$$

The term β is the compressibility of the medium. Note that the pressure function is phase shifted 90° compared to the displacement function.

Audible sound, that is sound of frequencies which the human ear can detect, is in the range of 20 Hz to 20 kHz. Sound of higher frequencies is called ultrasound, while sound of lower frequencies is known as infrasound.

4.2 Standing wave acoustics

Two moving waves with the same frequency propagating towards each other will interfere with each other and give rise to a new wave. The new wave is a product of position dependence and time dependence of the original two waves, which means that the wave will not move but instead stay in one place and pulsate. Each point of the wave will stand still and oscillate with an amplitude that is the sum or the difference of the two original colliding waves. A standing wave can basically be formed in two different ways. The first case is based on two opposing transducers where the interference of the two meeting waves results in a standing wave. The second way is the use of a single transducer and a reflector where the original

emitted wave will be reflected back and interfere with itself and thus give rise to a standing wave.

A standing wave can be discussed in terms of displacement, but can also be visualized in terms of pressure variations. A node for displacement is phase shifted 90° in relation to a pressure node. This means that wherever there is a displacement node, there will also be a pressure antinode and vice versa, see figure 4.1.

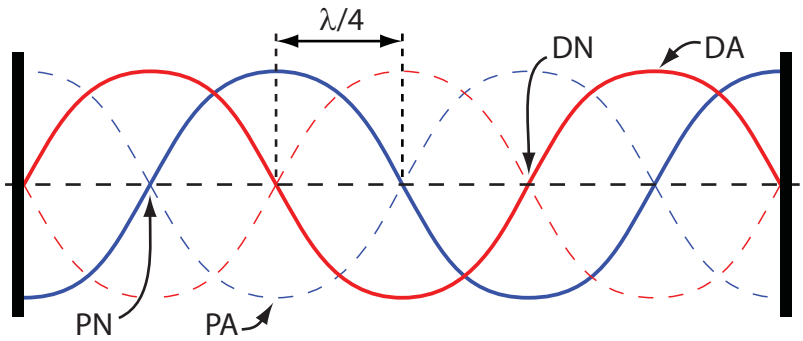

Figure 4.1. Standing waves. The blue line represents the pressure with pressure nodes (PN) and pressure antinodes (PA). The red line shows the displacement with displacement nodes (DN) and displacement antinodes (DA). As seen in the picture there is a phase shift between the pressure node and the displacement node which is λ/4.

The displacement and pressure function for a standing wave can be described as

$$y(x,t) = A_{SW} \cdot \cos(kx) \cdot \sin(\omega t) \qquad \text{Eq. 4.5}$$

$$p(x,t) = -p_{SW} \cdot \cos(kx) \cdot \cos(\omega t) \qquad \text{Eq. 4.6}$$

The equation expresses the displacement (y) and pressure (p) of a point in the standing wave corresponding to a certain position (x) and time (t). A_{sw} and p_{sw} are the sum of the amplitudes of the individual waves.

4.3 Acoustic forces on particles

The theories behind forces acting on particles in a sound field have been known for some time. King [23], Yosioka and Kawasima [24] and Nyborg [25] among others have reported extensively on the matter. The radiation force arises because any discontinuity in the propagating phase, i.e. a cell, particle or bubble, acquires a position dependent acoustic energy potential by just being located in the sound field. As seen in figure 4.2, the net acoustic force is a result of several force components. The primary radiation force (PRF) is responsible for the strongest force exerted on the particles while the secondary radiation force (SRF) is only active at close distances between the particles. A good example was shown by Ter Haar and Wyard [26] who estimated the PRF on an erythrocyte at 3 MHz and at an intensity of 1

W/cm^2 to be 2 x 10^{-12} N. The SRF, under the same conditions, for erythrocytes in contact is 10^{-13} N and 2 x 10^{-14} N for cells 10µm apart.

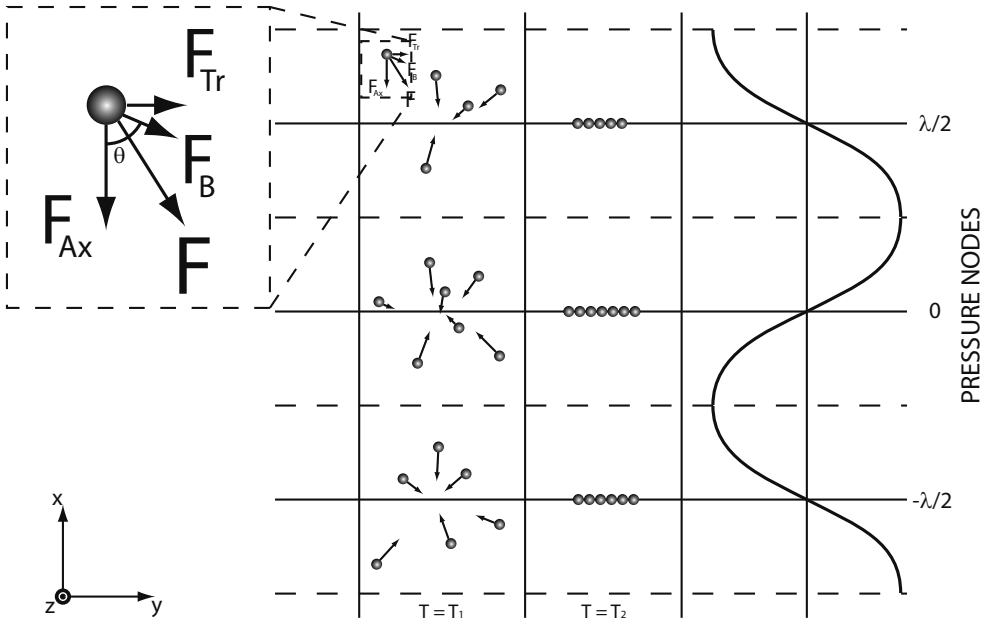

Figure 4.2. Acoustic forces acting on a particle in a wave field. F_{Ax} is the axial component of the primary radiation force, F_{Tr} is the transversal component and F_B is the secondary radiation force (Bjerknes force). At time T_1 the acoustic forces have just begun to affect the particles while at T_2, a steady state has been reached. Figure from Laurell et al. [27]

4.3.1 Primary radiation force

Gorkov [28] started out describing the force from an energy potential point of view and derived the force equation on a spherical object as

$$F_{Ax} = 4\pi \overline{E} R^2 (kR) \sin 2kx \left(\frac{\rho_p + \frac{2}{3}(\rho_p - \rho_f)}{2\rho_p + \rho_f} - \frac{1}{3} \frac{c_f^2 \rho_f}{c_p^2 \rho_p} \right) \qquad \text{Eq. 4.7}$$

where E is the average acoustic energy density, R the radius of the particle, ρ_p is the density of the particle and ρ_f is the density of the surrounding fluid. The speed of sound for the particle is denoted c_p and c_f is the speed of sound of the surrounding medium respectively. By utilizing a couple of relationships,

$$\overline{E} = \frac{\langle p^2 \rangle}{2\rho_p c_p^2} = \frac{P^2}{4\rho_p c_p^2} \qquad \text{Eq. 4.8}$$

and

$$\beta = \frac{1}{\rho c^2} \qquad \text{Eq. 4.9}$$

where P is the acoustic pressure amplitude and β is the compressibility, equation 4.7 can be rewritten into the more commonly known form used by Coakley et al.[29].

$$F_{Ax} = -\left(\frac{\pi P^2 V_c \beta_w}{2\lambda}\right) \cdot \phi(\beta, \rho) \cdot \sin(2kx) \qquad \text{Eq. 4.10}$$

$$\phi(\beta, \rho) = \frac{5\rho_p - 2\rho_f}{2\rho_p + \rho_f} - \frac{\beta_p}{\beta_f} \qquad \text{Eq. 4.11}$$

The axial primary radiation force is responsible for moving particles into the nodal planes of the pressure nodes or anti nodes. The force scales with the particle volume as well as the frequency of the ultrasound (through the wavelength λ). This means that large particles will move faster than smaller ones and that high frequencies will generate higher acoustic forces than lower frequencies, making ultrasound very preferable. The axial PRF is thus also dependent of the acoustic pressure amplitude, the compressibility and the density of the fluid.

The factor ϕ from equation 4.10 is generally denoted the acoustic contrast factor and comprises of the density and compressibility of the particle and the surrounding fluid. The sign of the contrast factor dictates if particles will move towards the pressure node (positive contrast factor) or the anti node (negative factor). As seen in figure 4.3 the blue particles have a positive contrast factor and end up in the pressure node, while the yellow particles with negative contrast factor end up in the pressure antinodes. Generally, rigid particles such as beads and cells will end up in the pressure node while liquids and air bubbles will move towards the pressure anti node. A suspension comprised of two types of particles with different contrast factor can thus be separated from each other [30].

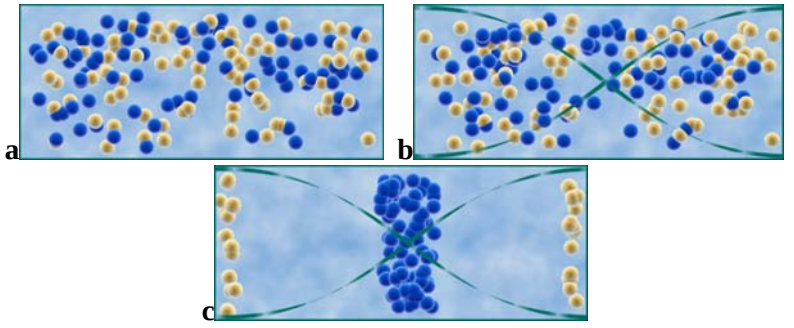

Figure 4.3. Blue particles have a positive acoustic contrast factor and will be moved towards the pressure node, the yellow particles have a negative contrast factor and will subsequently be moved towards the anti node.

Where the axial component of the PRF is the primary particle displacement source and responsible for moving particles into the nodes, the transversal component is responsible for packing the particles closer together in the nodes and to keep them aggregated. The equation for the transversal force was given by Woodside et al.[31].

$$F_{Tr} = V_p \nabla \overline{E} \left(\frac{3(\rho_p - \rho_f)}{\rho_f + \rho_p} \cos^2\left(\frac{2\pi x}{\lambda}\right) - \frac{\beta_f - \beta_p}{\beta_f} \sin^2\left(\frac{2\pi x}{\lambda}\right) \right) \quad \text{Eq. 4.12}$$

where ∇ is the transverse gradient operator.

4.3.2 Secondary radiation force

Suspended particles in an acoustic standing wave field will not only be affected by the primary radiation force, but also be affected by a secondary force which originates from scattering of the primary wave from other particles. This interparticle force, sometimes called the Bjerknes force after the man who pioneered the work [32], is only active at very short distances between particles. A simplified equation for the interparticle forces, valid when the acoustic wavelength is much greater than the particle radius and the distance between the particles, was derived by Weiser et al.[33] This work was based on results from Crum [34], which showed that it is possible to superimpose the equation for the force on a rigid sphere with the corresponding force for a compressible sphere. The force expression, as seen in equation 4.10, contains a velocity component as well as a pressure component [35].

$$F_B(x) = 4\pi R^6 \left[\frac{(\rho_p - \rho_f)^2 (3\cos^2\theta - 1)}{6\rho_f d^4} v^2(x) - \frac{\omega^2 \rho_f (\beta_p - \beta_f)^2}{9d^2} p^2(x) \right] \quad \text{Eq. 4.13}$$

where d is the distance between the particles and θ is the angle between the center line of the particles and the direction of propagation of the incident acoustic wave.

The left side of equation 4.10 depends on the particle velocity amplitude v(x) and the right side depends on the acoustic pressure amplitude p(x). When particles are lined up in the direction of the acoustic wave propagation (θ = 0°) the velocity-dependent term is zero and the net force thus repulsive, and likewise attractive when the particles are oriented perpendicular (θ = 90°) to the incident wave propagation. The pressure-dependent term is not affected by particle orientation at all and is always attractive. It is notable that the velocity-dependent term diminishes as particles are driven to the velocity node (pressure antinode) by F_{Ax}, as in the case of air bubbles and lipid vesicles. In a similar way the pressure dependent term diminishes as particles are driven towards the pressure node (velocity antinode), as are most solid particles in aqueous solutions. The secondary force is thus responsible for aligning particles into monolayers in the pressure node. If particles will remain in a monolayer structure is of course dependent of the particle concentration in the suspension and the relation between the PRF and the SRF.

4.4 Streaming

Because of inhomogenity of the ultrasonic wave field caused by absorption of acoustic energy by the fluid, pressure gradients will form in the medium exposed to the wave. In a fluid, these pressure gradients will cause movements of the fluid known as acoustic streaming [36]. There are basically three types of acoustic streaming: Eckart streaming, Rayleigh streaming, and Schlichting streaming [37]. Eckart and Rayleigh streaming is shown in figure 4.4.

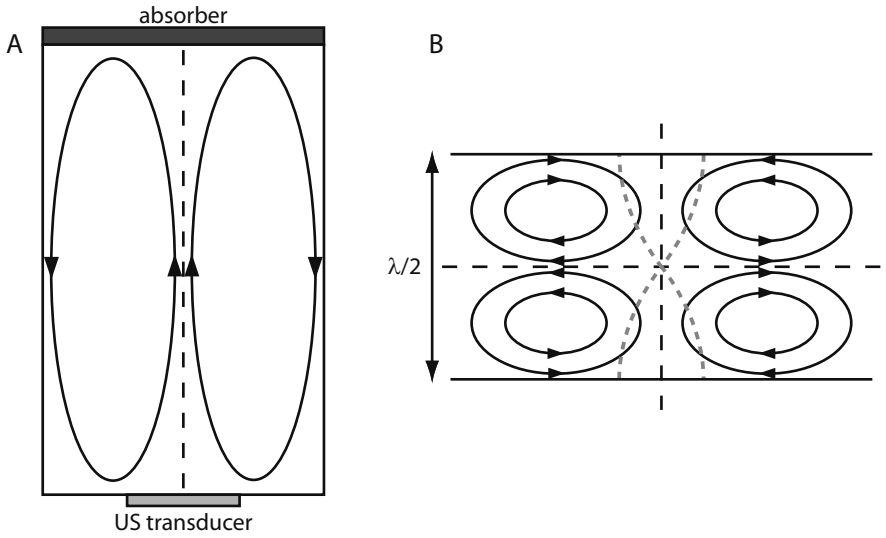

Figure 4.4. A) The large scale Eckart streaming and B) the wave length sized Rayleigh streaming.

Eckart streaming is caused by deposition through losses of acoustic energy along the travelling wave direction [38]. The Eckart streaming vortices is of much larger scale than the wave length and is determined by the fluid volume. Smaller than the container sized Eckart streaming is the Rayleigh streaming which has vortices about wavelength size. The Rayleigh streaming is generally due to energy losses into the viscous boundary layer near the container walls or other obstacles in the fluid. Schlichting streaming is similar to Rayleigh streaming but with the exception that it occurs inside the viscous boundary layer. The vortices extend about twice the boundary layer thickness, which at 2MHz in water is about 0.27 μm for a typical particle. The influence of Schlichting streaming for acoustic particle separation systems are very limited [39].

When working with acoustic particle manipulation, the streaming phenomenon is usually a distress since it counteracts the linearization desired when moving particles into desired positions. The particle size at which acoustic streaming starts to overtake the acoustic radiation force occurs for particles of about 1μm diameter. This has experimentally also been shown with PIV measurements by Hagsäter et al.[40].

Streaming effects can be advantageous if chaos is desired in the micro domain as in the case of mixing. Systems which rely on diffusion for reactions to take place may

be somewhat time-consuming and inefficient due to slow transport of reactants by diffusion. Acoustic streaming can in those cases be utilized to generate a rotation of the fluid and speed up the transport of reactant. Bengtsson et al. [41] have used Rayleigh streaming as a way to increase convective transport in micro enzyme reactors, and Liu et al. [42] used microstreaming to accelerate the hybridization process in DNA hybridization chips.

4.5 Actuation methods

When designing microfluidic systems as active acoustic units, the transducer selection and coupling to the microchip is of major importance. The transducer most commonly used is a piezo ceramic element, a PZT (Lead zirconate titanate) transducer. The three most commonly reported ways of actuating a microfluidic channel for separation experiments are discussed below.

The most straight forward is to use the strong axial PRF and set up the standing wave between the top and the bottom of the channel, see figure 4.5A. This is very common in layered separators. The second way is to place the transducer underneath the entire separation system or at any location on the chip surface where space is available [43], see figure 4.5B. This causes the whole separator chip to be actuated, not just the separation channel. By designing the separator channel carefully, it is possible to obtain a standing wave horizontally or vertically or in both ways in the microchannel. This way of actuating is used in many of the micro separators from the Lund group, and is thus sometimes called the Lund method [27]. The benefit of a translateral wave, as seen in 4.5B is that a transparent glass lid enables a clear visual inspection of what is going on inside the channel. It is easily seen if a separation is successful in contrast to the 4.5A actuation where a visual inspection does not immediately tell if a proper separation is obtained unless determined by optical measurements. The last way of actuating is using a wedge as seen in figure 4.5C. The function of the wedge is to guide the acoustic wave into the chip at an angle which enables further refraction in the layers below such that the incident wave eventually enters the fluid channel from the side and give rise to a horizontal standing wave. This technique has been developed by Wiklund et al. [44, 45]

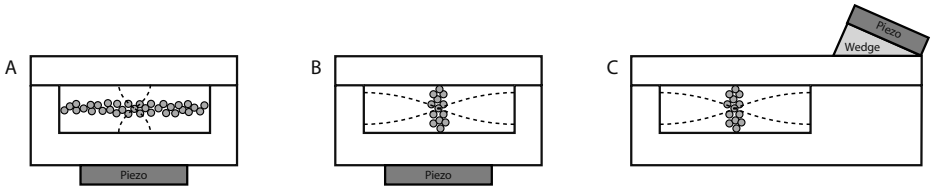

Figure 4.5. Different ways of acoustic actuation on a microfluidic system. A) Actuation the regular way using the strong axial wave component to create a standing wave between the top and the bottom of the channel. Used in layered resonators. B) Actuation from underneath the chip creating a resonance in the entire chip. The distance in lateral direction is matched to the standing wave criterion and thereby a standing wave is formed perpendicular to the incident wave. The actuation used in many of the micro separators from Lund, and is thus sometimes called the Lund method. C) Using a wedge it is possible to "bend" the axial PRF from the transducer with the layers the incident wave is passing and get the lateral standing wave.

4.6 Separator design and materials

The design of the flow splitters have proven to be of importance. Generally, the lesser angle of the side channels with regards to the main separation channel possible, the better the separation will get. The ideal case would be as shown in figure 4.6c, where practically infinitesimal thin walls (they are ~6μm wide) act as flow dividers. Unfortunately, this design has proven to be less usable since acoustic steaming will occur at the edges of the flow splitters and disrupt the separation severely.

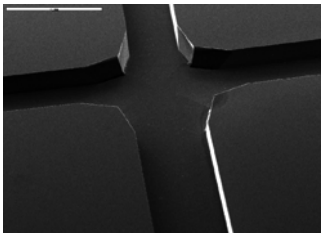

Figure 4.6a. Silicon flow channel with 90° flow splitters etched on a <100>-oriented silicon wafer.

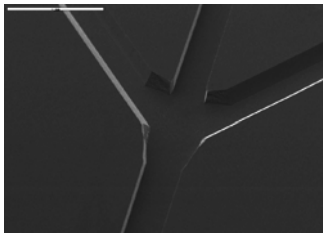

Figure 4.6b. Silicon flow channel with 45° flow splitters etched on a <100>-oriented silicon wafer.

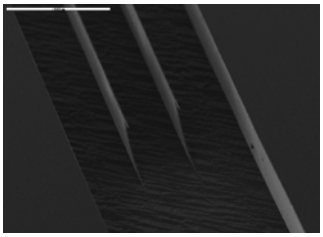

Figure 4.6c. Silicon flow channel with straight flow splitters etched on a <110>-oriented silicon wafer.

It was initially anticipated that totally smooth, vertical walls was a prerequisite to obtain an optimal acoustical separation. Thus making anisotropically etched silicon the ideal separation material as the surface smoothness and high aspect ratios are outstanding of the crystalline silicon. However, as shown in [46] this is not necessarily the case. Instead, an isotropic separation channel with slanted walls ending in a slight curve towards the flat bottom (figure 4.7a) has proven to have a matching performance compared to a corresponding silicon separator (figure 4.7b). For further details see Paper V in this thesis.

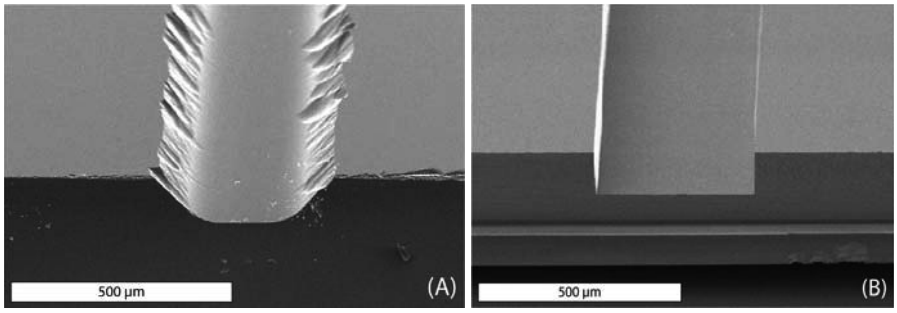

Figure 4.7. Scanning electron microscopy (SEM) images showing cross-section of A) isotropically etched glass and B) anisotropic silicon channels. From Evander et al. [46]

This proves that the channel design and smoothness are less crucial in a continuous flow system as well as the choice of material. Although it would have been practical to be able to use polymers as separation device materials, such as SU-8 [47] or the much popular PDMS [48, 49] which is used in many microfluidic applications, polymers are known to absorb ultrasound quite efficiently. The absorption also results in elevated temperature and possible material deformation, which can be so extreme that ultrasound can be used to weld plastic parts together [50]. Polymers do not have a distinct difference in reflection coefficient relative water either, thus making the separation channel walls poor as acoustic reflectors for building up the standing wave. However, polymers can be used if the acoustic resonance is made by two opposing transducers, as shown by Kapishnikov et al.[51]. In such cases, no reflecting walls are required and only the absorption may be of concern.

When focusing particles and cells using acoustic standing waves in microfluidic channels the obtained shape of the particle/cell stream is important. The 2D-distribution of particles in a half wavelength separation channel excited from underneath was recently investigated by Evander et al. [46]. A fluorescent particle separation was scanned confocally and the different line scans were added together to generate a cross-sectional view. As seen in figure 4.8, the particles are distributed in a sheet from top to bottom of the channel proving the USW to be active in the entire separation channel. The broadening of the particle sheet in the middle of the channel is due to the parabolic flow profile where the higher flow rate gives the particles less time in the acoustic field.

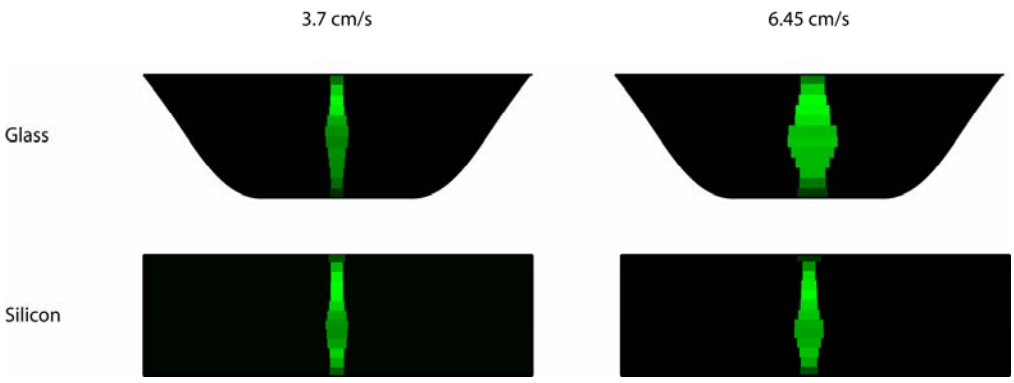

Figure 4.8. Cross-sectional view of the band formation in the channels based on confocal image data. The widening of the particle band in the center of the channel is due to the parabolic flow profile causing the particle in the center to have less time to focus into a narrow band. From Evander et al. [46]

4.7 Layered separators

One of the most straightforward ways of using ultrasound for acoustic particle manipulation is to use the full potential of the axial primary force in a layered resonator. This means that the particles will be focused in the same plane as the transducer, i.e. the resonance occurs between the bottom and the top of the chamber. In order to optimise these systems and obtain maximum acoustic standing wave energy in the flow channel it is important to design the resonator to match reflections and in the different layers.

Figure 4.9. Layered resonator.

The thickness of the layers is dependant of the acoustic impedance matching between the layers. The acoustic impedance, which is described as

$$Z = \rho c \qquad \text{Eq. 4.14}$$

is of major importance when calculating the reflection and transmission coefficient. For normal incidence the pressure reflection coefficient is:

$$R_p = \frac{Z_2 - Z_1}{Z_1 + Z_2} \qquad \text{Eq. 4.15}$$

where Z_1 is the acoustic impedance of the first medium and Z_2 of the second. The transmission coefficient of a wave of normal incidence is subsequently

$$T_p = 1 - R_p \qquad \text{Eq. 4.16}$$

To avoid acoustic losses due to reflection or absorbance, the acoustic impedances of two adjacent layers should match or be as close as possible. Generally, the thickness of the piezoelectric transducer is half a wavelength (at its fundamental frequency), the transmission layer a quarter wavelength, the fluid layer half a wavelength and the reflector a quarter wave length. Substantial modelling efforts have been performed to find the correct resonator parameters for the different layers. Gröschl [35] has done simulations of the layer thicknesses of different combinations and Hawkes et al. [52] have done predictions of the acoustic energies in the fluid layer and how to maximize the input with regards to the surrounding layers. It should be noted that investigations by Hill et al. [53] have shown that matching two resonant systems can be counter productive since a phenomena known as coincidence resonance or frequency splitting can occur. This means that if a resonator channel is designed to have the same resonance frequency as the fundamental frequency of the transducer, a frequency split can occur and one lower resonance and one higher resonance than the intended resonance will appear. At the intended resonance frequency, an unexpected null with no response at all is found. Precautions have to be taken when designing systems with layers with close matching resonances since even small parameter changes in the design are critical.

4.8 Eigenmode modelling

Currently, much effort is put into experimental verification and redesign before an accurate resonator is obtained. Accurate modelling tools would thus be very valuable and timesaving in the development of acoustic resonators. 1D approximation, such as predicting resonances from a channel cross-section point of view, can be accurate when talking about layered resonators where the axial wave component is the major contributor as the standing wave generator. When actuating the resonator chip from the side or underneath, figure 4.5 b&c, which is used in many of the silicon micro separators, the standing wave is generated in a translateral way which does not lend itself to alignment to the regular modelling tools reported. In those cases, the whole separator is actuated and multiple resonances are created in the entire chip. At resonances of such complexity, the equations in section 4.3 might not be entirely representative but may act as a good approximation. When it comes to modelling such a system, it becomes apparent that the 1D approximation is not sufficient when looking at a single channel separator with a micro bead suspension affected by an acoustic standing wave at zero flow. The micro beads affected by the acoustic force show a much more complex pattern than just the simple cross-section information that can be received from the 1D approximation of the PRF equation, see figure 4.10.

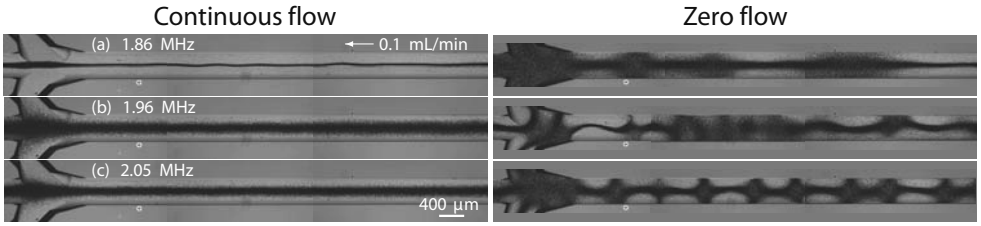

Figure 4.10. A simple separation channel driven at three different frequencies. Comparing the images of the continuous separation (the three images to the left), it can be seen that the results are very alike even though the force acting on particles at zero flow (three to the right) are very much unlike. The information of acoustic pinching regions is hidden in the integration of the total acoustic effect in a continuous flow mode.

In continuous flow mode the observer easily misinterprets the actual acoustic standing wave pattern in the flow channel because the actual acoustic standing wave pattern is lost during a continuous separation. The separator in figure 4.10 is tuned for a $\lambda/2$ resonance and the channel is characterized by some regions that focus the particles to the center and some regions that do not. The total force contribution from many small focusing regions along the channel is integrated as the particles flow through the channel, resulting in a well focused single band stream of particles. As seen from the zero flow images at 2.05, 1.96 and 1.86 MHz in figure 4.10, the acoustic force is acting in clusters or periodic patterns, creating multiple "pinches" along the separation channel, all with different spatial distributions. At the same time, the continuous flow operation shows straight bands of more or less focused particles which display the net integral particle focusing force along the flow channel.

An improved description of an acoustically actuated microfluidic system can be obtained by finding eigenmode solutions p_n to the Helmholtz eigenvalue equation $\nabla^2 p_n = -(\omega_n^2 / c_i^2) p_n$, where ω_n are the resonance angular frequencies, n is the mode number, and the index i of the sound velocities c_i is referring to the three material domains of silicon, water and glass in the chip [54]. This model of the system including the silicon substrate, water filled microchannels and glass lid, denoted the 3D model. In the case where the height of the system is less than half of a wavelength, the description can be approximated by a simpler (not least in respect to the requisite of computational power) 2D approach, where the eigenvalue problem is solved only in the center plane of the microchannels and the surrounding silicon substrate. This second model is denoted the 2D chip model. A further simplification is obtained by utilizing the large difference in acoustic impedance between water and silicon: the 2D Helmholtz eigenvalue equation is solved only for the fluidic part of the system, while the surrounding chip substrate appears only as a hard wall boundary condition on the walls of the microchannels. This third model, denoted the 2D chamber model, is valuable as it gives a more principal representation of the acoustic resonances that can be difficult to detect in the more accurate 2D chip model.

If the Helmholtz eigenvalue equation is solved for the idealized 2D chamber model of the acoustic separator, the result is much different to that suggested by an extended 1D model. Instead of a single solution for one specific frequency, the 2D chamber model suggests several solutions within a rather wide frequency span. More specifically, instead of a uniform pressure amplitude along the length of the channel, the solutions displays an increasing number of "pinching regions" along the channel, see figure 4.11.

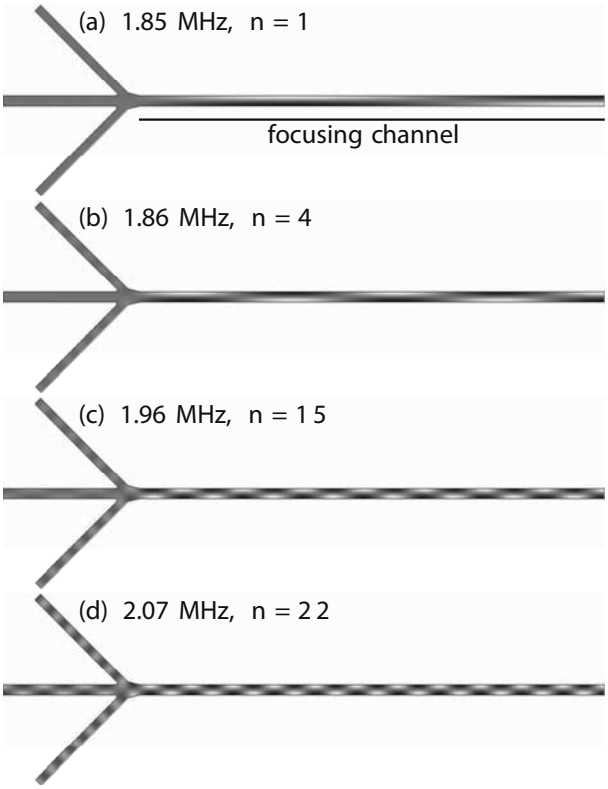

Figure 4.11. Gray-scale plots of the pressure eigenmodes p_n for the chamber model at (a) 1.85 MHz, (b) 1.86 MHz, (c) 1.96 MHz and (d) 2.07 MHz. The integer value n is the number of pinching regions in the focusing channel. From Hagsäter et al. [40]

It is apparent that the 2D model shows a much greater resemblance to the actual live results when running the chips than the 1D model. The simplified chamber model might be enough in most cases, but when it comes to the placement of the transducer a 2D chip model might have to be considered. If a larger transducer is used which cover a large area of the separator the placement might be less critical than if a smaller transducer is used. In those cases it can be devastating if the transducer is applied to an area which is less favourable in terms of transferring the acoustic energy. For more details of Eigenmode modelling, see Paper IV in this thesis.

4.9 Temperature and viability issues

An acoustic separation system is affected by temperature changes in many ways. One is the heating of the chip due to acoustic losses in the PZT transducer or sound absorption of the building blocks of the separator. The latter is of less importance when materials of high E-module compose the resonator, e.g. glass and silicon. The elevated temperature of the separator raises the fluid temperature which induces a mismatched frequency operation since the heat affects the speed of sound in the fluid medium [55]. The frequency drift causes the separation efficiency to decrease and thereby a loss in separation performance is observed. In order to overcome the temperature increase a couple of arrangements can be made. By using a larger transducer on a larger area, much acoustic energy can be transmitted into the chip at a low transducer driving voltage. If the same amount of acoustic energy was to be transferred by a much smaller transducer, higher driving voltages would have been needed and thereby higher electromechanical losses expressed as heat will appear. Another way is to use cooling elements such as Peltier elements and ultimately design the system with a temperature feed-back control.

Svennebring et al.[56] investigated the source of temperature elevation as well of ways to control it. They found that the major source of heat deposition to the fluid channel is due to the losses in the PZT element. They also concluded that heating of the fluid is less of a problem in flowthrough devices than in long-term ultrasonic manipulation traps.

It is commonly known to the scientific society that ultrasound can be used to lyse cells and there is always the question if there is any harm done to cells after being affected by an ultrasonic standing wave. What commonly is forgotten is that the frequency used for cell lysing is much lower, in the kHz range, and that MHz ultrasound is used in diagnostic ultrasonic imaging examinations every day. Nevertheless, many studies have been conducted in the ultrasonic standing wave community to investigate the influence the acoustic exposure on cells. Ryll et al. [57], Wang et al. [58] and Hultström et al. [59] have shown that the acoustical field has no negative effect on the proliferation of cells. Evander et al. [60] have cultured yeast cells for 6 hours in an acoustic trap proving that proliferation was not affected. They also made a viability assay on neural stem cells not observing any adverse effects on the cells after about 15 minutes of trapping. Finally Bazou et al. [61] have shown that the hydrodynamic stress imposed on cells by acoustic streaming is less than that imposed by gentle preparative centrifugation procedures, devices which are very common in every day laboratory work.

5 PARTICLE AND CELL MANIPULATION METHODS

Particle and cell manipulation in terms of separation, sorting and enrichment has always been important from an analytical or biomedical perspective. The development of microtechnology based fluidic devices enables these unit operations to be made at a reduced scale as compared to conventional methodology, thus requiring much smaller sample volumes. Small chemical or biological operations can thereby be implemented in a serial mode, and be made entirely at a chip level thus named Lab-on-a-chip. Medical or chemical operations are envisioned to be performed on a single cell or molecule on a routine basis in the future. Already today, this has been demonstrated in a wide range of applications [62-66]. Several of the early technique development focus on single cell and molecule analysis. However, the direction of cell and particle handling systems are currently moving into the continuous processes which can be integrated with microfluidics on-chip where complex sample suspensions from biofluidics are processed for integrated analysis [67-70]. Below follows an overview of different technologies.

5.1 Magnetophoresis

Magnetic separation is done using either a permanent magnet or electromagnets. The electromagnets matching the size microfluidic systems usually produce a weaker magnetic force than permanent magnets, and are therefore not that commonly used. The magnetic force can not only be used to manipulate magnetic particles or magnetically labelled cells which are magnetic or paramagnetic, but also non-magnetic (diamagnetic) objects which show a very weak repelling movement to the magnetic field [71]. The magnetic force on a particle with a volume V_p is given by equation 5.1:

$$F_{mag} = \frac{\Delta\chi \cdot V_p}{\mu_0} \cdot (\nabla B) \cdot B \qquad \text{Eq. 5.1}$$

where B is the magnetic flux density, ∇B is the gradient of the externally applied magnetic field, μ_0 is permeability of vacuum and $\Delta\chi$ is the difference in susceptibility between the particle and the fluid. In a homogeneous field with $\nabla B = 0$, the net force on a magnetic particle is zero.

Depending of the size of the particle or the magnetic core of a coated particle, the behaviour in the magnetic field differs between nanoparticles and microparticles. Nanoparticles display no hysteresis in the magnetic field, meaning that when the magnetic field is turned off they show no remanence and they disperse in the suspension. In contrast, microparticles display magnetic hysteresis which causes them to agglomerate into clusters [72]. The nanoparticles are therefore preferable

since they enable an on/off action of the magnetic interaction, which may be advantageous if several analytical steps are required for a process sequence.

The standard magnetic bead separation is basically composed of a plain chamber with an external magnet, or an integrated magnetic array as done by Bu et al. [73]. The beads are trapped by the magnetic force and pressed against the wall of the chamber, figure 5.1c. There they will remain until the magnetic field is removed. The magnetic bead separation is well suited for different assays where the beads have been surface modified or coated with antibodies or antigens.

Pamme et al. [74] reported a continuous magnetophoretic system, where multiple bifurcations provided inlets for buffer solution and a sample inlet at the bottom of the chamber, figure 5.1a. The suspended magnetic particles were separated according to size in the separation chamber as particles with the largest volume were affected the most by the magnetic force and subsequently ended up in an outlet closer to the magnet. By utilizing the same device but introducing different reagent buffer in layers, it is possible to perform multi-step biochemical processes on the magnetic particles as they move through the different buffer layers under the influence of the magnetic force [75].

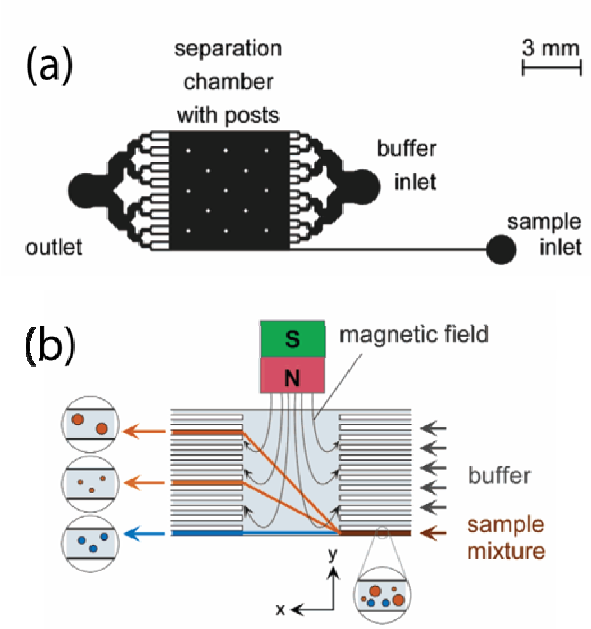

Figure 5.1a and b. Magnetophoresis according to Pamme et al. Sample suspension enters the separation chamber at the lower right and the particles will be displaced orthogonal to the flow in the upward direction by the magnetic force into the carrier buffer solution and separated. Reprinted with permission from [74]. Copyright 2004 American Chemical Society.

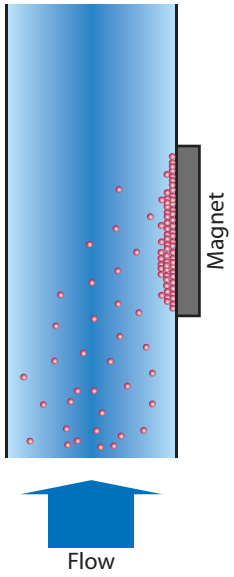

Figure 5.1c. Magnetic trapping. Suspended magnetized bead will be trapped at the channel wall by the magnetic force provided by the magnet. There they will remain until the magnetic force is removed.

Magnetic nanoparticles have shown to be useful in a number of biomedical applications, for example as drug carriers [76]. Furlani [77] have separated white blood cells (WBC) from red blood cells (RBC) using magnetic forces. This was possible since WBC behave as diamagnetic microparticles while RBC can be either paramagnetic or diamagnetic depending on the oxygenation state. Han and Frazier [78] also separated WBC and RBC but with a different approach. They included a ferromagnetic wire in the direction of the fluidic flow. The wire caused a high gradient in the magnetic flux which enhanced the magnetic separation.

5.2 Dielectrophoresis

Dielectrophoresis, or DEP, was first investigated by Herbert Pohl in the 1950's [79]. In DEP, a force is exerted on a dielectric particle in a non-uniform electric field. All particles are affected more or less in the presence of an electrical field, and the force does not require the particle itself to be charged. The strength of the force depends on the medium and the particle's electrical properties, on the shape and size of the particle and the frequency of the electrical field.

The DEP force on a homogenous sphere with the radius r can be expressed as:

$$F_{DEP} = 2\pi r^3 \varepsilon_m \mathrm{Re}(f_{CM}) \nabla E_{rms}^2 \qquad \text{Eq. 5.2}$$

where ∇ is the del vector operator and E_{rms} is the root mean square of the applied electric field. $\mathrm{Re}(f_{CM})$ refers to the real component of the Clausius-Mossotti factor:

$$f_{CM} = \frac{\varepsilon_p^* - \varepsilon_m^*}{\varepsilon_p^* + 2\varepsilon_m^*} \qquad \text{Eq. 5.3}$$

where ε_p^* and ε_m^* are the complex permittivity of the particle and the medium. The complex dielectric constant is:

$$\varepsilon^* = \varepsilon - \frac{j\sigma}{\omega} \qquad \text{Eq. 5.4}$$

where ε is the dielectric constant, j is $\sqrt{-1}$, σ is the conductivity and ω is the angular frequency of the applied electric field.

By varying the frequency of the applied voltage, it is possible to induce a dipole moment in a particle and thereby cause the particle to experience a movement. Particles having higher permeability than the surrounding fluid, $F_{CM}>0$, move to a region of stronger electric field i.e. the electrodes, and is called positive dielectrophoresis (pDEP). The opposite occurs when the particles have lower permeability than the fluid, in which case the particles are repelled from the

electrodes and is consequently called negative dielectrophoresis (nDEP). For continuous fractionation pDEP is not recommended since particles are attracted toward the electrodes and may cause damage to them [62]. Less stress is induced at field minima, which is especially good for living cells. Fiedler et al. [62] have used nDEP to create virtual flow channels with “channel walls” created by activating the electrodes. They have also used transients to temporarily switch off “the walls” in order to move particles between the flow channels. The choice of frequency is also very important for the DEP function. Gascoyne and Vykoukal [80] have presented a very useful frequency guide which shows at what frequencies different types of DEP is used and what the typical particle responses are.

For the DEP to be functional, a non-uniform electric field is required. One way is to use electrodes of various shapes and designs [81]. Another is to apply voltage along a channel that contains insulating obstacles such as posts [82] or ridges [83]. The electric field becomes non-uniform close to these objects, and particles flowing around them will be affected by the DEP force. DEP forces do not depend on the polarity of the electric field but rather the field gradient and either AC or DC or both [84] can be used in contrast to regular electrophoresis which uses DC only.

DEP is a very versatile tool which can be used for many of the standard particle and cell operations in the analytical field such as continuous separation [85], particle medium exchange [86], particle concentration [87], trapping [64] and positioning [88]. DEP can be used for a wide range of particle sizes. There is however a lower limit around 1μm when Brownian motion will start to influence and a higher limit around 10μm when sedimentation will start to dominate.

5.3 Pinched flow fractionation

In pinched flow fractionation, two inlets are used; one which contains a particle suspension with particles of different sizes and one particle free fluid. The particle free liquid flows at a higher rate and laminates the particles in the other suspension to one sidewall in the pinching region, regardless of particle size. The particles are pinched to the side wall at a distance which is equal to their radius and will move along streamlines that pass through their hydrodynamic centers. As the particles move out into the expansion chambers, the laminar streamlines are expanded and the particles are separated perpendicularly to the flow direction according to their sizes, see figure 5.2.

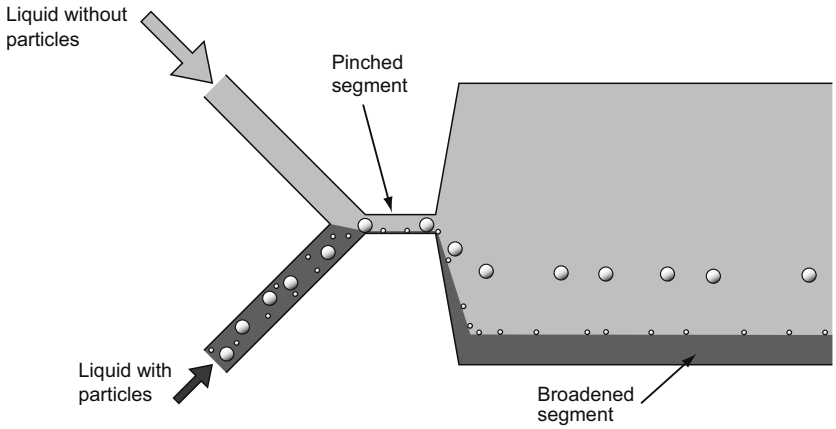

Figure 5.2. Principle of pinched flow fractionation. Particles in a suspension are focused along the side wall in a pinched segment with a clean buffer. As they enter the expansion chamber the broadening of the laminar streamlines separate the particles by size.

The expansion chamber is then split into many outlets collecting only particles of specific size. The basic principle was shown by Yamada et al. [89] and an improved device with asymmetrically arranged separation branches has also been shown [90, 91]. Further enhancement including flow rate control valves [92] as well as replacing the pressure driven flow with EOF have been done [93].

5.4 Hydrodynamic filtration

Hydrodynamic filtration is a principle which is similar to cross flow filtration [94, 95]. Both techniques utilize small capillary branches perpendicular to the main flow where excess fluid will exit. The removal of carrier fluid forces particles to the side walls of the main channel, but whereas the aim of cross flow filtration is to remove the carrier fluid, the gaps between the side branches are too small to let particles through. In hydrodynamic filtration the aim is not only to remove the suspension media, even though it certainly is possible, but to separate particles of different size from each other. The width of the side branches is thus wider and it is the flow control of the side branches that decides which fractions will be removed. As seen in figure 5.3 from Yamada and Seki [96], when the relative flow rate in the side channels is low a), no particles will be diverted to the side branches – only fluid. In b), medium flow rate is applied to the side channels letting small particles be separated with the medium but not large particles, while in c) relative high side flows will result in no particle fractionation. The dashed lines in figure 5.3a-c show the virtual boundaries of the layers of fluid in the main channel that will be diverted into the side branches. Before the separation branches there are multiple branches responsible for aligning and concentrating the particles by medium removal.

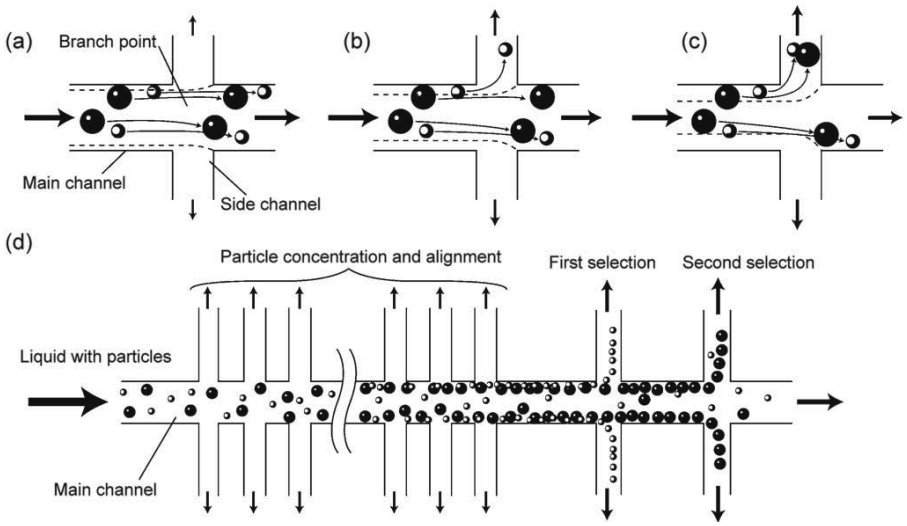

Figure 5.3. The principle of hydrodynamic filtration. Excess fluid is removed gradually from the side branches perpendicular to the main flow. This action will eventually line up particles along the main channel walls. By controlling the flow rate of the branch flow it is possible to remove particle fractions of a particular size while larger particle moves on to be separated later. From Yamada and Seki [96]. Reproduced by permission of The Royal Society of Chemistry.

The technique has also been demonstrated in the separation of WBC from RBC. An alternate design where the medium fractions removed during the concentration process have been recombined again with the main flow providing an improved particle alignment is shown in [97].

A related effect which can be used to separate particles or cells from their medium is the Fahraeus-Lindqvist effect. A suspension flowing through a tube with a small diameter (typically <500µm) will experience a viscosity gradient where particles tend to gather in the center of the tube with clear fluid at the walls. The viscosity will thereby be lower at the walls and higher in the center of the tube. In the case of blood, the low viscosity fluid by the walls will be blood plasma while the different cells will be concentrated in the high viscosity region in the tube. This makes it possible to remove some small fractions of blood plasma, and the effect is sometimes called plasma skimming. Jäggi et al. [98] utilized the effect in their microfluidic plasma separation chip. Their PMMA chip reached a separation efficiency of 59% for an initial hematocrit of 15% and 37% for initial hematocrit of 45% respectively for a flow rate of 2 ml/min.

Yang et al. [99] used the Zweifach-Fung effect which states that if blood is flowing through a bifurcating region in a capillaty vessel, the blood cells have a tendency to travel into the vessel with the highest flow rate leaving very few cells going into the low flow rate vessel. They used a PDMS chip with a main channel and five plasma skimming channels and achieved close to 100% cell free plasma from 45% hematocrit at a flow rate of 10 µl/h.

5.5 Field Flow Fractionation

Field Flow Fractionation or, FFF, is a technique where an external force is applied perpendicular to a flow to perform the separation mechanism [100]. The force can be almost any imaginable physical phenomena; examples are electric or magnetic fields, gravity, thermal or cross fluid flows. The motion of the particle depends on the physical parameters of the particle versus the interaction of the applied force and the parabolic flow profile. How the separation is performed depends on the size of the suspended particle. Particles approaching the dimensions of macromolecules, will be more affected by Brownian motion than larger ones and will therefore behave differently. The separation of the different components is determined by the retention time in the separator, i.e. depending on the physical parameters of the particles included and the applied external force, particles will exit the separator at various times and thereby enable fractionation. There are basically three modes of operation, the normal mode, the steric mode and the hyperlayer mode [67, 101].

The *normal mode* affects submicron particles and macromolecules. The external force drives them toward the wall opposite the side of the incident force, see figure 5.4a). An accumulation of particles and macromolecules will occur. The increased particle concentration by the wall is however counteracted by Brownian diffusion in the opposite direction of the force. The macromolecules, which are smaller in size than the submicron particles, will be more affected by the Brownian motion and move further away from the accumulation wall. Because of the parabolic flow profile, the macromolecules will thus exit the separator before the submicron particles.

The *steric mode* FFF acts differently on larger particles than the normal mode, typical particle sizes of 0.5-10µm. These particles are too large to be affected by the weak Brownian diffusion counter effect. Instead, the particles will form a thin layer close to the accumulation wall. The larger particles will protrude out of this layer into faster streamlines and exit the separator faster than the small particles that are caught into slower streamlines close to the wall. As this is the opposite reaction of the normal mode FFF, it is sometimes referred to as reversed mode. The residence time for the steric mode depends only on the size of the particle.

For larger particles, >10µm, the contact with the wall is very limited. Instead they are affected by an opposed force generated by hydrodynamic lift forces that moves them away from the wall. As they are moved a distance greater than their diameter, the retention mode is called *hyperlayer*, figure 5.4c. The separation in the field is still reversed, that is larger particles first, but the separation does not entirely rely on size but also on other physical properties of the particle.

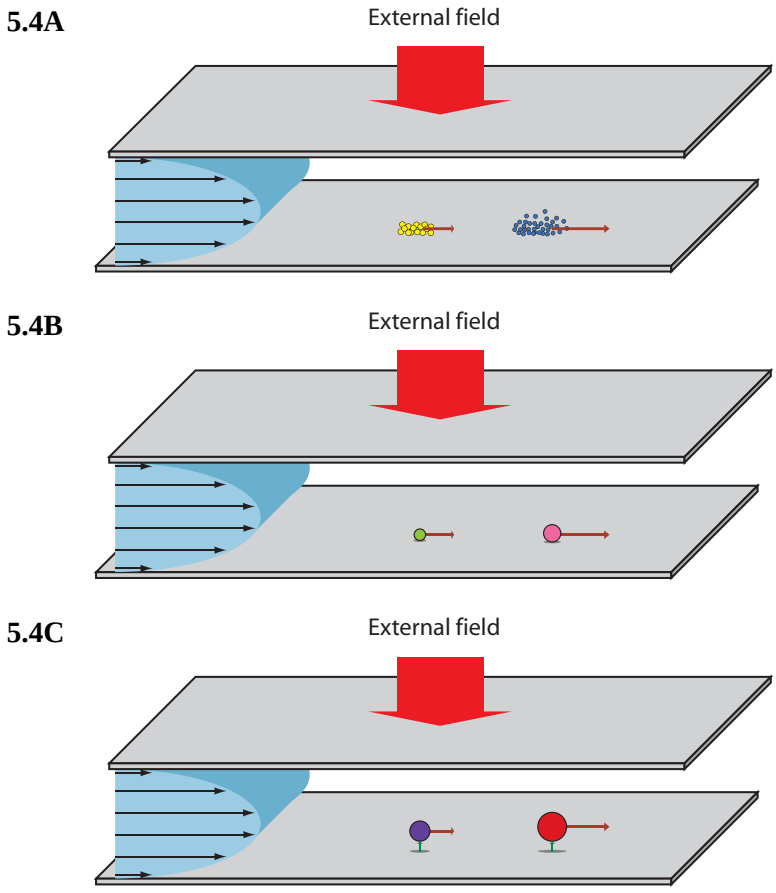

Figure 5.4. A) Normal mode FFF, B) Steric mode FFF, C) Hyperlayer mode FFF

The FFF family is a very versatile platform which enables separation over a wide size range, from hundreds of microns down to nanometer scale [102].

5.6 Obstacle induced separation

Deterministic lateral displacement is a method for separating particles by size [103]. An asymmetric array of posts or obstacles is created, i.e. the placement of the following post is shifted a short distance sideways. Depending on the size of the particle, it will be deflected towards a neighbouring flow stream as it passes between two posts and will thus display a sideways deviation in its course through the post array. The trajectory is dependent on the asymmetry of the array. The distance a post is shifted, δ, and the total distance between two posts G, will determine how many streamlines the separator will have, see figure 5.5A. The number of streamlines will also limit the amount of particle sizes that can be separated at the same time. The angle α of which particles will be deflected depends on the distance between the posts along the flow path, and can be calculated as $\tan^{-1}(\delta/\lambda)$, figure 5.5B. More

detailed theoretical models for deterministic lateral displacement were developed by Inglis et al. [104].

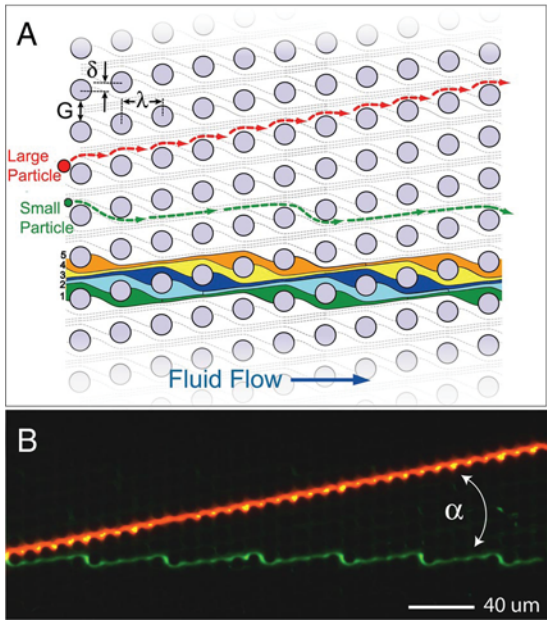

Figure 5.5. Deterministic lateral displacement. The asymmetrical placements of the posts in the array cause particles of different sizes to choose different flow streams. This results in an in lateral displacement and thus size separation. Printed with permission from Morton et al. [105]. Copyright 2008 National Academy of Sciences, U.S.A:

Morton et al. [105] experimented with many different post combinations, drawing parallels toward optical phenomena as refraction and deflection as well as focusing particles into jets. They showed that it is possible to direct streams of differently sized particles across laminar flows. This was utilized in [106] where E.coli cells were fractionated and subsequently directed into another flow line containing cell-lysing solution. The intracellular content was then further separated and the DNA recovered.

Another technique which relies on obstacles is the *Brownian ratchet*. The Brownian ratchet is comprised of asymmetrical posts in a symmetric array, i.e. the opposite of deterministic lateral displacement [107]. The ratchet will only work on small particles, such as macromolecules, which are affected by Brownian motion. As a suspended mix of particles flow through the ratchet they will bump into slanted obstacles which will deflect their trajectories. They will however also experience a lateral movement due to diffusion. Small particles will move farther by Brownian diffusion than larger ones and are therefore more likely to move further sideways.

The Brownian ratchet will thus separate by size in a lateral way. The geometry of the posts and the distance between them influence the mechanism and separation degree and have to be considered when designing the ratchet [108]. Since only very small particles can be used, DNA molecules are very suitable to separate [109]. Cabodi et al. [110] have made a system with a precisely controlled injection scheme which allows them to separate two different DNA into their components. Matthias and Müller [111] showed that it is possible to make a massively parallel Brownian ratchet using asymmetric pores in a silicon membrane which could be suitable for large-scale particle separations.

5.7 Optical methods

Optical tweezers is a method which uses a focused laser beam in which dielectric particles are trapped. With the tweezers, it is possible to hold or to move particles. It was first reported by Ashkin [112] in the early 1970´s of particles being affected by scattering and gradient force on particles of micron size. Objects of high refractive index were attracted toward the center of the beam and propelled away in the direction of the beam. Using two counter propagating beams, he was able to trap particles in three dimensions. Ashkin later developed of what became known as optical trapping where dielectric particles were to be trapped and held stable in three dimensions using a single focused beam of light.

The method operates with a Gaussian beam profile and utilizes the fact that there is a very strong electric field gradient in the narrowest part of a focused beam of light, known as the waist of the beam. When a particle enters the beam boundary, it will experience a net force towards the center of the beam because the larger optical momentum change towards the center of the beam, see figure 5.6a. Less intense beams will pass on a smaller momentum change away from the center, however, the net momentum will move the particle to the center where an equilibrium is met and thereby it will be trapped [113].

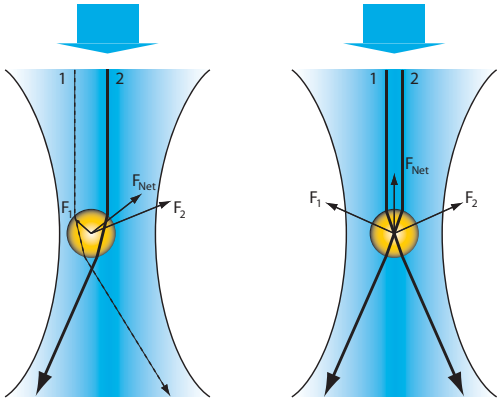

Fig 5.6a. The principle of optical tweezers. A particle will experience a net force towards the center of the beam because the more intense beams transfer a larger momentum change towards the center of the beam.

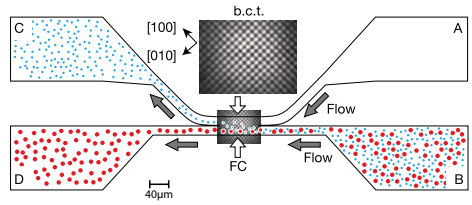

Figure 5.6b. The concept of optical fractionation presented by MacDonald et al. [114] The array of laser beams causes particles to be repeatedly deflected towards the center of a laser beam. Since the optical tweezer force is lower than the Stoke's drag, and the particles display a sideways trajectory dependent of the size and optical properties of each particle, a separation is obtained. Reprinted by permission of Macmillan Publishers Ltd: Nature, Copyright 2003

By using infrared lasers, Ashkin et al. [115] were able to perform damage-free trapping and manipulation of red blood cells and organelles located within living cells since the haemoglobin and chlorophyll absorption is reduced in the IR spectra.

Optical forces have been used in a wide range of applications. Perroud et al. [116] for instance used the optical gradient forces to displace particles into another streamline in a μFACS system. The system basically worked as a regular FACS but with the exception of using the optical force as actuator for the rare event fractionation.

An array of optical tweezers can be arranged as an optical lattice for a continuous particle fractionation system [114]. The lattice is a three dimensional structure which enables sorting of particles through a three-dimensional flow. When a flow of mixed particles passes through the lattice, MacDonald et al. [114] used 2μm silica and polymer spheres, the selected particles are deflected from their original trajectories while the others pass on, see figure 5.6b. The selectivity depends on the particles sensitivity to the optical potential. The result of the optical lattice will be similar to the deterministic lateral displacement system, with the exception that there will be no physical obstacles which could be subjected to clogging. Ladavac et al. [117] showed a similar device in two dimensions using twelve discrete optical tweezers.

5.8 Acoustical methods

Methods using acoustic forces provide a gentle and contact free way of manipulating cells and particles. Several different applications and inventive ways using acoustics, and especially acoustic standing waves, have been developed in recent years [27, 29]. Below follows an overview of acoustical macrofluidic and microfluidic systems, with the main focus on the microfluidical systems as those are the platform used in the papers included in this thesis.

5.8.1 Macrofluidic systems

Several of the early acoustic particle manipulation systems were large, in the sense that they were not microfluidic systems relying on laminar flow etc., and commonly effectuated separation according to the agglomeration/sedimentation principle [118, 119]. In this principle, the acoustic forces are used to gather the particles or cells into clusters, which at some time will gain such size that the buoyant lift force will be exceeded and they will subsequently sediment at the bottom of the chamber. These systems can be either continuous [120-123] or batch systems [124, 125]. The aggregation sedimentation processes may be well working, but are generally quite slow since they rely on sedimentation processes as a driving force. Gupta et al. [126, 127] proposed a semi-continuous separation system in which particles were passed through a porous medium in which the particles where trapped when the ultrasound was turned on. The porous medium had, however, the drawback of being saturated after operating a while and separation efficiency decreased. A purging procedure with the ultrasound turned off had to be performed before separation could be commenced. Continuous separation systems where particles are driven toward a designated area and subsequently separated by flow splitters [128] are much faster and can be placed in an arbitrary position [129]. The continuous separators are superior in the way that they work as particle filters without the apparent drawback of clogging, which ordinary filters are prone to do sooner or later.

By shrinking the dimensions of the separation chamber to half a wavelength, it is possible to line up particles in a single lane, rather than in cluster formations. Yasuda et al. [130] inserted a capillary into their fluidic chamber to act as a flow splitter where the single line of particles was collected.

5.8.2 Microfluidic systems

By reducing the size of the fluidic device into the microscale, several desirable features are accomplished. The flow in a microfluidic device is primarily laminar, making continuous separation using flow splitters very useful, as will be elaborated below. As the size of a fluidic channel decreases into micrometers, the frequency of the sound will rise into ultrasound regime, if a half wavelength channel width is to be retained. The higher the frequency, the higher the acoustic radiation force will be (see equation 4.10) and thus improved separation performance. The increased force also allows smaller particles or cells to be separated. It should be mentioned,

however, that acoustic streaming starts to affect the separation around particle sizes of ~1μm [54] and Brownian motion around 0.1μm [131].

5.8.2.1 Continuous flow systems

Microfluidic systems have the advantage over macrofluidic systems that smaller volumes are required and that reactions are much faster. The continuous format also enables fast sample solutions to be introduced for more complex chemical procedures. This in combination with microscale devices can result in a higher degree of integration of different types of modules to compose a lab on a chip system.

The basic way of making a separation of particles using acoustic standing waves in a continuous format is to use a standard three-way flow splitter, as in figure 5.7.

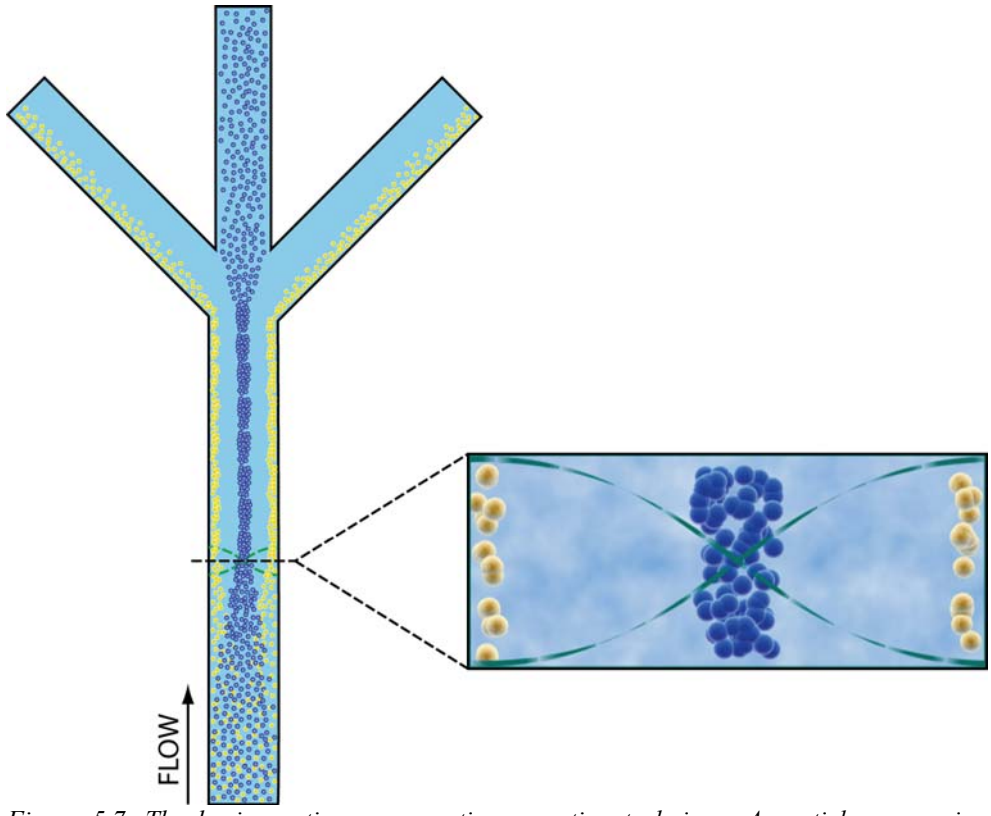

Figure 5.7. The basic continuous acoustic separation technique. A particle suspension enters the separation channel which has the width of half a wavelength. The USW moves particles with a positive acoustic contrast factor to the pressure node in the middle of the channel and particles with negative acoustic contrast factor to the pressure antinode along the sides of the channel. The laminar flow in the micro channel allows particle separation by a flow splitter since no mixing occurs.

Suspended particles enter from the bottom and the blue particles moves toward the acoustic pressure node in the center and the yellow particles move to the pressure antinode because of different physical properties. Because of the laminar flow in the

micro channel the particles remain in their lateral position even after they have passed the acoustic field and by introducing the flow splitter at the end it is possible to separate the two particle types from each other.

A variety of different separator materials have been used. Hawkes et al. [132] presented a half wavelength separator in stainless steel which was constructed by wire electro discharge machining. Kapishnikov et al. [51] made their separator in a polymer (SU-8). Since polymers do not reflect ultrasound sufficiently well in regards to an aqueous medium, the standing wave has to be created by other means. Kapishnikov et al. thus used two opposing transducers and the interference of the two incident waves created the standing wave. The separator itself reminds of a SPLITT-chip where particles large enough to be affecter by the USW are transferred to another clean buffer. Another disadvantage with polymers in the design of acoustically actuated microfluidic systems is that they normally display a substantial absorption coefficient for the employed ultrasound and the absorbed energy is mainly transformed into heat.

A material/material combination that is more suitable as a reflector and resonator is silicon and silicon/glass compound devices. The acoustic impedance difference between silicon and an aqueous solution is quite high, supporting the design of silicon cavity based resonators. Silicon also offers the properties of a crystalline material, which can be taken advantage of by anisotropic etching where selective etching of different crystal planes result in perfect vertical walls and thus well defined resonator chambers.

Harris et al. [133] made a layered resonator in silicon with a glass cavity lid where the resonance occurred between the bottom of the silicon channel and the glass lid as exemplified in figure 4.5A. As the device only had two outlets, instead of three as in figure 5.7, the performance of such a device is limited because there will always be some medium or undesired particles that follow with the desired particles into the enriched outlet. The device also displayed limited visual inspection possibilities since the focused particles were placed in a sheet parallel to the glass lid.

The alternative actuation principle where the transducer is placed underneath the silicon separator with the standing wave generated perpendicular to the transducer was utilized by Nilsson et al. [134], paper I in this thesis. This way of actuation have the advantage that it is possible to see the separation clearly via the glass lid and the performance of the separation can easily be monitored since there is a large contrast between particle dense band formation and clear, particle free fluid. This is illustrated in figure 5.8 which shows multiple band formations at higher harmonics of the fundamental resonance frequency.

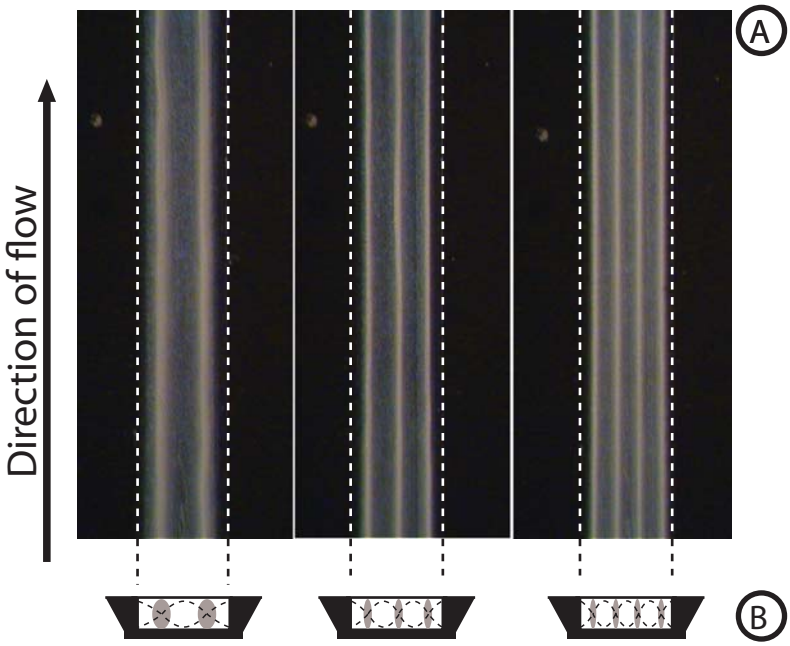

Figure 5.8. Microscope image of 5 µm polyamide particles aligned in parallel bands in a ~750 µm wide channel at different actuation frequencies. left: first harmonic (~2 MHz), middle: second harmonic (~3 MHz), right: third harmonic (~4 MHz), microscope image from above (A), illustrated cross-section (B). From Nilsson et al. [134]

Nilsson et al. also investigated different separator designs, one with the side channels directed 90° from the main separation channel and another design with the side channels at 45° angle, see figure 5.9. These are the two different designs possible to make while using <100>-oriented silicon. Even though the 45° angle design had side channels with non rectangular cross section (but rather a trapezoid shaped cross section) the design proved to be preferable since it eliminated the stagnant zones at the junction where air bubbles tended to be trapped and interfere with the separation. The performance of the chip was demonstrated using 5µm polyamide beads and showed 90% separation efficiency at ~2% bead concentration into the chip.

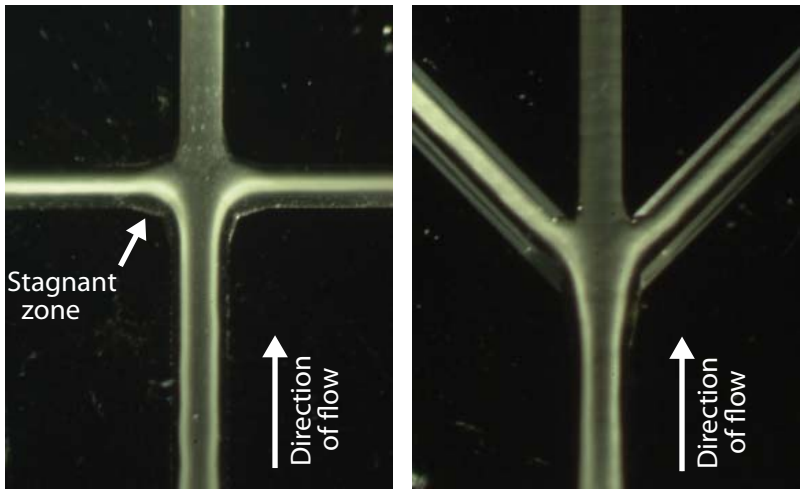

Figure 5.9. Microscope images of the two different designs investigated by Nilsson et al.[134]. Note the stagnant zone on the 90° side channel design (left). The structure with 45° side channels (right) is not bothered with such problems. From Nilsson et al. [134]

Blood wash

One of the first applications of the above described silicon microfabricated acoustic separation chip targeted blood wash in open-heart surgery. Normally during cardiac surgery, the blood shed during surgery is returned to the patient via a filter. The filter, however, does not remove the millions of small lipid particles mixed with the blood, which originates from adipose tissue ruptured when performing the surgery. The lipids, mainly triglycerides [135], instead pass through the filter and are returned into the patient's circulatory system where massive embolization will occur and subsequently local ischemic tissue damage. Animal studies have shown that almost all internal organs will be affected and especially organs with high blood perfusion rates such as the kidneys and the spleen [136]. It is however in the brain that the ischemic damage becomes most obvious [137]. Elevated levels of cognitive dysfunction have been linked to lipid microembolization of the brain [138]. A the moment, no medical equipment are dedicated at lipid removal from blood even though blood wash techniques based on centrifuges can be used at extensive blood loss. The centrifuges do have drawbacks of being committed to quite large volumes, exposing the blood cells to harmful mechanical stress and not being continuous.

Acoustic separation can however be used since, fortunately, the acoustic contrast factor of red blood cells and lipid particles have different sign. Erythrocytes have a positive ϕ-factor (~ +0.3) while lipid particles have negative ϕ-factor (~ -0.3). This means that the RBC and the lipid particles will move to different lateral positions in the acoustic standing wave and can thus be separated from each other as they pass through the acoustic separation channel, see figure 5.10. A laboratory model of tritium labeled triglycerides in saline solution was used to evaluate the lipid particle separation efficiency [30] (Paper II in this thesis).

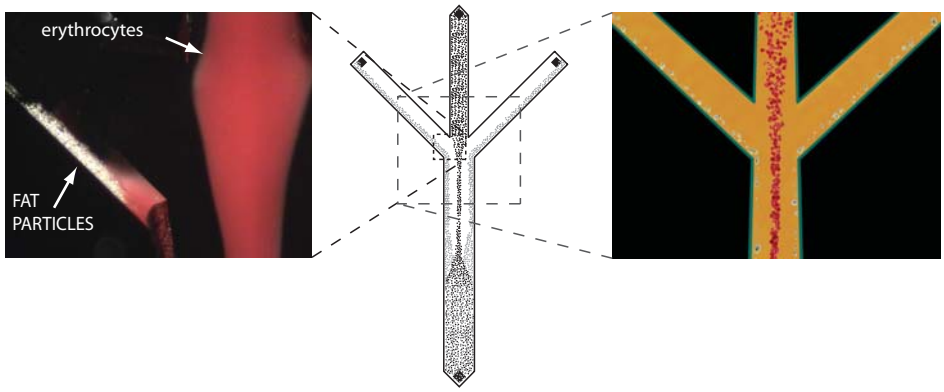

Figure 5.10. Lipid contaminated blood enter the chip from below. Because the lipids and the blood cells have different sign on the acoustic contrast factor, lipids move towards the antinodes at the channel walls while the blood cells move towards the pressure node in the middle of the channel. The microscope image to the left shows human blood and lipid particles being separated from each other.

Results showed that about 85% of the lipid particles were removed regardless of the RBC concentration while the RBC separation decreased with increasing concentration. The flow rate through a single separator was 0.3 ml/min, which needlessly to say is not very much. A chip with eight parallel separation channels connected in a bifurcation structure was constructed [139] proving that up-scaling of the separator device is possible, see figure 5.11. The multichannel chip handled flows of 0.5 ml/min with approximately the same separation efficiencies for blood cells and lipid particles. The degree of hemolysis, i.e. the rupture of red blood cells, was also studied and no increase in hemolysis was found, thereby concluding that the acoustic separation method posed no threat to cell viability. For more detailed information see Paper III in this thesis. An even larger structure with multiple parallel channels was proposed by Laurell et al. [27].

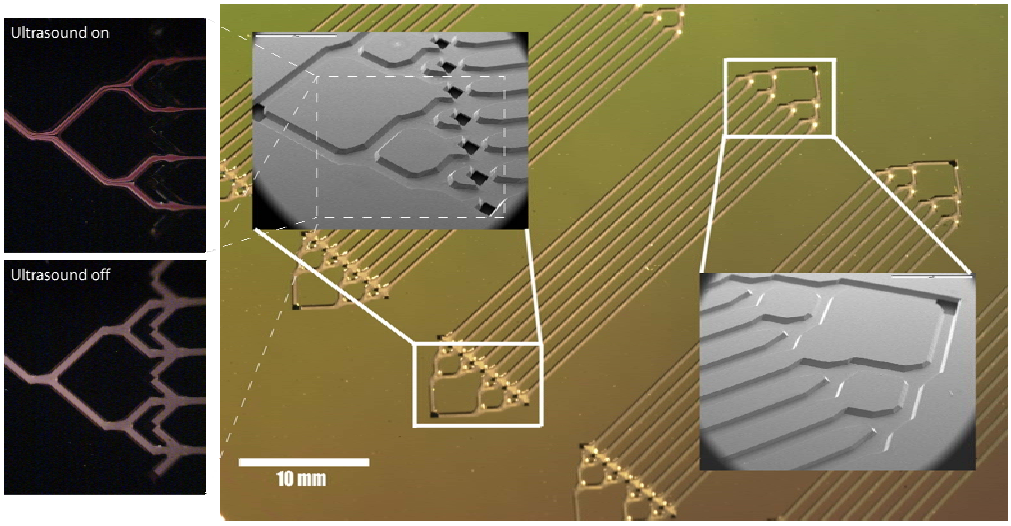

Figure 5.11. Separation chip with eight parallel separation channels for increased throughput.

Plasmapheresis

A procedure which is closely related to blood wash is plasmapheresis, i.e. the removal of the cellular content from the blood plasma. Many of the microfluidic devices presented in the literature display problems in handling fluids of high concentrations, such as whole blood. Often these separation devices are forced to work with dilute blood samples, which deteriorate the quality of the plasma from an analytical point of view. The acoustical chips presented earlier are no exception since the separation efficiency is known to decrease significantly by increasing hematocrit (<10%). However, a novel acoustic separation chip has been designed to manage the processing of whole blood [Lenshof, paper VI in this thesis]. The plasmaphersis chip is comprised of a separation channel as in [134] but with the exception of a series of outlets placed in the separator channel along the way. These outlets remove mainly red blood cells which already have been focused by the acoustic standing wave and thus sequentially lower the hematocrit along the separation channel, figure 5.12. At point D in figure 5.12, the concentrations of blood cells are sufficiently low for all remaining cells to be removed and the clean plasma fraction is extracted from outlet E.

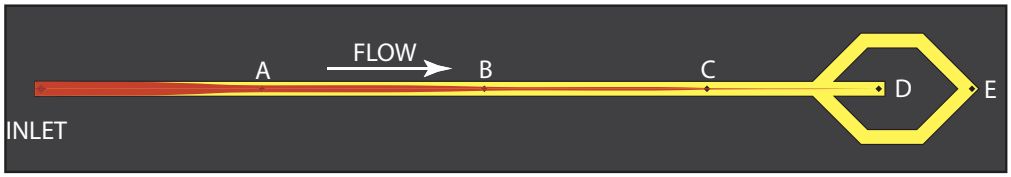

Figure 5.12. The principle behind the plasmapheresis chip. Multiple outlets are placed along the separation channel where red blood cells focused in the middle of the channel are subsequently removed. The clean plasma fraction is collected at outlet E.

By increasing the length of the separation channel, and fold it into a space saving meander, the duration in the acoustic field is longer and thus the time to focus particles even further after sequential removal of fractions is increased. The removal of particle fractions perpendicular to the flow is also advantageous, since it does not disrupt the acoustic radiation force on the remaining particles which would be the case in a trifurcation separation design. The total flow rate of the chip is 80 µl/min and the clean plasma fraction is 12.5% of the total blood volume. The separation of red blood cells is 100% and the total number of red blood cells is below $6x10^9$ per liter [140], a limit which has been set by the Council of Europe for plasma intended for transfusion.

The plasma generated by the plasmapheresis chip was also successfully linked to an antibody array chip for detection of Prostate Specific Antigen (PSA), a biomarker for prostate cancer. Increased levels of PSA present in male blood plasma can be an indicatior of prostate cancer. Being able to quickly detect the elevation of PSA is of major interest for detection of prostate cancer and to assess response to treatment of a patient already having established cancer. The successful combination of the plasmapheresis chip and the PSA antibody array chip opens up the possibility of creating a fully integrated lab on a chip solution for PSA detection.

Medium exchange through particle switching

Laminar flow microchannels offer the possibility to laminate different liquid media in a streaming system. This, combined with acoustic particle manipulation, can be utilized to move particles from one suspending medium to another using acoustic standing waves [141, 142]. By adding two extra inlets on each side of the original central inlet, it is possible to move particles from the medium streams on the side into the central, particle-free medium thus exchanging the medium the particles are suspended in. This can be of importance in applications where a more rigorous wash of particles or cells is required.

The medium exchange procedure was illustrated by translation of 5µm polyamide beads in a buffer contaminated by Evans blue into a clean medium [141]. About 95% of the contaminant was removed in this experiment while it should be mentioned that the degree of contamination was quite low. If medium of higher degree of contamination is used the cleaning efficiency will decrease, probably due to weakly absorbed contaminants on the bead surface or by tailing effects of the beads dragging contaminants with them into the clean buffer. The medium exchange efficiency mentioned above was also repeated with erythrocytes in saline solution and Evans blue as pollutant.

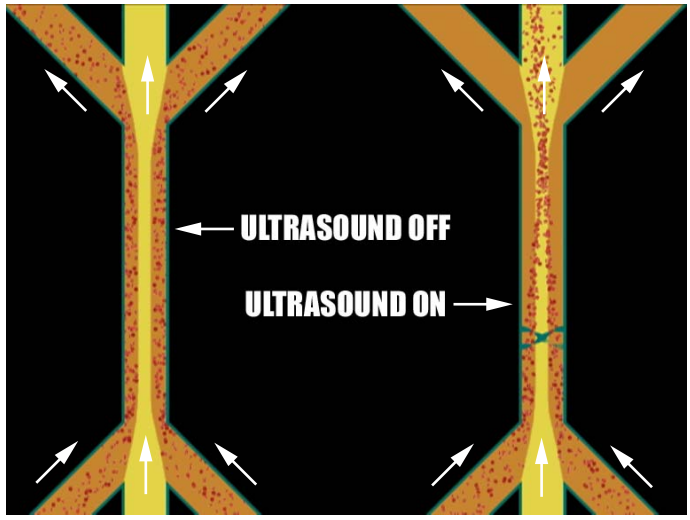

Figure 5.13. The particle wash and buffer media exchange chip. A contaminated particle suspension enters from the sides and a clean buffer enters through the middle. The acoustic standing wave moves the particles into the clean buffer which exits through the middle outlet while the contaminated medium exits through the sides. From Petersson et al. [141]

The described medium exchange method can be used to extend the applicability of the above described blood wash method to include post surgery blood recycling, i.e. when the patient is still bleeding in the post surgery intensive care unit and the shed blood is collected via a drain tube in the chest cavity. In this case the blood plasma can be heavily contaminated by drugs, immunologically active substances and coagulation factors that should not be returned to the patient [143]. To avoid this, the

erythrocytes can be moved from the contaminated plasma to clean plasma or saline solution for safe re-infusion.

Enhanced medium exchange

An enhanced medium exchange device with two integrated acoustic switching chips in sequel was presented by Augustsson et al. [43]. A similar protocol as used in [141] with Evans blue as a contaminant and 5μm polystyrene bead was used to verify the contaminant efficiency removal. While previous data showed a 95% removal of the contaminant, Augustsson et al. showed a provoking 99.995% efficiency. They also showed an application for phosphopeptide affinity extraction. Further work with the sequential medium exchange chip has involved affinity specific extraction of phage particles [144]. Microbeads with affinity specific coating were used to separate bound phages from unbound and thus being able to sort out specific phages from a library. The enhanced medium exchange chip proved to be at least as efficient as conventional separation approaches, and has the advantage of being much more flexible when it comes to handling different types of particles and can thus be adapted to virtually any kind of antigen carrier.

Medium exchange through side-washing

The side-washer principle is a bit different than previously described medium exchange technique [145]. The original buffer is phased out gradually through the addition of clean buffer along the channel while the acoustic radiation force keep the beads aligned in the channel, figure 5.15. Although the band of focused beads gets slightly displaced every time new clean buffer is added, the acoustic radiation force will refocus the beads. The retention time of the beads in the acoustic field is of major importance if the wash should be successful and not too many beads lost to the cross-flow stream. Each junction has an exchange rate of 25% of the main buffer flow resulting in the buffer injected at inlet 1 will end up in outlet 5. The chip had eight cross-flow junctions and each junction increase the buffer exchange ratio accordingly. Wash efficiencies up to 96.4% were accomplished with a 0.2% solid content bead suspension, using eight cross-flow junctions, effectively exchanging the carrier buffer twice.

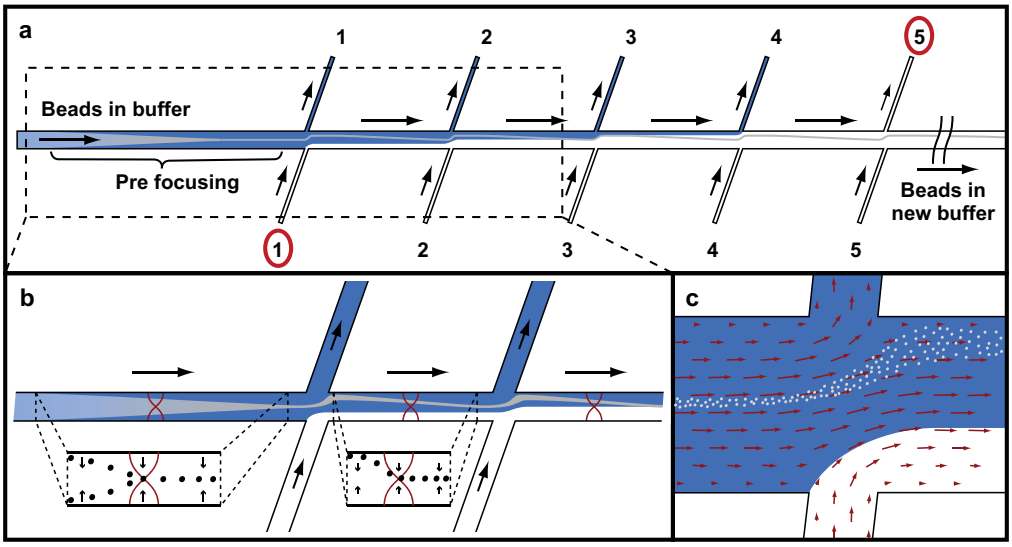

Figure 5.15. Side-washing chip. Beads in buffer enter the system and are focused in a band in the middle of the channel. At junction 1 the particle band will be displaced towards the upper wall because of the addition of clean buffer. The acoustic radiation force will however realign the particles in the middle and the cycle is repeated until the entire original medium has been shifted out and the beads are re-suspended in clean medium. From Augustsson et al. [145].

A alternative use of the side-washer was presented by Augustsson et al. [146] where the cross-flow channels were not used for washing buffer but instead each branch injected a pH-buffer of varying degree. This enabled the use of microbeads with ion-exchange properties and different surface bound peptides to be eluted from the beads during sequential exposure to higher pH in the channel. The advantages of such a chip include the ability to perform multiplex probing and wash of contaminating background, increasing the detection limit.

Size fractionation

The primary axial radiation force on a particle is dependent on the volume of the particle, see equation 4.10. This means that larger particles will experience a larger acoustic force than smaller sized particles and thus size fractionation could be possible if the force is tuned correctly [147]. Petersson et al. [148] made a silicon fractionation chip where a particle suspension containing particles of different sizes, although equal density and compressibility, was introduced along the side walls of the flow channel. In the middle of the channel a clean buffer was introduced. By tuning the acoustic force and the flow rate, the largest particles reached the pressure node shortly before entering the center outlet. The second largest fraction, located in a neighbouring laminar boundary, exited the chip through the next outlet and so forth. Thereby a size sorting device was achieved. The different sizes were thus spatially separated at the end of the separation channel and were collected via several outlets that addressed a defined laminar portion of the flow channel.

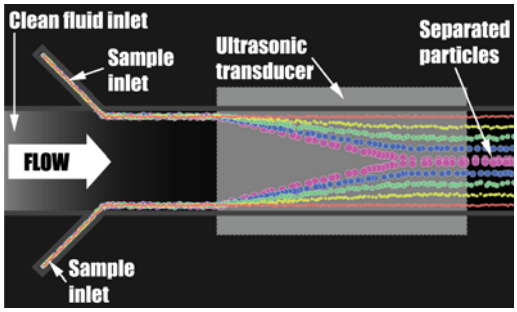

Figure 5.16a. Particle suspension entering at the sides of the channel. Pink particles are the largest and will thus reach the pressure node first. By adjusting the acoustic force such that only the pink particles reach the node before the multiplex output, fractionation is enabled.

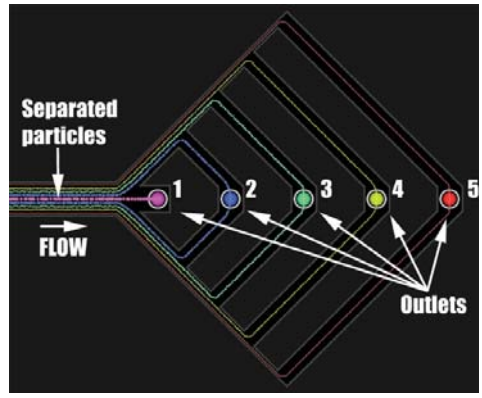

Figure 5.16b. Fractionation of the particle sizes. The largest particles exit through 1, second largest through exit no. 2 and so on. Reprinted with permission from Petersson et al. [148]. Copyright 2007 American Chemical Society.

By manipulating the density of the medium through the addition of cesium chloride, Petersson et al. [148] also managed to separate normally acoustically inseparable particles from each other. The medium manipulation in combination with the fractionation device realized the successful fractionation of erythrocytes, platelets and leucocytes from each other.

Size fractionation can also be realized by a frequency switching scheme [149]. Since the acoustic force is proportional to particle size, as described above, the particles will move an unequal distance when switching the frequency between two harmonics. At time T1 (Figure 5.17) a single wavelength standing wave (second harmonic, ~4 MHz) is applied, thus the particles are gathered in the pressure nodal planes one quarter of the channel width from each side wall. When switching over to the fundamental resonance frequency (half wavelength, ~2 MHz) the particles will start to migrate toward the pressure nodal plane in the center of the channel (T2). The larger particles move faster because they are affected by a stronger radiation force. If the frequency is switched back at the right moment the larger particles will be located close to the center of the channel, where the acoustic force is at its minimum (T3). The smaller particles, on the other hand, will have moved only a small distance and, at time T3, start to move back to their position seen at time T1. After switching again (T4) the larger particles will be closer to the center than at T2 while the smaller ones will be at approximately the same position as at T2. If the switching continues the larger particles will end up in the middle of the channel and the smaller ones one quarter of the channel width from each side wall when they reach the outlets (Figure 5.18b).

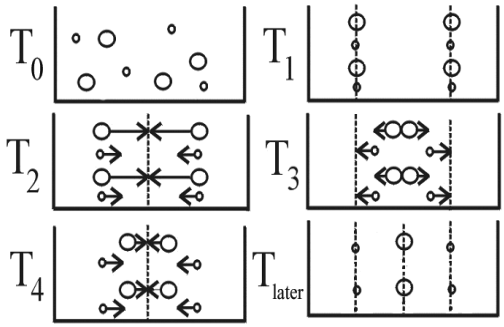

Figure 5.17. The frequency switching separation principle. At T_0 particles have entered the system and no ultrasound is applied. At T_1 and T_3 the second harmonic is applied and at T_2 and T_4 the frequency corresponds to the fundamental frequency. At T_{later} the two particle sizes have been separated from each other. From Laurell et al. [27]

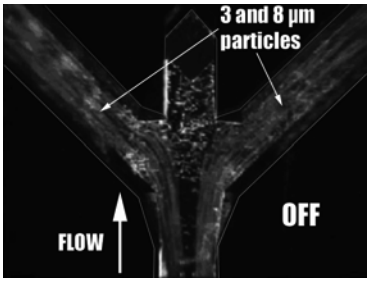

Figure 5.18a. Initial state with the ultrasound turned off. Both particle sizes exit through the side channels and the clear buffer through the middle. From Laurell et al. [27]

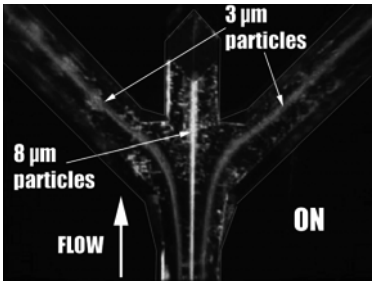

Figure 5.18b. The two particle sizes have been separated from each other and the 8µm particles are focused in the fundamental pressure node and exits through the central outlet. The 3 µm particles are focused in the node of the second harmonic and exits through the side outlets.

Using this method, it was demonstrated that at least 80% of the particles could be collected in the intended outlets when separating 3 µm polystyrene (1.05 g/cm^3) and 8 µm polymethylmethacrylate (1.22 g/cm^3) particles. The fundamental resonance and the second harmonic were typically active for 800 and 200 µs respectively (total flow rate: 90 µl/min).

Binary particle switching

The combination of the acoustic radiation force and laminar flow also enables valveless particle switching. As seen in figure 5.19a it is possible to deflect particle streams from one trajectory and outlet into another outlet. By connecting several acoustic valves into a tree structure, Sundin et al. [150] showed a possible discrimination of particles into four different outlets. If less concentrated samples are to be used, a rare event sorting of single particle types can be managed in a FACS type of way [27]. This technique would require fast switching and total control of the flow parts of the particle. One of the problems with fast acoustic switching has been the parabolic flow profile since particles flowing near walls have a slower flow rate

and do not respond fast enough at the acoustic radiation force. Grenvall et al. [151] solved the problem by making a 2D focusing of the particles streams, that is standing waves between the walls and bottom and the ceiling of the channel. The acoustic FACS showed promising results, however further development is needed. The acoustic FACS might have potential compared to the regular FACS as it shows higher degrees of differentiation as more parameters influence the acoustic force affecting the particles such as density and compressibility.

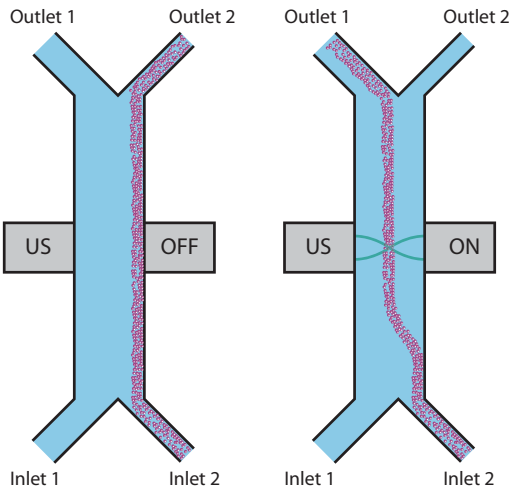

Figure 5.19a. Binary switching principle. Particles from inlet 2 will exit outlet 2 due to laminar flow unless affected by the USW. By switching the ultrasound on and off it is possible to decide which outlet the particles should exit through.

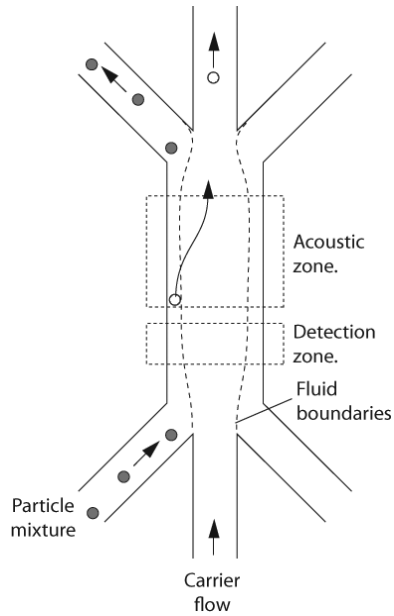

Figure 5.19b. Principle of rare event sorting based on acoustic valving. From Laurell et al. [27]

5.8.2.2 Acoustic trapping systems

If the acoustic force is larger than the drag force of the fluid the particle will be trapped in the acoustic field. Acoustic trapping can be utilized for enrichment, sorting out rare particles and performing chemistry on cells and particles by exposing them for different analytes. Lilliehorn et al. [152] presented an ultrasonic trapping system with integrated ultrasonic micro transducers in a PCB plate with a glass/polymer (SU-8) fluidic channel. The particle trapping was found to be strongly affected by near field pressure variations but still the trapping managed to withhold linear fluid flows of 1mm/s. They also presented a trapping array of three sequential trapping zones with individual controlled ultrasonic transducers [153]. The trapping zones also had individual cross-flow microchannels for adding external fluids and thereby enabling a non-contact and continuous flow bioassaying system utilizing e.g. antibody-activated microbeads.

Evander et al. [60] improved the trapping device of Lilliehorn by integrating the flow channel and reflector into a single glass unit. The system proved to be able to handle live cells and viability tests were made on trapped stem cells and yeast which showed no signs of being harmed by the ultrasonic trapping. An altered flow channel design was used to separate sperm cells from female epithelial cells in a forensic application which aimed at sample preparation for DNA-analysis in rape cases [154]. The acoustic technique is shown to achieve comparable purities of the separated DNA fraction in a substantially shorter time as compared to the standard methods used today.

Trapping in silicon cavities have been investigated by Manneberg et al. [155] where they showed 3D manipulation of particles and cells at an individual level. A combination of acoustic forces and DEP was presented by Wiklund et al.[44]. The principle is based on the competition between long-range ultrasonic forces, short-range dielectrophoretic forces and viscous drag forces from the fluid flow. The USW was used to move particles to the DEP electrodes and there the DEP forces could be applied to position, sort and separate the particles.

6 BLOOD

Since blood has a central position in this thesis, a short summary of the constituents and properties of blood is presented.

Whole blood comprises a cell population and plasma. The cellular content can be classified in three groups, red blood cells, white blood cells and platelets. An adult human body contains 6 – 8 liters of whole blood where the cellular components make up about 45% of the volume. The rest of the 55% is plasma, which consists of 90% water and 10% dissolved species, such as proteins, carbohydrates, electrolytes, lipids, vitamins etc. The term serum sometimes used refers to blood plasma without fibrinogen or other blood clotting factors.

6.1 Basic blood component knowledge

6.1.1 Red blood cells

The primary function of red blood cells, or erythrocytes, is to transport and deliver oxygen to tissues and organs in the body and to return carbon dioxide to the lungs. Adult blood typically holds 4.2 - 6.2×10^{12} erythrocytes per liter [156]. An erythrocyte has the shape of a biconcave disc, which has a diameter of 7µm and a thickness of 2µm. The biconcave shape makes them highly flexible and provides maximum surface area for oxygen transport. Hemoglobin, a highly abundant protein in erythrocytes, is responsible for the oxygen transporting properties. Highly oxygenated blood is bright red while it becomes dark red when oxygen has been released.

Unlike many other cells, the erythrocyte does not have a cell nucleus. The nucleus is lost when the erythrocyte is squeezed through the pore of the endothelial lining of the bone marrow capillary. There are three reasons for the absence of a nucleus: a nucleus will decrease the amount of oxygen possible to transport, it will cause the erythrocyte to be heavier which will increase the workload of the heart and it does not require a nucleus to be able to perform its tasks since it is fully differentiated.

The term hematocrit, which is one of the most important erythrocyte factors, is used to describe the percentage of red cells in the blood. The hematocrit differs between genders, whereas males have a hematocrit of 0.46-0.54, females have a slightly lower hematocrit 0.38-0.44.

6.1.2 White blood cells

White blood cells, or leucocytes, are an important part of the human immune system which protects the body from antigens, i.e. microorganisms and foreign matter. The majority of the leucocytes are found in the vascular and lymphatic systems. An average adult has approximately 75 billion leucocytes circulating and the normal

amount of leucocytes in a blood sample is about 4.5 - $11x10^9$ per liter. An increased amount of leucocytes is an indicator of infection.

The leucocytes are divided into numerous sub groups since there is a wide diversity of cells with different functions. The three main groups are granulocytes, monocytes and lymphocytes [157].

Granulocytes are basically named after the granules, or small grains, present in their cytoplasm. The granulocytes are in turn are categorized into neutrophils, eosinophils and basophils.

Neutrophils measure from 10-15µm and are the most common white blood cell and make up 65% of all white cells. Neutrophils defend against bacterial or fungal infection and other very small inflammatory processes. They are generally the first responders to microbial infection and their activity and death in large numbers form pus.

Eosinophils measure from 12-17µm and primarily deal with parasitic infections and an increase in them may indicate such. Eosinophils are also the predominant inflammatory cells in allergic reactions.

Basophils measure about 5-7µm and the main function is to release the anticoagulant heparin in case of external cell damage so that the white blood cells can address foreign matter before clotting starts. Basophils are also responsible for allergic response by releasing histamine causing inflammation.

Monocytes migrate from the bloodstream to other tissues and differentiate into tissue resident macrophages or dendritic cells. The macrophage is a large cell, 12-20µm, which performs phagocytosis (engulfment and digestion) of cellular debris and foreign matter. The dendritic cells main function is to act as antigen-presenting cell (APC) to activate T lymphocytes, since T lymphocytes cannot recognize protein antigens on their own.

Lymphocytes are a part of the immune system and are activated when they recognize foreign matter as nonself. Lymphocytes measure from 5-12µm in diameter and are divided into B cells, T cells and natural killer (NK) cells [158].

B cells are responsible for making antibodies toward antigens, such as bacteria and viruses, and thereby induce immunity towards the antigen. The B cells also have the function as memory cells, remembering different antigens that the host has been exposed to in the past.

T cells themselves are categorized into three different types: cytotoxic T cells, helper T cells and suppressor T cells. The cytotoxic T cells have the ability to kill cells, such as transplanted tissue or cells which have been altered by antigens or viruses. The helper T cells have the ability to recognize antigens and produce

cytokines to direct other T cells to the infected area. The suppressor T cell is responsible for keeping the immune system in a healthy balance by neutralizing too aggressive lymphocytes, for instance when an infection already has been supressed.

NK cells play a major role in defending the host from both tumors and virally infected cells. They differ from other lymphocytes in the way that they do not require prior exposure to antigen and thus do not require prior activation in order to destroy cells. Because of this ability they were named “natural killers”.

6.1.3 Platelets

Platelets, or thrombocytes, have the main function of preventing blood loss. This is done in two ways: they act as a plug over the endothelial damage area and they also provide a platelet factor-3, a phospholipid found on the surface of the platelet needed for activation of coagulation factors.

The thrombocyte is a colorless cell which is about 2-4μm in size. A blood sample of an average adult contains about $150\text{-}450 \times 10^9$ platelets per liter.

7 CONCLUSIONS

Acoustic force driven particle and cell manipulation has proven to be a successful base in developing continuous flow microseparators. This thesis demonstrates an acoustic standing wave microchip solution that discriminate between particle types of different acoustic contrast factors and an application of cleaning shed blood from lipid particles as encountered in open heart surgery has been investigated. The blood/lipid separation provided promising results and further investigations also proved that the acoustic separation technique does not inflict any damage to the processed cell. A separation device with parallel channels for higher throughput has also been presented.

Furthermore, the principle of acoustic radiation force acting on particles has been investigated. It has been shown that the radiation force does not act uniformly on particles in a flow channel but rather in pinching regions. It has also been shown that acoustic streaming is present in the separation channel and mainly influences particle sizes of about 1μm and smaller. For larger particles the primary acoustic radiation force dominates over hydrodynamic drag in the acoustic streaming. The effect of streaming and uneven force distribution in the channel is decreased due to the continuous flow and thereby the integration of the effect of the force along the flow channel.

The influence of separation device material and the shape of the cross-section of the separation channel have also been investigated. Results show that a separator in glass works equally well as its silicon based counterpart. Investigations also indicate that the shape and the surface smoothness of the cross-section is of less importance although more investigations need to be done.

Confocal measurements on the particle separation show that the particles are lined up in a vertical sheet located in the center of the half wavelength separation channel. This can be utilized in a separation device handling high concentration fluids, like for instance whole blood. By sequentially removing high particle concentrated fractions from the center of the channel, the total concentration of particles in the channel can be reduced gradually. An acoustic plasmapheresis chip for whole blood processing have been developed and proven successful in generating high quality plasma for subsequent diagnostic purposes.

The acoustic particle manipulation platform has proven to be very versatile and is clearly showing several interesting results. The applications of the technique are numerous and the future of microfluidics combined with acoustics will be exciting.

8 POPULÄRVETENSKAPLIG SAMMANFATTNING

Ultraljud är ljud av så hög frekvens att det mänskliga örat inte kan höra det. De flesta associerar säkert termen ultraljud med diagnostiskt ultraljud som utövas på foster under en graviditet. Tänker man lite längre kanske man erinrar sig om att delfiner och fladdermöss kommunicerar och navigerar med hjälp av ultraljud. Det finns dock så mycket mer man kan använda ultraljud till. Man kan till exempel påverka och flytta celler eller partiklar i vätska. Om detta handlar denna avhandling.

Ljud brukar oftast beskrivas som en våg, en ljudvåg. Ljud kan ju som bekant studsa när det möter en vägg, som ett eko. Studsar ljudet mellan två motstående väggar kan en stående våg uppsåt. Den stående vågen flyttar sig inte utan befinner sig på samma ställe hela tiden, ungefär som när man slår an en gitarrsträng. Att vågen ser lika dan ut hela tiden gör att man kan utnyttja det faktum att man vet positionerna för svängningarna.

Partiklar i en vätska som utsätts för ett ljudfält kommer att uppleva en akustisk kraft. Är ljudfältet en stående våg kommer de att bli påverkade av en mycket större kraft än om ljudet bara fortsatt rakt fram eftersom det återkommande ljudet också påverkar partikeln. När den återkommande ljudvågen blandas med sig själv kommer den växelvis att förstärka sig själv respektive ta ut sig själv. Vi får alltså noder med noll i ljudintensitet samt bukar med maximalt ljud. Partiklarna kommer att förflytta sig mot noden och samlas där. Om man flödar en vätska med partiklar i en kanal av den bredden att den rymmer en ljudnod i mitten av kanalen och ljudbukar längs kanterna av kanalen, så innebär det att alla partiklarna kommer att samlas i ett band i mitten av kanalen. Längs kanterna av flödeskanalen finns nu enbart ren vätska. Genom att dela upp sin kanal i tre olika utflöden kommer de av ljudet separerade partiklarna att ledas ut i mitten utloppet medan den rena västan längs kanterna kommer att gå ut i de två sidoutloppen.

Olika typer av partiklar eller celler kommer att uppföra sig olika i ljudfältet beroende på deras fysikaliska egenskaper. De flesta solida partiklar och celler kommer att röra sig mot en ljudnod, medan luftbubblor och fetter (som olja) kommer att röra sig mot en buk. Detta resulterar i att man kan skilja två olika partiklar med olika fysikaliska egenskaper från varandra med en stående vågfält. Detta faktum utnyttjades i en applikation i avhandlingen där blod från en hjärtoperation renades från skadliga fettpartiklar. Om blodkropparna kan renas från fettpartiklar är det möjligt att återföra patientens eget blod som den förlorat under hjärtoperationen på ett säkert sätt utan att de förorenade fetterna följer med in i blodomloppet. Hade fetterna kommit in i blodet hade risken funnits att de hade täpp till de små ömtåliga kapillärerna i exempelvis hjärnan som tillför den näring och syre. Om kapillärer blockeras i hjärnan uppstår snabbt små skador i hjärnvävnaden och om antalet blockerade kapillärer blir stort erhålls bestående men för patienten.

En annan tillämpning i avhandlingen handlar om att med samma teknik filtrera bort alla blodkroppar från blodplasman. Plasman är blodkropparnas bärvätska som innehåller en massa näringsämnen och slaggprodukter. Blodplasma innehåller även ett stort antal sk. biomarkörer som mäts i samband med sjukdom. En sådan markör är prostata specifikt antigen (PSA) som vid förhöjda nivåer indikerar risk för prostata cancer. PSA nivån i plasma står i proportion till hur långt cancern är gången. Det är alltså svårare att upptäcka en eventuell cancer tidigt. Biomarköranalys inklusive PSA görs normalt på plasma vilket innebär att alla blodprover måste genomgå ett centrifugeringssteg innan analys kan genomföras. Avhandlingsarbetet har här visat på möjligheten att nyttja akustiska mikrochip för produktion av ren plasma och direkt koppla denna till PSA diagnostik. Tanken är att i slutändan kunna göra ett kombinerat analyschip med ett akustiskt filter för en snabb prostata cancer diagnos.

9 ACKNOWLEDGEMENTS

I am now writing the final chapter of this thesis and it really gives you some perspective of the time spent during these years. I remember when I started looking for a project for my master thesis. I had taken some courses at the Solid State Physics department since silicon and microelectronics fascinated me. However, it turned out that semiconductor components and excited electrons was not that intriguing. But I still had the attraction towards micromachining of silicon and thought that it must be something else you could do with it besides semiconductor electronics. Then I took the course of Micro Sensors at Electrical Measurements and found out about the chemical and biomedical world beyond the barrier of semiconductors. I talked to Professor Thomas Laurell and he presented an interesting idea he had of manipulating particles with ultrasound in microfluidic channels. I knew this was the right project as I had taken the course of Ultrasonic Physics before at the department and found that I liked the subject as well as the people working there. One thing led to the other, and I eventually ended up as a Ph.D-student. The rest, as they say, is history…

With this, I would firstly like to start with special thanks my supervisor Thomas Laurell. Without his inspiration and visions, this thesis would never have been completed. I am also very grateful that he had patience with me at times when the research and the results did not go my way.

I would also like to thank my assistant supervisor Johan Nilsson for many interesting discussions, on and off the golf course. My former room mate and collaborator Filip Petersson, who showed me the meaning of true ambition. Mikael Evander for all the good times at the golf course, in the mushroom forest and in the lab. Simon Ekström for reintroducing me to computer games, making me spend too much time and money at the pub (I still cannot believe we earned our self an invitation to a gathering for loyal customers at the Bishop's Arms) and for all amusing anecdotes.

I would also like to thank all current and former colleagues at Elmät for all good times. Sus Levin for being a good friend and always being there to help me when whenever I need it, with the exception of always needing to finish some urgent stuff first… Martin Bengtsson and Lars Wallman for keeping the clean room going and providing heavy resistance in the Snood competitions. Magnus Cinthio for having a personal vendetta with me every time at the florball court. Tomas Jansson, the superior winner of the famous "most hairy chest contest", for answering tricky questions on ultrasound even though "standing waves are an abomination" and for being a really funny dude. My master thesis students Filip Petersson and Melker Hagsäter, who ironically both made Ph.Ds before me. Kerstin Järås and Asilah Ahmad Tajudin for really working their asses off for helping me finalize the last manuscript before printing the thesis. Lennart Nilsson for all nice devices, mechanical assistance and advice on growing tomatoes (mine grew into a 3m high, dense, jungle after that). Eva Everitt for helping me with the university bureaucracy. Monica Almqvist for delivering fiery answers at music pop-quizzes. Hans Persson

for stressing the fact that ultrasonics is a complex field and for amusing evasive maneuvers for postponing his comeback at the floorball field. Elly Schlyter for taking care of the coffee room. Carl Grenvall for an endless enthusiasm (which hit a temporary low at the visit of the San Diego Zoo when all animals were hidden indoors sleeping). Per Augustsson for perfecting the art of beard-scratching. Christian Antfolk for interesting discussions on Premier League football. Josefin Starkhammar for general stubbornness, supporting the cookie empire and finishing up cakes, and everyone else I have forgotten.

A special acknowledgement goes to the Blizzard gamers at Elmät. Especially “the whistling warmonger”, “the back stabbing bastard” and “the silent but deadly Queen of the dead” - you know who you are. A battle with colleagues is an amazing way of letting out frustration, even though you sometimes end up more frustrated than you were before you started playing.

I would also like to thank the people at ErySave AB, the company of which I worked half time for three years of my time as a PhD-student. Special thanks to my everyday colleagues Filip Petersson, Thomas Hertz, Karin Arvidsson, Jesper Sjögren and Axel Roos. Without your good spirits the work would have been so much harder. Although the job was very challenging and I learned very much, it is my experience that working part time and do research as a Ph.D-student is a difficult combination. The time spent and the time needed is an equation which really does not add up.

Finally I would like to thank all of my families, and especially my lovely wife Tina. Life would be so much duller and less exciting without you.

10 REFERENCES

1. Feynman, R.P., *There's plenty of room at the bottom (data storage).* Microelectromechanical Systems, Journal of, 1992. **1**(1): p. 60-66.
2. Manz, A., N. Graber, and H.M. Widmer, *Miniaturized total chemical analysis systems: A novel concept for chemical sensing.* Sensors & Actuators: B. Chemical, 1990. **1**(1-6): p. 244-248.
3. Whitesides, G.M., *The origins and the future of microfluidics.* Nature, 2006. **442**(7101): p. 368-373.
4. Kundt, A. and O. Lehmann, *Longitudinal vibrations and acoustic figures in cylindrical columns of liquids.* Annalen der Physik und Chemie, 1874. **153**: p. 1.
5. Petersen, K.E., *Silicon as a mechanical material.* Proceedings of the IEEE, 1982. **70**(5): p. 420-457.
6. Sze, S.M., *Semiconductor Devices, Physics and Technology*. 1985, New York: John Wiley & Sons.
7. Williams, K.R. and R.S. Muller, *Etch rates for micromachining processing.* Journal of Microelectromechanical Systems, 1996. **5**(4): p. 256-269.
8. Williams, K.R., K. Gupta, and M. Wasilik, *Etch rates for micromachining processing - Part II.* Journal of Microelectromechanical Systems, 2003. **12**(6): p. 761-778.
9. Elwenspoek, M. and H.V. Jansen, *Silicon Micromachining*. 1998, Cambridge: Cambridge University Press.
10. Squires, T.M. and S.R. Quake, *Microfluidics: Fluid physics at the nanoliter scale.* Reviews of Modern Physics, 2005. **77**(3): p. 977-1026.
11. Weibel, D.B. and G.M. Whitesides, *Applications of microfluidics in chemical biology.* Current Opinion in Chemical Biology, 2006. **10**(6): p. 584-591.
12. Grover, W.H., et al., *Monolithic membrane valves and diaphragm pumps for practical large-scale integration into glass microfluidic devices.* Sensors and Actuators B-Chemical, 2003. **89**(3): p. 315-323.
13. Unger, M.A., et al., *Monolithic microfabricated valves and pumps by multilayer soft lithography.* Science, 2000. **288**(5463): p. 113-116.
14. Bessoth, F.G., A.J. deMello, and A. Manz, *Microstructure for efficient continuous flow mixing.* Analytical Communications, 1999. **36**(6): p. 213-215.
15. Elwenspoek, M., et al., *Towards integrated microliquid handling systems.* Journal of Micromechanics and Microengineering, 1994. **4**(4): p. 227-245.
16. Laser, D.J. and J.G. Santiago, *A review of micropumps.* Journal of Micromechanics and Microengineering, 2004. **14**(6): p. R35-R64.
17. Janasek, D., J. Franzke, and A. Manz, *Scaling and the design of miniaturized chemical-analysis systems.* Nature, 2006. **442**(7101): p. 374-380.
18. Nguyen, N.-T. and S.T. Wereley, *Fundamentals and applications of Microfluidics*. Microelectromechanical system series. 2002, Norwood, MA: Artech House, Inc.

19. Einstein, A., *Investigations on the Theory of the Brownian Movements*. 1956, New York: Dover Publications.
20. Tabeling, P., *Introduction to Microfluidics*. 2005: Oxford University Press.
21. White, F.M., *Fluid Mechanics*. 4th ed. 1999, Singapore: McGraw-Hill Book Co.
22. Leighton, T.G., *What is ultrasound?* Progress in Biophysics & Molecular Biology, 2007. **93**(1-3): p. 3-83.
23. King, L.V., *On the acoustic radiation pressure on spheres.* Proc. Roy. Soc. Lond., 1934. **A147**: p. 212–240.
24. Yosioka, K. and Y. Kawasima, *Acoustic radiation pressure on a compressible sphere.* Acustica, 1955. **5**: p. 167-173.
25. Nyborg, W.L., *Radiation Pressure on a Small Rigid Sphere.* Journal of the Acoustical Society of America, 1967. **42**(5): p. 947-952.
26. Haar, G.T. and S.J. Wyard, *Blood cell banding in ultrasonic standing wave fields: A physical analysis.* Ultrasound in Medicine and Biology, 1978. **4**: p. 111-123.
27. Laurell, T., F. Petersson, and A. Nilsson, *Chip integrated strategies for acoustic separation and manipulation of cells and particles.* Chemical Society Reviews, 2007. **36**(3): p. 492-506.
28. Gorkov, L.P., *On the forces acting on a small particle in an acoustic field in an ideal fluid.* Sov. Phys. Doklady, 1962. **6**(9): p. 773-775.
29. Coakley, W.T., *Ultrasonic separations in analytical biotechnology.* Trends in Biotechnology, 1997. **15**(12): p. 506-511.
30. Petersson, F., et al., *Separation of lipids from blood utilizing ultrasonic standing waves in microfluidic channels.* Analyst, 2004. **129**(10): p. 938-943.
31. Woodside, S.M., B.D. Bowen, and J.M. Piret, *Measurement of ultrasonic forces for particle-liquid separations.* Aiche Journal, 1997. **43**(7): p. 1727-1736.
32. Bjerknes, V.F.K., *Die Kraftfelder*. 1909, Vieweg und Sohn: Braunschweig, Germany.
33. Weiser, M.A.H., R.E. Apfel, and E.A. Neppiras, *Interparticle Forces on Red-Cells in a Standing Wave Field.* Acustica, 1984. **56**(2): p. 114-119.
34. Crum, L.A., *Acoustic Force on a Liquid Droplet in an Acoustic Stationary Wave.* Journal of the Acoustical Society of America, 1971. **50**(1): p. 157-&.
35. Groschl, M., *Ultrasonic separation of suspended particles - Part I: Fundamentals.* Acustica, 1998. **84**(3): p. 432-447.
36. Spengler, J.F., W.T. Coakley, and K.T. Christensen, *Microstreaming effects on particle concentration in an ultrasonic standing wave.* Aiche Journal, 2003. **49**(11): p. 2773-2782.
37. Hertz, T.G., *Applications of Acoustic Streaming*, in *Dept. of Electrical Measurements*. 1993, Lund University: Lund.
38. Eckart, C., *Vortices and streams caused by sound waves.* Physical Review, 1948. **73**(1): p. 68-76.
39. Kuznetsova, L.A., S.P. Martin, and W.T. Coakley, *Sub-micron particle behaviour and capture at an immuno-sensor surface in an ultrasonic standing wave.* Biosensors & Bioelectronics, 2005. **21**(6): p. 940-948.

40. Hagsater, S.M., et al., *Acoustic resonances in straight micro channels: Beyond the 1D-approximation.* Lab on a Chip, 2008. **8**(7): p. 1178-1184.
41. Bengtsson, M. and T. Laurell, *Ultrasonic agitation in microchannels.* Analytical and Bioanalytical Chemistry, 2004. **378**(7): p. 1716-1721.
42. Liu, R.H., et al., *Hybridization enhancement using cavitation microstreaming.* Analytical Chemistry, 2003. **75**(8): p. 1911-1917.
43. Augustsson, P., et al., *Decomplexing biofluids using microchip based acoustophoresis.* Lab on a Chip, 2009.
44. Wiklund, M., et al., *Ultrasonic standing wave manipulation technology integrated into a dielectrophoretic chip.* Lab on a Chip, 2006. **6**(12): p. 1537-1544.
45. Manneberg, O., et al., *Wedge transducer design for two-dimensional ultrasonic manipulation in a microfluidic chip.* Journal of Micromechanics and Microengineering, 2008. **18**(9).
46. Evander, M., et al., *Acoustophoresis in wet-etched glass chips.* Analytical Chemistry, 2008. **80**(13): p. 5178-5185.
47. Abgrall, P., et al., *SU-8 as a structural material for labs-on-chips and microelectromechanical systems.* Electrophoresis, 2007. **28**(24): p. 4539-4551.
48. Duffy, D.C., et al., *Rapid prototyping of microfluidic systems in poly(dimethylsiloxane).* Analytical Chemistry, 1998. **70**(23): p. 4974-4984.
49. Whitesides, G.M., et al., *Soft lithography in biology and biochemistry.* Annual Review of Biomedical Engineering, 2001. **3**: p. 335-373.
50. Shoh, A., *Welding of thermoplastics by ultrasound.* Ultrasonics, 1976. **14**(5): p. 209-217.
51. Kapishnikov, S., V. Kantsler, and V. Steinberg, *Continuous particle size separation and size sorting using ultrasound in a microchannel.* Journal of Statistical Mechanics-Theory and Experiment, 2006.
52. Hawkes, J.J., et al. *Positioning particles within liquids using ultrasound force fields*. in *Proc. Forum Acusticum 2002 Sevilla*. 2002. Sevilla, Spain.
53. Hill, M., Y.J. Shen, and J.J. Hawkes, *Modelling of layered resonators for ultrasonic separation.* Ultrasonics, 2002. **40**(1-8): p. 385-392.
54. Hagsater, S.M., et al., *Acoustic resonances in microfluidic chips: full-image micro-PIV experiments and numerical simulations.* Lab on a Chip, 2007. **7**(10): p. 1336-1344.
55. Greenspan, M. and C.E. Tschiegg, *Tables of the speed of sound in water.* Journal of the Acoustical Society of America, 1959. **31**(1): p. 75-76.
56. Svennebring, J., O. Manneberg, and M. Wiklund, *Temperature regulation during ultrasonic manipulation for long-term cell handling in a microfluidic chip.* Journal of Micromechanics and Microengineering, 2007. **17**(12): p. 2469-2474.
57. Ryll, T., et al., *Performance of small-scale CHO perfusion cultures using an acoustic cell filtration device for cell retention: Characterization of separation efficiency and impact of perfusion on product quality.* Biotechnology and Bioengineering, 2000. **69**(4): p. 440-449.

58. Wang, Z., et al., *Retention and Viability Characteristics of Mammalian Cells in an Acoustically Driven Polymer Mesh.* Biotechnology progress, 2004. **20**(1): p. 384-387.
59. Hultstrom, J., et al., *Proliferation and viability of adherent cells manipulated by standing-wave ultrasound in a microfluidic chip.* Ultrasound in Medicine and Biology, 2007. **33**(1): p. 145-151.
60. Evander, M., et al., *Noninvasive acoustic cell trapping in a microfluidic perfusion system for online bioassays.* Analytical Chemistry, 2007. **79**(7): p. 2984-2991.
61. Bazou, D., L.A. Kuznetsova, and W.T. Coakley, *Physical enviroment of 2-D animal cell aggregates formed in a short pathlength ultrasound standing wave trap.* Ultrasound in Medicine & Biology, 2005. **31**: p. 423-430.
62. Fiedler, S., et al., *Dielectrophoretic sorting of particles and cells in a microsystem.* Analytical Chemistry, 1998. **70**(9): p. 1909-1915.
63. Muller, T., et al., *A 3-D microelectrode system for handling and caging single cells and particles.* Biosensors & Bioelectronics, 1999. **14**(3): p. 247-256.
64. Taff, B.M. and J. Voldman, *A Scalable Addressable Positive-Dielectrophoretic Cell-Sorting Array.* Analytical Chemistry, 2005. **77**(24): p. 7976-7983.
65. Garces-Chavez, V., et al., *Simultaneous micromanipulation in multiple planes using a self-reconstructing light beam.* Nature, 2002. **419**(6903): p. 145-147.
66. Funatsu, T., et al., *Imaging of single fluorescent molecules and individual ATP turnovers by single myosin molecules in aqueous-solution.* Nature, 1995. **374**(6522): p. 555-559.
67. Kulrattanarak, T., et al., *Classification and evaluation of microfluidic devices for continuous suspension fractionation.* Advances in Colloid and Interface Science, 2008. **142**(1-2): p. 53-66.
68. Pamme, N., *Continuous flow separations in microfluidic devices.* Lab on a Chip, 2007. **7**(12): p. 1644-1659.
69. Chou, C.F., et al., *Sorting biomolecules with microdevices.* Electrophoresis, 2000. **21**(1): p. 81-90.
70. Tegenfeldt, J.O., et al., *Micro- and nanofluidics for DNA analysis.* Analytical and Bioanalytical Chemistry, 2004. **378**(7): p. 1678-1692.
71. Pamme, N., *Magnetism and microfluidics.* Lab on a Chip, 2006. **6**(1): p. 24-38.
72. Gijs, M.A.M., *Magnetic bead handling on-chip: new opportunities for analytical applications.* Microfluidics and Nanofluidics, 2004. **1**(1): p. 22-40.
73. Bu, M.Q., et al., *Characterization of a microfluidic magnetic bead separator for high-throughput applications.* Sensors and Actuators a-Physical, 2008. **145**: p. 430-436.
74. Pamme, N. and A. Manz, *On-chip free-flow magnetophoresis: Continuous flow separation of magnetic particles and agglomerates.* Analytical Chemistry, 2004. **76**(24): p. 7250-7256.

75. Peyman, S.A., A. Iles, and N. Pamme, *Rapid on-chip multi-step (bio)chemical procedures in continuous flow - manoeuvring particles through co-laminar reagent streams.* Chemical Communications, 2008(10): p. 1220-1222.
76. Pankhurst, Q.A., et al., *Applications of magnetic nanoparticles in biomedicine.* Journal of Physics D-Applied Physics, 2003. **36**(13): p. R167-R181.
77. Furlani, E.P., *Magnetophoretic separation of blood cells at the microscale.* Journal of Physics D-Applied Physics, 2007. **40**(5): p. 1313-1319.
78. Han, K.H. and A.B. Frazier, *Continuous magnetophoretic separation of blood cells in microdevice format.* Journal of Applied Physics, 2004. **96**(10): p. 5797-5802.
79. Pohl, H.A., *The motion and precipitation of suspensoids in divergent electric fields.* Journal of Applied Physics, 1951. **22**(7): p. 869-871.
80. Gascoyne, P.R.C. and J. Vykoukal, *Particle separation by dielectrophoresis.* Electrophoresis, 2002. **23**(13): p. 1973-1983.
81. Gonzalez, C.F. and V.T. Remcho, *Harnessing dielectric forces for separations of cells, fine particles and macromolecules.* Journal of Chromatography A, 2005. **1079**(1-2): p. 59-68.
82. Cummings, E.B. and A.K. Singh, *Dielectrophoresis in microchips containing arrays of insulating posts: Theoretical and experimental results.* Analytical Chemistry, 2003. **75**(18): p. 4724-4731.
83. Barrett, L.M., et al., *Dielectrophoretic manipulation of particles and cells using insulating ridges in faceted prism microchannels.* Analytical Chemistry, 2005. **77**(21): p. 6798-6804.
84. Huang, Y., et al., *Electric Manipulation of Bioparticles and Macromolecules on Microfabricated Electrodes.* Analytical Chemistry, 2001. **73**(7): p. 1549-1559.
85. Doh, I. and Y.H. Cho, *A continuous cell separation chip using hydrodynamic dielectrophoresis (DEP) process.* Sensors and Actuators a-Physical, 2005. **121**(1): p. 59-65.
86. Tornay, R.L., et al., *Dielectrophoresis-based particle exchanger for the manipulation and surface functionalization of particles.* Lab on a Chip, 2008. **8**(2): p. 267-273.
87. Gadish, N. and J. Voldman, *High-throughput positive-dielectrophoretic bioparticle microconcentrator.* Analytical Chemistry, 2006. **78**(22): p. 7870-7876.
88. Suehiro, J. and R. Pethig, *The dielectrophoretic movement and positioning of a biological cell using a three-dimensional grid electrode system.* Journal of Physics D-Applied Physics, 1998. **31**(22): p. 3298-3305.
89. Yamada, M., M. Nakashima, and M. Seki, *Pinched flow fractionation: Continuous size separation of particles utilizing a laminar flow profile in a pinched microchannel.* Analytical Chemistry, 2004. **76**(18): p. 5465-5471.
90. Takagi, J., et al., *Continuous particle separation in a microchannel having asymmetrically arranged multiple branches.* Lab on a Chip, 2005. **5**(7): p. 778-784.

91. Zhang, X.L., et al., *Continuous flow separation of particles within an asymmetric microfluidic device.* Lab on a Chip, 2006. **6**(4): p. 561-566.
92. Sai, Y., et al., *Continuous separation of particles using a microfluidic device equipped with flow rate control valves.* Journal of Chromatography A, 2006. **1127**(1-2): p. 214-220.
93. Kawamata, T., et al., *Continuous and precise particle separation by electroosmotic flow control in microfluidic devices.* Electrophoresis, 2008. **29**(7): p. 1423-1430.
94. Crowley, T.A. and V. Pizziconi, *Isolation of plasma from whole blood using planar microfilters for lab-on-a-chip applications.* Lab on a Chip, 2005. **5**(9): p. 922-929.
95. VanDelinder, V. and A. Groisman, *Separation of plasma from whole human blood in a continuous cross-flow in a molded microfluidic device.* Analytical Chemistry, 2006. **78**(11): p. 3765-3771.
96. Yamada, M. and M. Seki, *Hydrodynamic filtration for on-chip particle concentration and classification utilizing microfluidics.* Lab on a Chip, 2005. **5**(11): p. 1233-1239.
97. Yamada, M. and M. Seki, *Microfluidic particle sorter employing flow splitting and recombining.* Analytical Chemistry, 2006. **78**(4): p. 1357-1362.
98. Jaggi, R.D., R. Sandoz, and C.S. Effenhauser, *Microfluidic depletion of red blood cells from whole blood in high-aspect-ratio microchannels.* Microfluidics and Nanofluidics, 2007. **3**(1): p. 47-53.
99. Yang, S., A. Undar, and J.D. Zahn, *A microfluidic device for continuous, real time blood plasma separation.* Lab on a Chip, 2006. **6**(7): p. 871-880.
100. Giddings, J.C., *Field-Flow Fractionation - Analysis of Macromolecular, Colloidal, and Particulate Materials.* Science, 1993. **260**(5113): p. 1456-1465.
101. Reschiglian, P., et al., *Field-flow fractionation and biotechnology.* Trends in Biotechnology, 2005. **23**(9): p. 475-483.
102. Giddings, J.C., *Unified Separation Science*. 1991, New York: John Wiley & Sons, Inc.
103. Huang, L.R., et al., *Continuous particle separation through deterministic lateral displacement.* Science, 2004. **304**(5673): p. 987-990.
104. Inglis, D.W., et al., *Critical particle size for fractionation by deterministic lateral displacement.* Lab on a Chip, 2006. **6**(5): p. 655-658.
105. Morton, K.J., et al., *Hydrodynamic metamaterials: Microfabricated arrays to steer, refract, and focus streams of biomaterials.* Proceedings of the National Academy of Sciences of the United States of America, 2008. **105**(21): p. 7434-7438.
106. Morton, K.J., et al., *Crossing microfluidic streamlines to lyse, label and wash cells.* Lab on a Chip, 2008. **8**(9): p. 1448-1453.
107. Duke, T.A.J. and R.H. Austin, *Microfabricated sieve for the continuous sorting of macromolecules.* Physical Review Letters, 1998. **80**(7): p. 1552-1555.
108. Huang, L.R., et al., *Role of molecular size in ratchet fractionation.* Physical Review Letters, 2002. **89**(17).

109. Chou, C.F., et al., *Sorting by diffusion: An asymmetric obstacle course for continuous molecular separation.* Proceedings of the National Academy of Sciences of the United States of America, 1999. **96**(24): p. 13762-13765.
110. Cabodi, M., et al., *Continuous separation of biomolecules by the laterally asymmetric diffusion array with out-of-plane sample injection.* Electrophoresis, 2002. **23**(20): p. 3496-3503.
111. Matthias, S. and F. Muller, *Asymmetric pores in a silicon membrane acting as massively parallel brownian ratchets.* Nature, 2003. **424**(6944): p. 53-57.
112. Ashkin, A., *Acceleration and trapping of particles by radiation pressure.* Physical Review Letters, 1970. **24**(4): p. 156-&.
113. Molloy, J.E. and M.J. Padgett, *Lights, action: optical tweezers.* Contemporary Physics, 2002. **43**(4): p. 241-258.
114. MacDonald, M.P., G.C. Spalding, and K. Dholakia, *Microfluidic sorting in an optical lattice.* Nature, 2003. **426**(6965): p. 421-424.
115. Ashkin, A. and J.M. Dziedzic, *Optical Trapping and Manipulation of Viruses and Bacteria.* Science, 1987. **3-235**(4795): p. 1517-1520.
116. Perroud, T.D., et al., *Microfluidic-based cell sorting of Francisella tularensis infected macrophages using optical forces.* Analytical Chemistry, 2008. **80**(16): p. 6365-6372.
117. Ladavac, K., K. Kasza, and D.G. Grier, *Sorting mesoscopic objects with periodic potential landscapes: Optical fractionation.* Physical Review E, 2004. **70**(1).
118. Baker, N.V., *Segregation and sedimentation of red blood-cells in ultrasonic standing waves.* Nature, 1972. **239**(5372): p. 398-&.
119. Peterson, S., G. Perkins, and C. Baker. *Development of an ultrasonic blood separator*. in *IEEE/Eighth Annual Conference of the Engineering in Medicine and Biology Society*. 1986.
120. Trampler, F., et al., *Acoustic Cell Filter for High-Density Perfusion Culture of Hybridoma Cells.* Bio-Technology, 1994. **12**(3): p. 281-284.
121. Pui, P.W.S., et al., *Batch and semicontinuous aggregation and sedimentatin of hybridoma cells by acoustic-resonance fields.* Biotechnology progress, 1995. **11**: p. 146-152.
122. Groschl, M., et al., *Ultrasonic separation of suspended particles - Part III: Application in biotechnology.* Acustica, 1998. **84**(5): p. 815-822.
123. Hawkes, J.J. and W.T. Coakley, *A continuous flow ultrasonic cell-filtering method.* Enzyme and Microbial Technology, 1996. **19**(1): p. 57-62.
124. Whitworth, G., M.A. Grundy, and W.T. Coakley, *Transport and harvesting of suspended particles using modulated ultrasound.* Ultrasonics, 1991. **29**(6): p. 439-444.
125. Cousins, C.M., et al., *Plasma preparation from whole blood using ultrasound.* Ultrasound in Medicine and Biology, 2000. **26**(5): p. 881-888.
126. Gupta, S. and D.L. Feke, *Acoustically driven collection of suspended particles within porous media.* Ultrasonics, 1997. **35**(2): p. 131-139.
127. Gupta, S. and D.L. Feke, *Filtration of particulate suspensions in acoustically driven porous media.* Aiche Journal, 1998. **44**(5): p. 1005-1014.
128. Benes, E., et al., *Ultrasonic separation of suspended particles.* Ultrasonics Symposium, 2001 IEEE, 2001. **1**: p. 649-659 vol.1.

129. Bohm, H., et al., *Quantification of a novel h-shaped ultrasonic resonator for separation of biomaterials under terrestrial gravity and microgravity conditions.* Biotechnology and Bioengineering, 2003. **82**(1): p. 74-85.
130. Yasuda, K., S. Umemura, and K. Takeda, *Concentration and Fractionation of Small Particles in Liquid by Ultrasound.* Japanese Journal of Applied Physics Part 1-Regular Papers Short Notes & Review Papers, 1995. **34**(5B): p. 2715-2720.
131. Higashitani, K., M. Fukushima, and Y. Matsuno, *Migration of suspended particles in plane stationary ultrasonic field.* Chemical Engineering Science, 1981. **36**(12): p. 1877-1882.
132. Hawkes, J.J. and W.T. Coakley, *Force field particle filter, combining ultrasound standing waves and laminar flow.* Sensors and Actuators B: Chemical, 2001. **75**(3): p. 213-222.
133. Harris, N.R., et al., *A silicon microfluidic ultrasonic separator.* Sensors and Actuators B: Chemical, 2003. **95**(1-3): p. 425-434.
134. Nilsson, A., et al., *Acoustic control of suspended particles in micro fluidic chips.* Lab on a Chip, 2004. **4**(2): p. 131-135.
135. Eyjolfsson, A., et al., *Characterization of lipid particles in shed mediastinal blood.* Annals of Thoracic Surgery, 2008. **85**(3): p. 978-981.
136. Bronden, B., et al., *Differential distribution of lipid microemboli after cardiac surgery.* Annals of Thoracic Surgery, 2006. **81**(2): p. 643-649.
137. Moody, D.M., et al., *Brain Microemboli Associated With Cardiopulmonary Bypass: A Histologic and Magnetic Resonance Imaging Study.* The Annals of Thoracic Surgery, 1995. **59**(5): p. 1304-1307.
138. Mahanna, E.P., et al., *Defining neuropsychological dysfunction after coronary artery bypass grafting.* The Annals of Thoracic Surgery, 1996. **61**(5): p. 1342-1347.
139. Jonsson, H., et al., *Particle separation using ultrasound can radically reduce embolic load to brain after cardiac surgery.* Annals of Thoracic Surgery, 2004. **78**(5): p. 1572-1578.
140. *Guide to the preparation, use and quality assurance of blood components*. 1996, Council of Europe Publishing: Strasbourg.
141. Petersson, F., et al., *Carrier medium exchange through ultrasonic particle switching in microfluidic channels.* Analytical Chemistry, 2005. **77**(5): p. 1216-1221.
142. Hawkes, J.J., et al., *Continuous cell washing and mixing driven by an ultrasound standing wave within a microfluidic channel.* Lab on a Chip, 2004. **4**(5): p. 446-452.
143. Rudmann, S.V., *Textbook of Blood Banking and Transfusion Medicine*. Second ed. 2005, Philadelphia, PA, USA: Elsevier Saunders.
144. Persson, J., et al., *Acoustic microfluidic chip technology to facilitate automation of phage display selection.* Febs Journal, 2008. **275**(22): p. 5657-5666.
145. Augustsson, P., et al., *Buffer medium exchange in continuous cell and particle streams using ultrasonic standing wave focusing.* Microchimica Acta, 2009.

146. Augustsson, P., T. Laurell, and S. Ekström. *Flow-through chip for sequential treatment and analyte elution from beads or cells*. in *Micro Total Analysis Systems 2008*. 2008. San Diego, CA, USA.
147. Semyonov, S.N. and K.I. Maslow, *Acoustic Field-Flow Fractionation.* Journal of Chromatography, 1988. **446**: p. 151-156.
148. Petersson, F., et al., *Free flow acoustophoresis: Microfluidic-based mode of particle and cell separation.* Analytical Chemistry, 2007. **79**(14): p. 5117-5123.
149. Siversson, C., et al. *Acoustic particle sizing in microchannels by means of ultrasonic frequency switching*. in *8th International Conference on Miniaturized Systems for Chemistry and Life Sciences*. 2004. Malmo, SWEDEN.
150. Sundin, M., et al. *Binary valving of particles using acoustic forces*. in *8th International Conference on Miniaturized Systems for Chemistry and Life Sciences*. 2004. Malmo, SWEDEN.
151. Grenvall, C., et al. *Fluorescent activated cell sorter using ultrasound standing waves in micro channels*. in *Micro Total Analysis Systems 2007*. 2007. Paris, France.
152. Lilliehorn, T., et al., *Trapping of microparticles in the near field of an ultrasonic transducer.* Ultrasonics, 2005. **43**(5): p. 293-304.
153. Lilliehorn, T., et al., *Dynamic arraying of microbeads for bioassays in microfluidic channels.* Sensors and Actuators B: Chemical, 2005. **106**(2): p. 851-858.
154. Evander, M., et al. *Acoustic Differential Extraction to enhance analysis of sexual assualt evidence on a valveless glass microdevice*. in *10th International Conference on Miniaturized Systems for Chemistry and Life Sciences*. 2006. Tokyo, Japan.
155. Manneberg, O., et al., *A three-dimensional ultrasonic cage for characterization of individual cells.* Applied Physics Letters, 2008. **93**(6).
156. Dailey, J.F., *Dailey's Notes on Blood*. Fourth ed. 2002, Arlington, MA, USA: Medical Consulting Group.
157. Eales, L.-J., *Immunology for life scientists*. 1997, Chichester, UK: John Wiley & Sons, Ltd.
158. Jacobson, B., *Medicin och Teknik*. Fourth ed. 1995, Lund, Sweden: Studentlitteratur.

I

PAPER

www.rsc.org/loc

Acoustic control of suspended particles in micro fluidic chips

Andreas Nilsson,[a] Filip Petersson,[a] Henrik Jönsson[b] and Thomas Laurell[a]

[a] *Department of Electrical Measurements, Lund Institute of Technology, P.O. Box 118, S-222 10 Lund, Sweden*

[b] *Department of Cardiothoracic Surgery, Lund University Hospital, Lund, Sweden*

Received 24th October 2003, Accepted 11th December 2003
First published as an Advance Article on the web 9th February 2004

A method to separate suspended particles from their medium in a continuous mode at microchip level is described. The method combines an ultrasonic standing wave field with the extreme laminar flow properties obtained in a silicon micro channel. The channel was 750 μm wide and 250 μm deep with vertical side walls defined by anisotropic wet etching. The suspension comprised "Orgasol 5μm" polyamide spheres and distilled water. The channel was perfused by applying an under pressure (suction) to the outlets. The channel was ultrasonically actuated from the back side of the chip by a piezoceramic plate. When operating the acoustic separator at the fundamental resonance frequency the acoustic forces were not strong enough to focus the particles into a well defined single band in the centre of the channel. The frequency was therefore changed to about 2 MHz, the first harmonic with two pressure nodes in the standing wave, and consequently two lines of particles were formed which were collected *via* the side outlets. Two different microchip separator designs were investigated with exit channels branching off from the separation channel at angles of 90° and 45° respectively. The 45° separator displayed the most optimal fluid dynamic properties and 90% of the particles were gathered in 2/3 of the original fluid volume.

1 Introduction

Several particle separation techniques utilizing ultrasound have previously been presented.[1–8] These are based on the fact that suspended particles exposed to an ultrasonic standing wave field are affected by an acoustic radiation force. This force will move the particles towards either the pressure nodes or the pressure anti-nodes depending on the density and compressibility of the particles and the medium. In order to realise these systems conventional precision engineering has been utilized to create well defined flow-through acoustic resonance cavities in which particles can be manipulated under controlled conditions. To obtain good particle aggregation in such cavities the sidewalls reflecting the acoustic wave must have a low surface roughness and the wall spacing must be constant throughout the separation region. The separation method presented herein is based on the same principle but proposes a different orientation of the piezoceramic actuator. Also, most importantly, modern micro fabrication technologies were utilized in order to address the issue of tedious manufacturing using traditional machining techniques to realise the micro fluidic system. The anisotropic wet etching properties of silicon ensure a perfect alignment of the reflecting walls in the channel. As in all micro fabrication the production of such particle separation structures also benefits from batch fabrication. The particle suspension is fed into a separation channel where it is exposed to an acoustic standing wave field induced by a piezoceramic plate glued to the back side of the silicon structure. The ultrasound frequency is tuned to match one half of the wavelength to the channel width. This results in a pressure nodal plane along the middle of the channel and one pressure anti-nodal plane along each channel side wall. If the density and compressibility of the particles are suitable, compared to the medium, they will move towards the nodal plane while travelling along the separation channel. The end of the channel is split into three outlets and when operating the system in the first harmonic resonance mode ($2*\lambda/2$) the particles are focused in two pressure nodes leaving the separation channel through the side outlets and a particle free clear medium thus exits through the centre outlet.

2 Theory

2.1 Acoustic force

An acoustic standing wave is commonly described according to eqn. (1).

$$y = A \cdot \cos\left(\frac{2\pi x}{\lambda} + \frac{\phi}{2}\right) \cdot \sin\left(\frac{2\pi t}{T} + \frac{\phi}{2}\right) \quad (1)$$

Eqn. (1) expresses the displacement (y) of a point in the standing wave corresponding to a certain position (x) and time (t). The displacement is also dependent of the amplitude of the standing wave (A), the wavelength (λ), the time for one full period (T) and the phase difference between the two travelling waves (ϕ). By looking at the cosine part of the equation it becomes evident that the distance between two consecutive nodes is $\lambda/2$.

If particles in a liquid are subjected to an ultrasonic field they experience pressure fluctuations. These fluctuations arise from the displacement of the molecules of the medium. If the acoustic field is in the form of a standing wave, eqn. (1) can be rewritten in terms of pressure [eqn. (2)].

$$p = p_0 \cdot \sin(kx) \cdot \cos(\omega t) \quad (2)$$

The constants $k = (2\pi/\lambda)$ and $\omega = (2\pi/T)$ have been introduced and the phase difference has been omitted since it only results in a lateral displacement of the wave. Sonic acoustic waves in a liquid are longitudinal which means that the particles are displaced along the wave. This results in compression and decompression of the particles in the medium. At the pressure nodes the molecular displacement is at its maximum and at the pressure anti-nodes at its minimum. The pressure fluctuations result in forces that act laterally on the particles in the x-direction. According to the acoustic force theory presented by Yosioka and Kawasima[9] the force on a particle can be expressed in the following way [eqn. (3)].

$$F_r = -\left(\frac{\pi p_0^2 V_c \beta_w}{2\lambda}\right) \cdot \phi(\beta, \rho) \cdot \sin(2kx) \quad (3)$$

DOI: 10.1039/b313493h

$$\phi = \frac{5\rho_c - 2\rho_w}{2\rho_c + \rho_w} - \frac{\beta_c}{\beta_w} \quad (4)$$

V_c is the volume of the particle, p_0 is the pressure amplitude from eqn. (2) and ϕ is defined by eqn. (4). The density of the medium and particles are denoted ρ_w and ρ_c respectively and the corresponding compressibilities β_w and β_c.

Small particles can generally be trapped in an acoustic standing wave. The first criterion is that the particle diameter must be less than half the wavelength, otherwise the acoustic force will act in more than one direction on the particle. The second criterion is that ϕ must not equal zero, otherwise there will be no net force exerted on the particle.

3 Materials and methods

3.1 Micro fabrication

In order for the acoustic separator to work, precise channel structures with vertical walls and good reflective properties are required. Silicon fits these requirements very well. By using photolithography and anisotropic wet etching it is simple to produce structures of rectangular cross-section using <100> silicon. If a cross-type structure with vertical channel walls is desired, the separation channels on the photo mask are turned 45° in relation to the primary flat of the wafer, (design I, Fig. 1). The separation structure will thereby obtain vertical walls in all flow channels. Optionally, the side channels can be anisotropically defined according to design II (Fig. 1). This separation structure will however get a V-groove cross-section of the side channels due to the slanted <111>-planes that define the stop etch conditions (Fig. 2). For clarity this design is henceforth denoted "45°-separation structure".

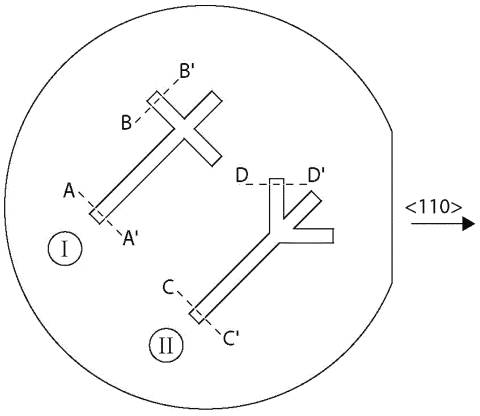

Fig. 1 Separation structures defined on a <100> silicon wafer. Design I – Cross-type separator; Design II – 45° separation structure.

Double sided photolithography and etching in KOH (potassium hydroxide, Merck KGaA, 64271 Darmstadt, Germany), 40 g in 100 ml deionised water, yielded micro channels with a depth and width of 250 μm and 750 μm respectively and inlets and outlets etched from the rear side. The micro separator was sealed with a glass lid by means of anodic bonding to achieve a closed separation structure with optical access (Fig. 3).

3.2 Device assembly

The ultrasonic standing waves were generated by PZ26 piezoelectric ceramics (Ferroperm Piezoceramics A/S, Kvistgard, Denmark) with resonance frequencies of 1 MHz and 2 MHz. To achieve an actuation with the highest energy transmission possible, the transducer was glued to the back side of the separation chip with epoxy (2 Ton Clear Epoxy, ITWDevcon, Danvers, MA, USA). The fact that it was glued to the rear side also provided air backing to the transducer, minimizing acoustic losses.

3.3 Experimental arrangement

Silicone rubber tubing was glued to the inlets and outlets on the back side of the separation chip, acting as docking ports to the syringe pump (WPI SP260P, World Precision Instruments, USA) *via* standard 1/16" od Teflon tubing. The particle suspension used was a Doppler fluid (Dansk Fantom Service, Gondolvej 25, 4040 Jyllinge, Denmark) that consisted of suspended Orgasol particles of 5 μm diameter mixed with distilled water. The piezoceramic element was operated *via* a high frequency power amplifier (Amplifier Research Model 50A15, Amplifier Research, Souderton, PA, USA). The frequency was set by a function generator (HP 3325A, Hewlett-Packard Inc, Palo Alto, CA, USA). After the separation step, particle content of the clear and the enriched fluid was measured by centrifugation using a Haematokrit 2010 (Hettich Zentrifugen, D-78532 Tuttlingen, Germany). Each sample was centrifuged for two minutes at 13000 rpm after which the length of the solid and fluid fraction in the capillaries was measured to determine the percentage solid in each collected volume, A and B. The separation efficiency was subsequently determined as the ratio of the percentage solid fraction in the side outlets from the chip (B)

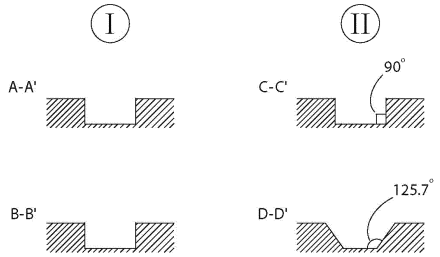

Fig. 2 Cross-sections of the two different designs: I) The cross-type separation structure and II) the 45°-separation structure.

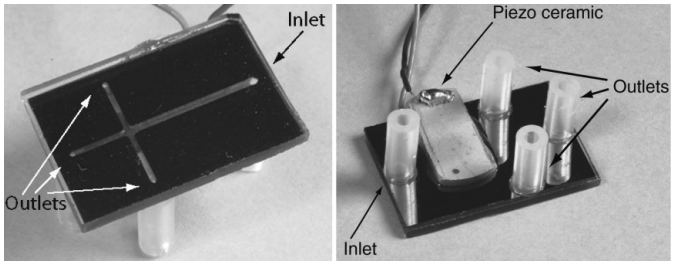

Fig. 3 Front and rear side of a cross-type separation chip.

to the percentage total solid fraction in the fluid colleted at all three outlets ($A + B$), eqn. (5).

$$\text{Separation efficiency} = 100*B/(A + B) \quad (5)$$

where:

A = relative particle fraction of the fluid collected from the centre outlet

B = relative particle fraction of the fluid collected from the side outlets

4 Results and discussion

4.1 Actuation

A benefit of arranging the actuator in plane with the separation chip is the large contact surface area for the piezoceramic actuator enabling a good coupling of the acoustic energy into the silicon chip. In spite of the fact that the actuator provides the acoustic signal from the back/bottom of the chip, the standing wave is obtained in plane with the silicon chip and orthogonal to the flow channel (Fig. 4) enabling continuous flow separation of particles.

4.2 Band formation

When particles are exposed to an acoustic force they will gather in the nodes or anti-nodes of the standing wave. Because of the laminar conditions in a small flow channel, particles once gathered in a defined lateral position will stay there even after leaving the acoustic force field, forming long bands of particles in the channel. When operating the separation channel in its fundamental resonance mode ($\lambda/2$) a single band formation was observed in the middle of the channel. However, the acoustic forces in the fundamental resonance mode were too weak to generate a well-defined particle band in the centre of the channel. The chips were therefore operated and the performance was investigated at the first harmonic ($2*\lambda/2$), where two bands were seen (Fig. 5 left). The higher operating frequency provided an improved particle focusing force as reasoned above, eqn. (3). There is also the possibility to generate multiple bands (Fig. 5 centre and right) in the separation channel at even higher harmonics.

4.3 Particle separator designs

Two different separators were designed and fabricated in silicon. Initially a cross-type design with the side outlet channels perpendicular to the inlet channel was made (Fig. 6a). The structure was 250 μm deep and the width and length of the inlet channel was 750 μm and 13 mm respectively. The cross-type design however displayed problems with stagnant zones as the fluid turned around the 90° corner into the side channels. Any air bubble or debris that entered the system was easily caught in the stagnant zone and was very hard to remove without disturbing the on-going separation. To solve that problem a new chip was designed, with the side channels leaving the separation channel at a 45° angle (Fig. 6b). In an attempt to make the separation structure even shorter, the inlet channel length was also reduced to 9 mm.

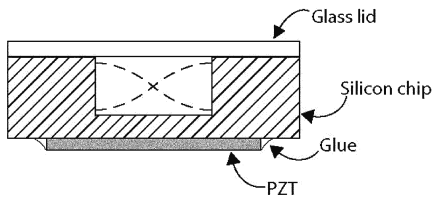

Fig. 4 A principal cross-section drawing of the assembled separation device, showing the separation channel with the piezoceramic element glued to the rear side of the microchip. The acoustic signal is tuned to fit the resonance criterion defined by the channel width, generating an acoustic standing wave (dashed) in plane with the silicon chip, orthogonal to the flow channel.

4.4 Results and discussion

The cross-type separator was operated in a two node mode ($2*\lambda/2$) with two bands and thus enriched particles were leaving *via* the side outlets as seen in Fig. 6. Studies of a varying operating voltage to the piezoceramic element (Fig. 7), at constant frequency of 1.956 MHz, constant flow of 0.3 ml min^{-1} and constant blood phantom concentration of 10%, show, as expected, that a higher separation efficiency was achieved with increasing voltage.

To operate the piezoceramic element at voltages exceeding 22 volts at a flow of 0.3 ml min^{-1} was not possible due to the fact that the high radiation forces trapped the particles in the ultrasonic field forming stationary particle clusters in the flow channel, which disturbed the laminar flow profile. High operating voltages will also cause an increase of temperature in the piezoceramic element, which may not exceed the Curie temperature of the ceramic since that will destroy the piezoelectric properties of the actuator.

The flow rate tests (Fig. 8) clearly show that lower flow rates provide a higher separation efficiency, which is the result of exposing the particles to the standing wave field for a longer time period, allowing more particles to reach their nodal position in the standing wave. The flow rate, voltage and the blood phantom concentration were maintained constant at 1.956 MHz, 15 Vpp (Voltage peak to peak) and 10% respectively. The voltage 15 Vpp was chosen since higher voltages in the lower flow rate range, below 0.1 ml min^{-1}, caused particle trapping/clustering and subsequent blocking of the flow channel.

Tests with different blood phantom concentrations (Fig. 9) showed, as expected, that the lower concentration yielded higher

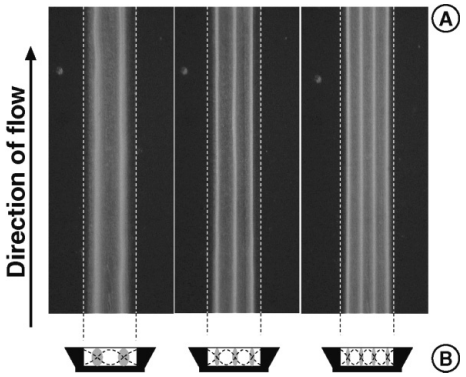

Fig. 5 Particle enrichment in the micro channel. The bands show the enriched particles in resonance mode, 1st, 2nd and 3rd harmonic with 2, 3 and 4 bands respectively, A) top view microscope photographs and B) principal separation channel cross-sections. Channel width: 750 μm, channel depth: 250 μm.

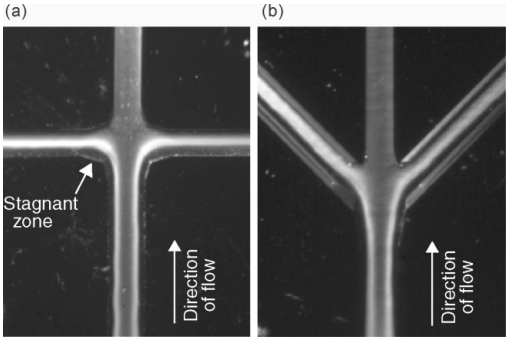

Fig. 6 a. Cross-type structure with a two band formation. b. 45°-structure with a two band formation.

separation efficiency. With increasing particle concentration, the side channels collecting the enriched particles will eventually be saturated, spilling over into the centre channel, which results in a decreased separation efficiency. As the blood phantom concentration increased, the separation efficiency decreased towards 67% (not shown), which would be the case when equal amounts of particles exit all outlets. This is also the case when no ultrasound is applied.

At its best, a separation efficiency of approximately 90% was achieved for the cross-type structure, *i.e.* almost 90% of the particles were collected through the side channels together with 2/3 of the fluid volume, at flow velocities less than 0.2 ml min^{-1}. The structure had however problems with stagnant zones as the fluid turned around the 90° corner. By changing the orientation of the side channels to 45° [Fig. 6b] the stagnant zones were reduced, and the separation process was improved.

Besides the change of the side channel angle for the 45°-structure, the inlet channel length was also shortened from 13 to 9 mm. In the investigation of the influence of the actuation voltage the 45°-structure showed approximately 10% higher separation efficiency at lower voltages (10 Vpp) as compared to the cross-structure; compare Fig. 7 and Fig. 10. At higher voltages both structures approached a separation efficiency close to 90%. It should be noted that the 45°-structure outperforms the cross-structure in spite of the fact that the separation channel was 4 mm shorter than the cross-structure.

The shorter separation channel resulted in a reduced retention time in the acoustic force field and thus the time for the particles to be focused were reduced by approximately 30%. A comparison of the separation efficiency of the two chip designs regarding the influence of flow rate (Fig. 8 and Fig. 11) and concentration of blood phantom (Fig. 9 and Fig. 12) respectively also disclosed that the 45°-structure performs better than the cross-structure. Much of the improved performance for the 45°-structure is attributed to the better flow profiles, avoiding rapid changes of the flow directions. This was also visually confirmed while performing the experiments. Commonly the cross-structure displayed a loss of particles from the focused bands into the centre outlet as the two bands turned around the 90° corner to its outlets. This was not as clearly seen for the 45°-structure. Both separator types displayed a maximum separation ratio of about 90% at extreme operating parameters.

In order to further optimise the proposed acoustic separation technology it would be preferable to move forward with a theoretical model describing the microfluidic and particle separation efficiency properties of the micro chip. The current state of

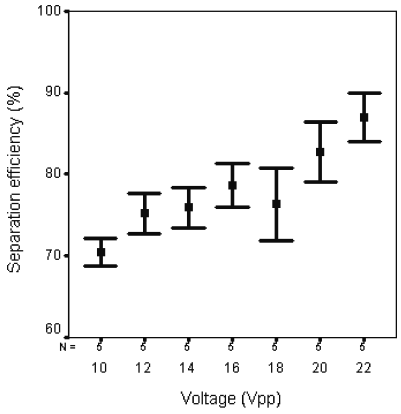

Fig. 7 Separation efficiency of a cross-type structure as a function of the excitation voltage to the piezoceramic element. Constant frequency of 1.956 MHz, a flow of 0.3 ml min^{-1} and 10% concentration of blood phantom were used.

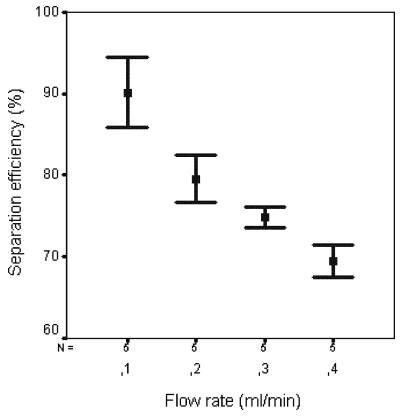

Fig. 8 Separation efficiency of a cross-type structure as a function of the flow. A constant frequency of 1.956 MHz, 15 Vpp, and 10% concentration of blood phantom was used.

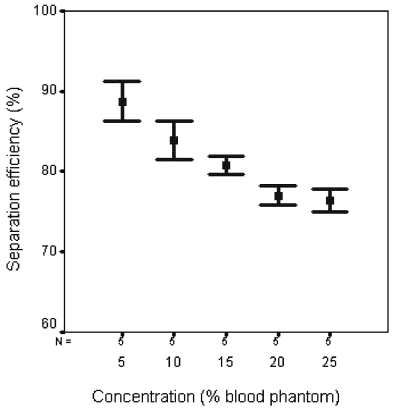

Fig. 9 Separation efficiency of a cross-type structure as a function of the concentration of the blood phantom. Constant frequency of 1.956 MHz, 20 Vpp and a flow of 0.3 ml min^{-1}.

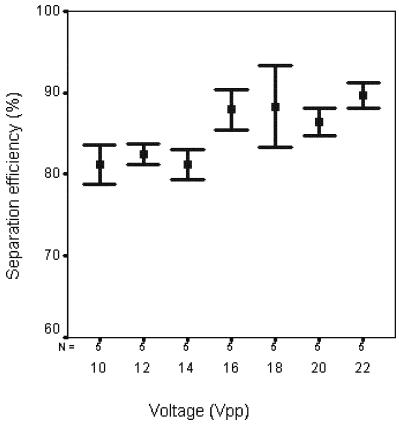

Fig. 10 Separation efficiency of a 45°-structure as a function of the excitation voltage to the piezoceramic element. A constant frequency of 1.970 MHz, a flow of 0.3 ml min^{-1} and 10% concentration of blood phantom was used.

modelling such a system still holds seemingly large deviations from experimental data. Hawkes and Coakley[1] have presented theoretical modelling of acoustic particle separation and compared these with experimental data demonstrating promising results. However, a further improvement of the model would be desired in order to predict the experimental outcome of a new separation device. Before a theoretical model actually would provide useful data in the work presented herein a much more detailed investigation of several physical parameters is needed, *e.g.* the acoustic field distribution in the separation channel is not easily derived as it is dependent on the coupling of the mechanical oscillation from the piezoceramic actuator to the separation channel *via* the bulk silicon. The wave propagation in the silicon chip and hence the obtained acoustic interference pattern is a complex modelling task. The modelling of the fluidics does not pose a problem as the system is operated in an laminar flow regime, Reynolds number ≈ 20. A further complication in defining a correct model is the fact that the fluid temporally undergoes a spatial reconfiguration with a change in physical properties, *e.g.* apparent density and viscosity (due to changing particle densities), while passing through the separation channel. Also, the effect of secondary forces on the particles, Bjerknes forces,[10,11] pose a further complex addition to the total model needed as the mean interparticle distance is varying in the separation channel along the channel length.

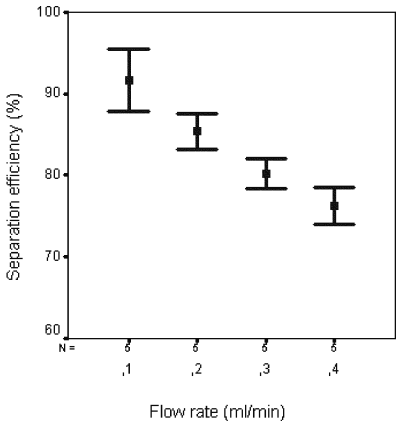

Fig. 11 Separation efficiency of a 45°-structure as a function of the flow rate. A constant frequency of 1.970 MHz, 15 Vpp and 10% concentration of blood phantom was used.

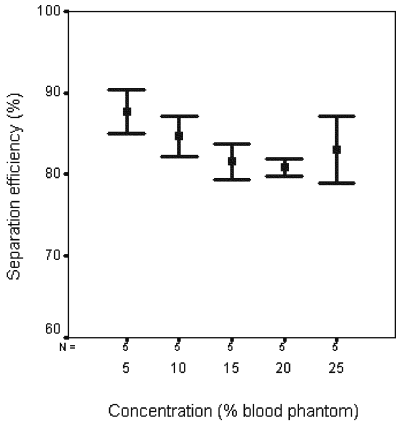

Fig. 12 Separation efficiency of a 45°-structure as a function of the concentration of the blood phantom. Constant frequency of 1.970 MHz, 20 Vpp and a flow of 0.3 ml min^{-1}.

5 Conclusions

This paper demonstrates successful on-line particle separation in silicon microchips using acoustic forces. Ultrasonic excitation of the micro fluidic channel, matching the ultrasound frequency to the channel width, enabled the focusing of particles to defined flow lines in the streaming fluid and thus the collection of a particle enriched fluid in the side channel outlets. 90% of the particles were recovered in 67% of the original volume. By increasing the frequency to higher resonance harmonics, controlled higher order particle band formation (3 and 4 bands) was demonstrated. The chip based separation approach will in future versions enable serial connection of separators for a sequential enrichment and at the end a net total higher particle enrichment factor than currently obtained. In order to improve the separation efficiency it would be desirable to confine the particles to a smaller zone. By reducing the channel width the particles are expected to be focused in a narrower band as the force on the particles increases with increasing frequency since a narrower channel has a higher resonance frequency.

References

1 J. J. Hawkes and W. T. Coakley, Force field particle filter, combining ultrasound standing waves and laminar flow, *Sens. Actuators B*, 2001, **75**, 213–222.
2 M. Gröschl, Ultrasonic separation of suspended particles – Part I: Fundamentals, *Acust. Acta Acust.*, 1998, **84**, 432–447.
3 M. Gröschl, Ultrasonic separation of suspended particles – Part II: Design and operation of separation devices, *Acust. Acta Acust.*, 1998, **84**, 632–642.
4 T. L. Tolt and D. L. Feke, Separation of dispersed phases from liquids in acoustically driven chambers, *Chem. Eng. Sci.*, 1993, **48**, 527–540.
5 D. A. Johnson and D. L. Feke, Methodology for fractionating suspended particles using ultrasonic standing wave and divided flow fields, *Sep. Technol.*, 1995, **5**, 251–258.
6 K. Yasuda, S. Umemura and K. Takeda, Studies on particle separation by acoustic radiation force and electrostatic force, *Jpn. J. Appl. Phys.*, 1996, **1**, 3295–3299.
7 K. Yasuda, S. Umemura and K. Takeda, Concentration and fractionation of small particles in liquid by ultrasound, *Jpn. J. Appl. Phys.*, 1995, **1**, 2715–2720.
8 J. J. Hawkes, W. T. Coakley, M. Gröschl, E. Benes, S. Armstrong, P. J. Tasker and H. Nowotny, Single half-wavelength ultrasonic particle filter: Predictions of the transfer matrix multilayer resonator model and experimental filtration results, *J. Acoust. Soc. Am.*, 2002, **111**.
9 K. Yosioka and Y. Kawasima, Acoustic radiation pressure on a compressible sphere, *Acustica*, 1955, **5**, 167–173.
10 L. A. Crum, Bjerknes forces on bubbles in a stationary sound field, *J. Acoust. Soc. Am.*, 1975, **57**(6), 1363–1370.
11 M. A. H. Weiser and R. E. Apfel, Interparticle forces on red cells in a standing wave field, *Acustica*, 1984, **56**, 114–119.

II

ARTICLE

THE ANALYST
www.rsc.org/analyst

Separation of lipids from blood utilizing ultrasonic standing waves in microfluidic channels

Filip Petersson,[a] Andreas Nilsson,[a] Cecilia Holm,[b] Henrik Jönsson[c] and Thomas Laurell[a]

[a] *Department of Electrical Measurements, Lund Institute of Technology, P.O. Box 118, S-221 00 Lund, Sweden*

[b] *Section for Molecular Signalling, Department of Cell and Molecular Biology, Lund University, Lund, Sweden*

[c] *Department of Cardiothoracic Surgery, Lund University Hospital, Lund, Sweden*

Received 16th April 2004, Accepted 21st June 2004
First published as an Advance Article on the web 18th August 2004

A method to continuously separate different particle types in a suspension is reported. Acoustic forces in a standing wave field were utilized to discriminate lipid particles from erythrocytes in whole blood. The presented technology proposes a new method of cleaning, *i.e.* removing lipid emboli from, shed blood recovered during cardiac surgery. Blood contaminated with lipid particles enter a laminar flow micro channel. Erythrocytes and lipid particles suspended in blood plasma are exposed to a half wavelength standing wave field orthogonal to the direction of flow as they pass through the channel. Because of differences in compressibility and density the two particle types move in different directions, the erythrocytes towards the centre of the channel and the lipid particles towards the side walls. The end of the channel is split into three outlet channels conducting the erythrocytes to the centre outlet and the lipid particles to the side outlets due to the laminar flow profile. The separation channel was evaluated *in vitro* using polyamide spheres suspended in water, showing separation efficiencies approaching 100%. The system was also evaluated on whole blood using tritium labelled lipid particles added to bovine blood. More than 80% of the lipid particles could be removed while approximately 70% of the erythrocytes were collected in one third of the original fluid volume. The study showed that the further reduced micro channel dimensions provided improved performance with respect to; (i) separation efficiency, (ii) actuation voltage, and (iii) volumetric throughput as compared to earlier work.

1 Introduction

Suspended particles in an acoustic standing wave field are affected by acoustic forces. The primary acoustic radiation force was thoroughly described for the first time by King in 1934.[1] King limited his work to incompressible spheres but his acoustic force theory was later extended by Yosioka and Kawasima[2] and by Gorkov[3] to include compressible spheres. Several groups have since used these theoretical results to increase the concentration of various particles in different media.[4–10] This has commonly been done by moving the particles into one fraction of the medium where after some of the particle free medium has been removed. However, there are two fundamental problems associated with the use of acoustic standing waves to separate particles. First of all the resonance cavity has to be very precisely fabricated to satisfy the resonance criterion. This leads to a difficult design and fabrication process. Secondly the cavity has to be coupled to an ultrasonic actuator in a way such that the power loss to the bulk material is minimised, which further increases the complexity of the separation device.

A separation cavity in silicon including improved means of coupling the acoustic actuator to the device has been proposed by Nilsson *et al.*[4] Briefly, micro channels were wet etched into a silicon wafer and sealed using anodic bonding. This resulted in very well defined structures and a fairly simple design and fabrication process. Silicon has also been used by Harris *et al.*[9,10] to fabricate separation cavities of a different design. Nilsson *et al.*[4] realized the ultrasonic actuation by applying a piezoceramic plate to the back-side of the silicon wafer using ultrasound gel. This actuation method resulted in good acoustic coupling of the ultrasound to the separation chip. The width of the channel (750 μm) was chosen to correspond to one wavelength of the applied ultrasound. This gave rise to a standing wave, with two pressure nodes and three pressure anti-nodes. When 5 μm polyamide spheres suspended in water entered the channel they moved into the pressure nodes and remained there throughout the length of the channel because of the laminar flow properties. The end of the channel was split into three outlets and the particles were collected *via* the side outlets while the main part of the particle free medium exited through the centre outlet. The results showed that 90% of the particles could be gathered in 2/3 of the original fluid volume.

This paper proposes the use of a smaller channel, 350 μm wide, and a standing wave with only one pressure node. The purpose of using only one node is that particles can be gathered in the centre outlet while the main part of the medium exits through the side outlets. Also, the smaller channel width enables the use of the same high actuation frequency even though operating at a half wave length mode, which should provide a strong acoustic force on the particles. Another advantage is that two types of particles can be separated from each other if their physical characteristics are appropriate in relation to the carrier fluid. This effect can be used in a medical application to remove lipid particles from blood collected during open heart surgery. The lipid particles originate from adipose tissue that is a part of the dissection field. When shed blood is collected and returned to the patient lipid droplets formed by triglycerides originating from adipose cells are also introduced into the circulatory system. Since the lipid particles commonly are larger than the erythrocytes these are dispersed throughout the capillary network of the body causing massive embolisation of various organs, of which the brain is most sensitive. Lipid micro embolisation of the brain in conjunction

DOI: 10.1039/b409139f

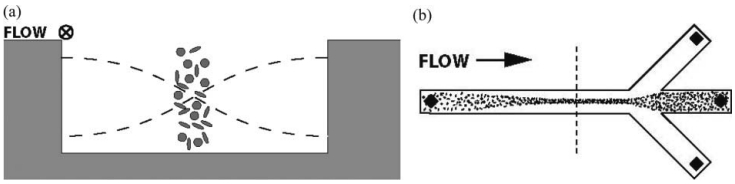

Fig. 1 (a) Particles positioned, by the acoustic forces, in the pressure nodal plane of a standing wave. (Cross section of the channel in (b), dashed line.) (b) Top view of a continuous separation of particles, positioned in the pressure node, from a fraction of their medium.

to cardiac surgery have previously been reported[11] and linked to a temporary or permanent cognitive decay.[12]

2 Theory

2.1 Separation principle

Pressure fluctuations in a liquid medium result in acoustic radiation forces on suspended particles. As long as the diameter of the particles is much smaller than half the wavelength of the standing wave[2] these forces will act mainly in one direction and the particles will move towards either a pressure node, a pressure anti-node or not at all. The direction and size of the force can be estimated by the acoustic force theory[13] (eqn. (1)).

$$F_r = -\left(\frac{\pi p_0^2 V_c \beta_w}{2\lambda}\right)\phi(\beta,\rho)\sin(2kx) \quad (1)$$

$$\phi = \frac{5\rho_c - 2\rho_w}{2\rho_c + \rho_w} - \frac{\beta_c}{\beta_w} \quad (2)$$

The densities of the medium and particles are denoted ρ_w and ρ_c respectively and the corresponding compressibilities β_w and β_c respectively, p_0 is the pressure amplitude, V_c is the volume of the particle, λ is the ultrasonic wavelength, ϕ is a dimensionless constant defined by eqn. (2), k is defined by $2\pi/\lambda$ and x is the distance from a pressure node. The direction of the force is determined by the sign of the ϕ-factor, a positive ϕ-factor results in a movement towards a pressure node and a negative towards a pressure anti-node correspondingly. For example, the theoretic value of the ϕ-factor for polyamide particles in water is about 0.8 and hence they should move towards a pressure node.

The force described by eqn. (1) is referred to as the primary acoustic force. Understanding of the characteristics of the primary acoustic radiation force is sufficient to understand the acoustic particle manipulating concept of this paper but there is a group of other related acoustic forces that also influence the movement of the suspended particles. The secondary acoustic radiation forces and other relevant forces in this context have been thoroughly discussed by Ter Haar and Wyard[14] and Weiser *et al.*[15] The relative magnitude of these forces was also investigated in ref. 14.

If a micro channel is actuated at its fundamental resonance frequency, pressure anti-nodes will be present along the side walls of the channel and a pressure node along the centre. If the channel dimensions are small the flow will be laminar provided that the flow rate is reasonably low. When suspended particles enter the channel they will be affected by the acoustic forces and move towards either the pressure node (Fig. 1a) or the pressure anti-nodes (Fig. 2a) depending on the densities and compressibilities of the particles and the medium respectively. Since laminar flow conditions prevail, the particles will remain in their lateral positions even though being outside the acoustic field region until they reach the end of the channel, which is split into three different outlets. The particles can subsequently be collected in the centre outlet (Fig. 1b) or the two side outlets (Fig. 2b). By controlling the flow rate through the three outlets independently the fraction of the medium that exits together with the particles can be controlled.

2.2 Separation of particles with different physical properties

A consequence of eqns. (1) and (2) is that it in principle should be possible to separate two types of particles suspended in the same liquid medium from each other. If the ϕ-factors (eqn. (2)) have opposite signs the two particle types will move in different directions in the acoustic force field. Eventually, one particle type will end up in the pressure node and the other type in the pressure anti-nodes (Fig. 3a). This effect can be used to separate different particle types in a continuous flow if the flow is laminar. If a half wavelength acoustic standing wave is used, one particle type will be located in the middle of the channel and the other along the side walls (Fig. 3b). When the channel is split into the three outlets one particle type will exit through the centre outlet and the other through the side outlets. For example, if the particles are erythrocytes and lipid particles (triglycerides) in blood plasma, $\phi \approx 0.3$ and $\phi \approx -0.3$ respectively, the erythrocytes should exit through the centre outlet while the lipid particles exit through the side outlets.

2.3 Downsizing

If two different particle types are to be separated from each other it is essential that the acoustic forces are sufficiently strong. Alternative ways to increase the acoustic force can be identified by considering eqn. (1), which tells us that one possibility is to increase the applied pressure amplitude. However, this can only be done to a certain extent since high pressure amplitudes also result in increased power dissipation and thus heating of the surrounding material and ultimately, cavitation and formation of gas bubbles in the system. Another

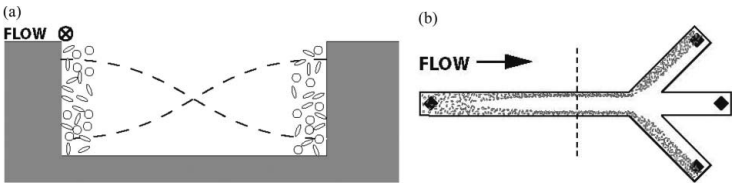

Fig. 2 (a) Particles positioned, by the acoustic forces, in the pressure anti-nodal plane of a standing wave. (Cross section of the channel in (b), dashed line.) (b) Top view of a continuous separation of particles, positioned in the pressure anti-nodes, from a fraction of their medium.

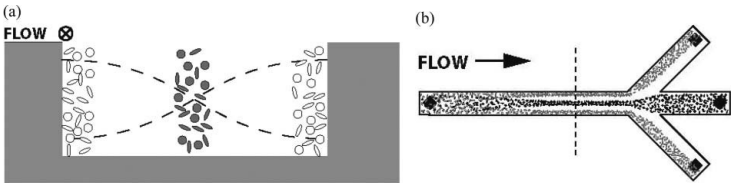

Fig. 3 (a) Two particle types positioned, by the acoustic forces, in the pressure nodal and anti-nodal planes of a standing wave. (Cross section of the channel in (b), dashed line.) (b) Top view of a continuous separation of two particle types from each other and/or a fraction of their medium.

alternative is to change the properties of the medium. This is more difficult and in some applications even impossible. The best way to increase the acoustic force is to decrease the ultrasound wavelength and the width of the separation channel accordingly.

3 Method and materials

3.1 Micro machining

The separation chips were manufactured in silicon since the material displays good acoustic properties and the high precision fabrication process is well known. By using photolithography and anisotropic wet etching techniques a separation channel with perfectly vertical walls was obtained according to the method used in ref. 4. A structure with a 350 μm wide and 125 μm deep separation channel and a trifurcation outlet was designed (Fig. 4) and fabricated. A borosilicate glass lid was attached to the silicon chip by anodic bonding to provide closed flow channels.

3.2 Experimental arrangement

The piezoceramic element (PZ26, Ferroperm Piezoceramics AS, Kvistgard, Denmark) was powered by an in-house built sinusoidal signal power amplifier. The transducer was acoustically coupled to the rear side of the separation chip using ultrasound gel (Aquasonic Clear, Parker Laboratories Inc., Fairfield, NJ, USA). Silicone rubber tubings were glued to the inlets and outlets on the back side of the separation chip, acting as docking ports to the syringe pump (WPI SP260P, World Precision Instruments Inc., Sarasota, FL, USA) *via* standard 1/16′ od teflon tubings. The flow rates through all three outlets were identical. The 5 μm polyamide spheres used were suspended in a doppler blood phantom (Dansk Fantom Service AS, Jyllinge, Denmark) containing 20% particles. The bovine blood used was mixed with saline solution (9 mg ml^{-1}, Fresenius Kabi Norge AS, Halden, Norway) in order to achieve different concentrations of erythrocytes. The lipid particles used were derived from a phospholipid-stabilized emulsion of triolein, which was prepared as described in detail in ref. 16 with some modifications. Briefly, a total amount of 320 mg triolein, tritium labelled and unlabelled, and 3.2 mg of phospholipids were sonicated in 7.2 ml of PBS. Following sonication, 0.8 ml of 20% BSA in PBS was added. The lipid emulsions were always used within 5 h from the time of preparation. The degree of hemolysis was measured using a HemoCue Plasma/Low Hb meter (HemoCue AB, Ängelholm, Sweden).

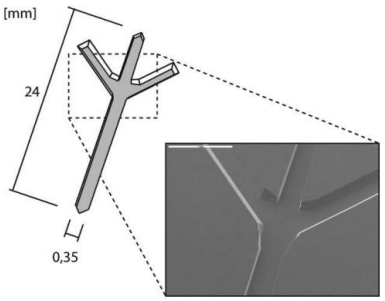

Fig. 4 Schematic drawing and scanning electron microscopy image of the trifurcation region of the 350 μm wide separation chip.

To measure the fraction of particles (polyamide spheres or erythrocytes) recovered, *i.e.* the separation efficiency, samples from the centre and side outlets were collected in capillaries (Bloodcaps 50 μl, VWR International AB, Stockholm, Sweden). Each sample was centrifuged (Haematokrit 2010, Hettich Zentrifugen, Tuttlingen, Germany) for 2 min at 13000 rpm after which the height of the particle pillars in the capillaries were measured, A (fluid collected from centre channel) and B (fluid collected from side channel). The separation efficiency was defined as $A/(A + 2B)$.

The lipid content was measured by a scintillation counter (Wallac Guardian 1414 Liquid Scintillation Counter, Perkin-Elmer Life and Analytical Sciences Inc., Boston, MA, USA), according to standard scintillation counting protocol,[17] with the modification of using Ultima Gold (Packard Biosciences, Boston, MA, USA) as scintillation liquid. The lipid separation efficiency was calculated in line with that of the other particle types.

4 Results and discussion

4.1 Separator design

The earlier reported separation channel (750 μm wide and 250 μm deep) was operated in a single wavelength standing wave mode.[4] The new design (350 μm wide and 125 μm deep), allowed the system to use a half wavelength standing wave in the 2 MHz range for acoustic separation. The use of a single pressure node made it possible to collect the particles in 1/3 of the total fluid volume. Another improvement was the use of ultrasound gel as an interface between the piezo ceramic element and the silicon, instead of epoxy. The advantage of not gluing the transducer to the chip was the possibility to reuse the same transducer several times. The Reynolds number for the 350 μm channel was calculated to 40, as compared to 20 for the earlier reported larger separation channel,[4] which still guarantees a stable laminar flow

4.2 Separator performance

As seen in Fig. 5, the particle separation efficiency was found to be very close to 100% at 12 V_{pp} (voltage peak-to-peak). It can be noted that voltage needed was lower as compared to the earlier design yet obtaining a high separation efficiency. The fast decrease in separation efficiency as the voltage was decreased can be explained by the fact that the force is proportional to the square of the voltage, *i.e.* applied pressure.

The flow rate tests (Fig. 6) showed that low flow rates resulted in high separation efficiencies. The reason for this was that the suspended particles were exposed to the ultrasound

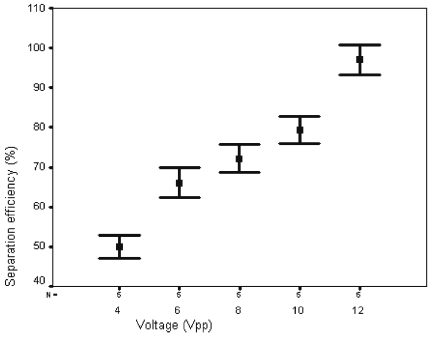

Fig. 5 Separation efficiency of the 350 μm structure *versus* voltage applied to the piezo ceramic element. The total flow rate was 0.3 ml min^{-1} and the blood phantom concentration was 10%.

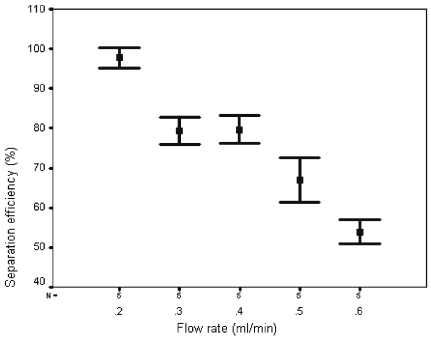

Fig. 6 Separation efficiency of the 350 μm structure *versus* total flow rate. A voltage of 10 V_{pp} was applied to the piezo ceramic element and a blood phantom concentration of 10% was used.

field for a longer time period while travelling through the separation channel. The separation efficiency of the 350 μm design was better than the 750 μm design at the peak efficiency of the latter (between 95–100% compared to around 90%), even though the voltage was considerably lower (10 V_{pp} compared to 15 V_{pp}) and the flow rate was higher (0.2 ml min^{-1} compared to 0.1 ml min^{-1}).

At low particle concentrations very high separation efficiency was achieved (Fig. 7). The efficiency dropped as higher particle concentrations were investigated, mainly because a large number of particles demanded stronger acoustic forces to gather in well defined bands. Also, the centre outlet was overloaded by particles trying to exit the system that some particles were forced into the side outlets. It should also be commented that at higher particle concentrations secondary forces will eventually put a limit to the density of particles that can be accomplished in the centre of the channel as these will eventually counteract the primary force.[15]

4.3 Separating lipids from blood

The average adult has four to six litres of blood in the circulatory system. Particles (erythrocytes, leukocytes and thrombocytes) compose about 45% of this volume and the rest is blood plasma. The plasma is composed of 90% water and 10% solved substances. The number of erythrocytes (red blood cells) is three orders of magnitude greater than the number of leukocytes (white blood cells) and more than ten times greater than the number of thrombocytes (platelets).

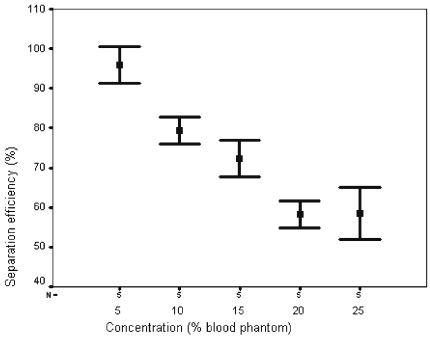

Fig. 7 Separation efficiency of the 350 μm structure *versus* blood phantom concentration. The total flow rate was 0.3 ml min^{-1} and a voltage of 10 V_{pp} was applied to the piezo ceramic element.

A major health care problem is the lack of allogeneic blood (donor blood). To reduce this demand shed blood can be collected and returned to the patient during or after surgery. There are several advantages associated with this method, called autologous blood recovery or blood wash. In addition to reducing the demand for allogeneic blood it reduces or eliminates transfusion transmitted disease and immunologic reactions to allogeneic blood. It also eliminates the risk of blood group incompatibility. Existing autologous blood recovery methods are based on centrifuges. A large volume of shed blood, typically 500 ml, is collected and centrifuged, the supernatant is removed and the collected erythrocytes are subsequently returned to the patient. However, this method suffers from three major shortcomings. First of all it can not remove lipids derived from surgery of adipose tissue efficiently and therefore offers no solution to the lipid emboli problem. Secondly, the erythrocytes experience high gravitational forces deforming them during the centrifugation process, and centrifugation is known to induce hemolysis.[18] Finally, the process is not continuous and demands a large volume of blood to initiate a cell wash cycle, which makes it inappropriate for many applications. The presented ultrasonic method is not burdened with these problems.

The different physical properties of erythrocytes and lipid particles yield a shift in sign of the Φ-factor of eqn. (1), thus resulting in forces with opposite signs for the two particle types. This enables the gathering of lipid particles and erythrocytes at different locations in the acoustic standing wave field. Milk was used in initial tests (Fig. 8a – ultrasound off and 8b – ultrasound on) to confirm that lipid particles gathered in the pressure anti-nodes of the standing wave, along the side walls. A mixture of milk and blood was also successfully processed. When the ultrasound was turned on, the lipid particles moved towards the walls of the separation channel and the erythrocytes moved towards the centre (Fig. 8b) as expected.

The separation efficiency of the chip was determined using tritium labelled triolein. The results showed that approximately 70% of the erythrocytes could be enriched in the centre outlet (Fig. 9) while more than 80% of the lipid particles were removed through the side outlets (Fig. 10). An interesting result was that the removed fraction of lipid particles was quite independent of the erythrocyte concentration.

The lipids occasionally formed clusters that tumbled along the channel walls, temporarily causing a decrease in erythrocyte separation efficiency since the laminar flow was disturbed and the straight flow lines of separated particles lost shape and destination.

The tritium labelled triolein offered a possibility to evaluate

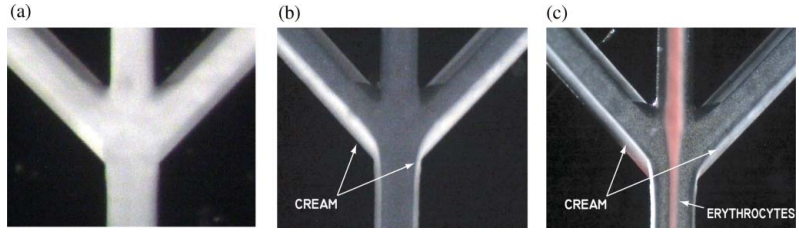

Fig. 8 (a) Milk flowing through the 350 μm separation chip with ultrasound turned off. (b) Milk flowing through the 350 μm separation chip with ultrasound turned on. (c) A mixture of milk and blood flowing through the 350 μm separation chip with ultrasound turned on.

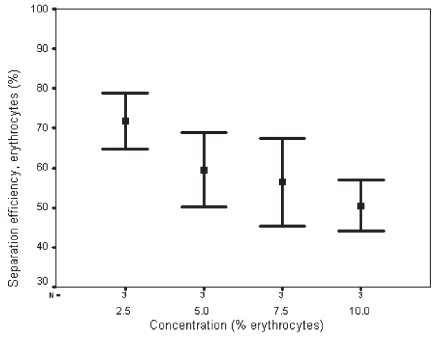

Fig. 9 Separation efficiency *versus* erythrocyte concentration. The total flow rate was 0.3 ml min^{-1} and a voltage of 10 V_{pp} was applied to the piezo ceramic element.

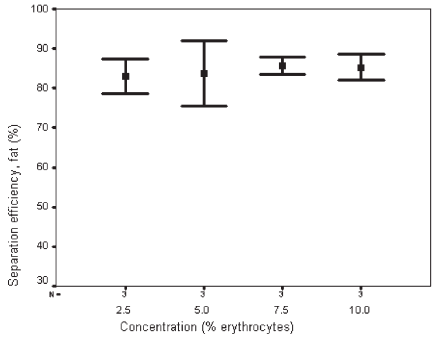

Fig. 10 Separation efficiency of lipid particles *versus* erythrocyte concentration. The total flow rate was 0.3 ml min^{-1} and a voltage of 10 V_{pp} was applied to the piezo ceramic element. All suspensions contained 1% lipids.

the lipid separation efficiency of the chip. Unfortunately, it was not possible to evaluate the chip's ability to remove lipids from human blood collected during cardiac surgery, because these lipids could obviously not be radioactively labeled. Neither could it be distinguished from the lipids contributed by lipoproteins upon measurement of total acylglycerides in plasma. However, a visual evaluation of the separation process indicated that it worked very well indeed (Fig. 11). The suspended lipid particles in blood collected during surgery are, in general, much larger than the lipid particles in the triolein emulsion used in this investigation and should be easier to remove since they are affected by stronger acoustic forces.

The degree of hemolysis was measured before and after separation and no increase was detected. This indicated that the separation process was gentle and harmless for the

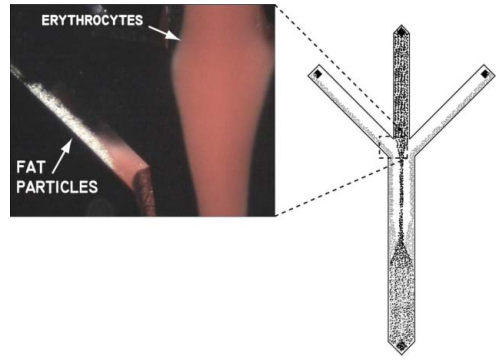

Fig. 11 Lipid particles separated from erythrocytes at the trifurcation of 350 μm separation chip with ultrasound turned on.

erythrocytes. In this context it should also be mentioned that the ultrasound frequency used was within the frequency range used in diagnostic ultrasound and thus the risk of causing cell lysis by means of the applied ultrasound should not be a problem in the current setting.

5 Conclusions

It has been shown that the new design of the particle separator, 350 μm wide, surpassed the earlier reported separator, 750 μm, in terms of separation performance. A separation efficiency of almost 100% could be reached for polyamide spheres.

Most importantly, separation of two different particles types in a homogenous mixture was demonstrated. The fact that particles with different physical properties moved to different locations in the ultrasonic standing wave field, combined with the laminar flow micro channel with a trifurcation outlet, made this possible. Separation of erythrocytes from lipid particles was confirmed. In these initial experiments approximately 70% of the erythrocytes were recovered while more than 80% of the lipid particles were removed. These results in combination with the fact that no hemolysis was detected indicated that the method may be appropriate for the suggested intraoperative blood wash application.

Although the linear flow rate was increased in the new design, it was still insufficient for processing large volumes. A design with parallel separation channels for increased throughput is therefore desired.

Acknowledgements

The authors wish to thank The Swedish Research Council for financial support. The authors also wish to thank Ellco Food AB (Kävlinge, Sweden) for their kind donations of bovine blood.

References

1 L. V. King, *Proc. R.. Soc. Lond.*, 1994, **A147**, 212–240.
2 K. Yosioka and Y. Kawasima, *Acustica*, 1955, **5**, 167–173.
3 L. P. Gorkov, *Sov. Phys. Doklady*, 1962, **6**(9), 773–775.
4 A. Nilsson, F. Petersson, H. Jönsson and T. Laurell, *Lab Chip*, 2004, **4**, 131–135.
5 M. Gröschl, *Acust. Acta Acust.*, 1998, **84**, 432–447.
6 J. J. Hawkes and W. T. Coakley, *Sens. Actuators, B*, 2001, **75**, 213–222.
7 D. A. Johnson and D. L. Feke, *Sep. Tech.*, 1995, **5**, 251–258.
8 K. Yasuda, S. Umemura and K. Takeda, *Jpn. J. Appl. Phys.*, 1995, **1**(34:5B), 2715–2720.
9 N. R. Harris, M. Hill, S. Beeby, Y. Shen, N. M. White, J. J. Hawkes and W. T. Coakley, *Sens. Actuators, B*, 2003, **95**, 425–434.
10 N. Harris, N. Hill, Y. Shen, R. J. Townsend, S. Beeby and N. White, *Ultrasonics*, 2004, **42**, 139–144.
11 D. M. Moody, W. R. Brown, V. R. Challa, D. A. Stump, D. M. Reboussin and C. Legault, *Ann. Neurol.*, 1990, **28**(4), 477–486.
12 E. P. Mahanna, J. A. Blumenthal, W. D. White, N. D. Croughwell, C. P. Clancy, L. R. Smith and M. F. Newman, *Ann. Thorac. Surg.*, 1996, **61**(5), 1342–1347.
13 W. L. Nyborg, in *Ultrasound: Its Applications in Medicine and Biology*, ed. F. J. Fry, Elsevier, New York, 1978, Part 1, pp. 1–76.
14 G. Ter Haar and S. J. Wyard, *Ultrasound Med. Biol.*, 1978, **4**, 111–123.
15 M. A. H. Weiser, R. E. Apfel and E. A. Neppiras, *Acustica*, 1984, **56**, 114–119.
16 C. Holm and T. Österlund, *Methods in Molecular Biology: Lipase and Phospholipase Protocols*, ed. M. H. Doolittle and K. Reue, Humana Press Inc., Totwa, NJ, 1999, **vol. 109**.
17 S. Evangelista, P. Cochet, N. Bromet, M. Criscuoli and C. A. Maggi, *Drug Metab. Dispos.*, 2000, **28**, 643–647.
18 C. T. Klodell, J. D. Richardson, T. M. Berdamini and D. A. Spain, *Am. Surg.*, 2001, **67**(1), 44–47.

III

CARDIOVASCULAR

Particle Separation Using Ultrasound Can Radically Reduce Embolic Load to Brain After Cardiac Surgery

Henrik Jönsson, MD, PhD, Cecilia Holm, PhD, Andreas Nilsson, MS, Filip Petersson, MS, Per Johnsson, MD, PhD, and Thomas Laurell, PhD

Department of Cardiothoracic Surgery, Center for Heart and Lung Disease, Lund University Hospital, Section for Molecular Signaling, Department of Cell and Molecular Biology, Biomedical Centre, Lund University, and Department of Electrical Measurements, Lund Institute of Technology, Lund, Sweden

Background. **Microembolism during cardiopulmonary bypass has been suggested as being the predominant cause of neurocognitive disorders after cardiac surgery. Shed blood, normally retransfused into the patient during cardiopulmonary bypass, is a major source of lipid microemboli in the brain capillaries. A newly developed technique based on acoustic standing-wave separation of particles in fluid in microchannels, with the capacity to remove lipid particles in blood, is presented.**

Methods. **A separator consisting of eight parallel, high-fidelity microfabricated channels was actuated with an ultrasound field to create a standing wave. Three different concentrations of lipid particles (diameter, 0.3 μm) were added to blood samples with increasing hematocrits and introduced into the separator channels to separate lipid particles and erythrocytes.**

Results. **The mean separation rates for lipid particles were 81.9% ± 7.6% and for erythrocytes 79.8% ± 9.9%, and both were related to the hematocrit level of the incoming blood sample. The procedure was atraumatic and did not cause hemolysis.**

Conclusions. **Particle separation by means of an acoustic standing-wave technique can be used for atraumatic and effective removal of lipid particles from blood, with the possible clinical implication of reducing neurocognitive complications after cardiopulmonary bypass.**

(Ann Thorac Surg 2004;78:1572–8)

For the majority of patients undergoing cardiac surgery, the outcome in terms of cardiac function is excellent, and, for some, predicted long-term survival is increased. Despite improvements in surgical techniques during the recent decades, complications resulting from surgery persist. Of all the possible complications, cerebral complications are by far the most feared and costly. A meta-analysis showed an overall incidence of 1.7% of postoperative stroke [1]. Cognitive dysfunction after surgery, with symptoms dominated by deficits of memory retention and attention together with inability to learn new tasks, is more frequent, and figures ranging from 10% to 70% have been reported [2]. What is even more alarming is that many of these deficits are permanent. In a recent long-term follow-up, it was reported that 42% of patients suffered from cognitive dysfunction 5 years after surgery [3].

The origin of these cognitive deficits has been discussed for many years. Evidence is mounting that microemboli play a major role in this type of subtle brain damage [4–7]. Moody and coworkers [8, 9] reported massive embolization of lipid particles to the brain, amounting to millions of emboli in the capillaries of the brain. The source of the emboli was found to be the shed blood from the surgical field, into which lipids leak into the pericardial cavity from adipocytes in the mediastinum, subcutis, and bone marrow (Fig 1A) [10]. These emboli are often referred to as lipid microemboli, and the blood containing these lipid particles is normally retransfused into the patient if a heart-lung machine is used, leading to massive embolization of lipid particles, ranging in size from 5 to 50 μm.

As the currently available techniques for particle separation (filters and centrifuges) are inadequate to remove these lipid particles satisfactorily [11, 12], we set out to develop a new separation technique based on ultrasonic standing waves, realized in microfluidic channels. The separation of suspended particles using standing waves is itself not new, and has been described previously [13, 14]. Both these methods were, however, hampered by serious limitations, and cannot be used for this application.

The separation technique described here is based on silicon microstructure development, which enables the manufacture of high-fidelity, microchannel arrays in silicon wafers for online acoustic separation of microparticles in a parallel fashion for increased throughput.

Accepted for publication April 21, 2004.

Address reprint requests to Dr Jönsson, Department of Cardiothoracic Surgery, Lund University Hospital, SE-221 85 Lund, Sweden; e-mail: henrik.jonsson@thorax.lu.se.

Drs Jönsson, Laurell, Nilsson, and Petersson disclose that they have a financial relationship with ErySave AB.

Published by Elsevier Inc

0003-4975/04/$30.00
doi:10.1016/j.athoracsur.2004.04.071

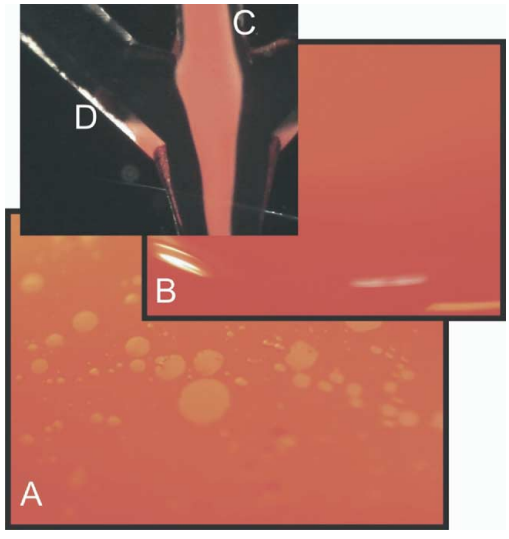

Fig 1. Shed human blood from the pericardial cavity with lipid particles visible on the surface (A). The same blood after being processed using particle separation with ultrasound standing-wave technique (B). A still from a video sequence during separation of a human blood sample showing erythrocytes in the center outlet (C) and lipid particles in the side outlets (D). The lipid particles can be seen as a white patch against the inferior wall of the side outlet. The direction of flow is from the bottom to the top of the image.

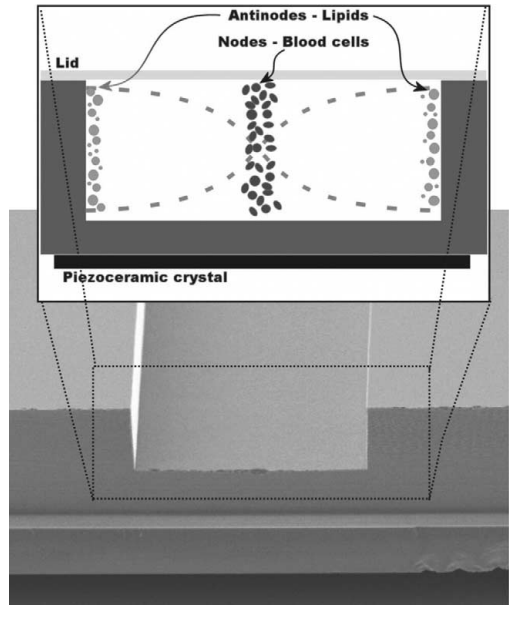

Fig 2. The principle of particle separation with ultrasound standing-wave technology. A scanning electron microscopy image shows the high-fidelity channels with vertical walls where separation is performed. Less-compressible particles with higher density (eg, erythrocytes) than the medium will move to the nodes, whereas more-compressible particles with a lower density (eg, lipid emboli) will gather at the antinodes.

The aim of this investigation was to test the efficiency of this separation method for erythrocytes and lipid particles and to demonstrate the feasibility of the technique for this specific purpose in cardiac surgery, possibly leading to a future role in reducing complications after cardiac surgery.

Material and Methods

Microchip Development

The microfluidic separation chip was manufactured by means of standard silicon processing techniques [15]. This microfabrication technique provides, in principle, perfectly vertical side walls of the microchannels as seen in the scanning electron micrograph (Fig 2). The fine accuracy of the side walls are a prerequisite for obtaining high-quality acoustic resonance in the microfluidic device. One benefit of this technique is that although the ultrasonic element is placed underneath the separation channel, the acoustic standing wave is obtained in the same plane as the silicon wafer, orthogonal to the direction of fluid flow (Fig 3). The high fidelity of the microfabrication process enables the manufacture of a separation device based on a parallel microchannel array. In this study, a separator with eight parallel channels was used (Fig 4).

The acoustic forces exerted on the particles are dependent on the density, compressibility, and size of the particles. The acoustic properties of lipid particles and erythrocytes are such that the acoustic force field acts in opposite directions on the two types of particles, thus

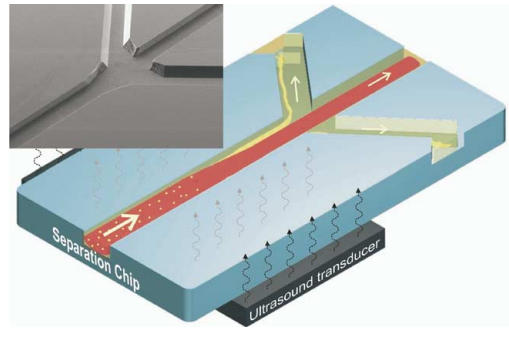

Fig 3. Schematic view of one 375-μm-wide separation channel and a scanning electron microscopic image of the trifurcation forming the center and side outlets in which the flow is be divided depending on the acoustic properties of the particles. The orthogonal placement of the ultrasonic transducer is also depicted.

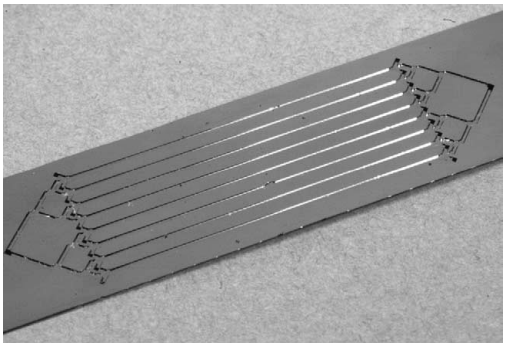

Fig 4. Photograph of a structure consisting of eight parallel channels, which was used in the study. The parallel channels are a prerequisite for increased throughput.

collecting the erythrocytes in the standing-wave pressure node and the lipid particles in the antinode [15, 16]. At the end of each separation channel, a trifurcation divides the flow of fluid and particles according to their spatial distribution in the channel (Fig 3) because the flow is completely laminar. Particles collected in the node of the standing wave (erythrocytes) are collected in the center outlet, and the lipid particles are collected in the side outlets of the microseparator.

Study Model

A lipid–blood phantom was constructed for the separation experiments. Bovine blood was anticoagulated with citrate and diluted with 0.9% saline solution to obtain predetermined hematocrit levels. Lipid particles mimicking lipid emboli were produced according to a standard protocol for sonicating tritium-labeled triolein with phospholipids [17] with minor modifications. A total amount of 800 mg of triolein (of which 1.875 mg was radioactive; 61 μCi/mg) and 8 mg of phospholipids were sonicated in 18 mL of phosphate-buffered saline. After sonication, 2 mL of 20% fatty-acid-free bovine serum albumin in phosphate-buffered saline was added. The resulting 4% triolein emulsion was diluted to obtain the various working solutions of triolein used in the experiments. This procedure yielded emulsified triglycerides with a mean diameter of 0.3 μm. Both blood and lipid emulsions were always used within 48 hours of preparation.

Eighteen different aliquots of blood and lipid with increasing concentrations of erythrocytes (hematocrits of 5%, 10%, 15%, 20%, 25%, and 30%) and lipid particles (0.5%, 1%, and 2%) were prepared. However, the aliquot with a hematocrit of 30% and 2% lipids would not mix owing to the high concentrations of particles, and had to be excluded from the study. For each of the 17 unique mixtures of blood and lipid particles, we made three independent measurements of hematocrit, hemolysis (measured as free hemoglobin in plasma), and lipid content (measured as beta radiation) in samples taken at the center and the side outlets, and before separation.

The flow was controlled with syringe pumps, and the flow rate was maintained at 0.5 mL/min for both center and side outlets by applying the syringe pumps after the structure. The ultrasonic transducer was operated with an 18.0 to 28.3 Voltage peak to peak sinusoidal signal at frequencies between 1.9739 and 2.0343 MHz.

The separation efficiency was measured as the ratio of particles collected from the center and the side outlets divided by particles collected in the side and center outlets combined, that is, the ratio of lipid particles in the side outlets to the center and side outlets, and the ratio of erythrocytes in the center outlet to the center and side outlets. This method for determining efficiency would yield 100% if all erythrocytes were recovered. Hematocrit determinations were performed with a standard hematocrit centrifuge. The lipid particle load was determined by measuring the radioactivity in whole blood, according to a standard scintillation counting protocol [18]. Hemolysis was determined using a HemoCue Low-HB device (Hemocue, Ängelholm, Sweden). The cutoff level for the device was 0.3 g/L. Levels below this value were set to 0.2 g/L for calculations.

Statistics

Group values are expressed as the mean ± standard deviation. For measurements of hemolysis (Table 1), data were grouped according to their predetermined hemat-

Table 1. Concentration of Red Blood Cells Expressed as Hematocrit, Before Separation and After Separation at Different Initial Concentrations, Together With the Hemolysis Before Separation and After Separation in Both Center and Side Outlets[a]

Predetermined Hematocrit	Measured Hematocrit in Phantom (%)		Hemolysis (g/L)		
	Before Separation	Center Outlet	Before Separation	Center Outlet	Side Outlets
5%	4.65 ± 0.40	7.89 ± 0.41	0.47 ± 0.21	0.41 ± 0.32	0.48 ± 0.29
10%	9.14 ± 0.03	15.14 ± 2.63	0.67 ± 0.40	0.56 ± 0.26	0.6 ± 0.38
15%	13.86 ± 0.34	21.62 ± 1.54	0.67 ± 0.45	0.58 ± 0.24	0.69 ± 0.39
20%	20.25 ± 4.95	25.09 ± 2.90	0.70 ± 0.40	0.64 ± 0.26	0.79 ± 0.42
25%	23.31 ± 2.68	30.64 ± 1.94	0.9 ± 0.0	1.41 ± 0.81	1.07 ± 0.26
30%	28.16 ± 0.58	38.06 ± 2.61	1.35 ± 0.21	1.05 ± 0.05	1.35 ± 0.23

[a] Values are grouped according to their predetermined hematocrit, ie, different lipid particle concentrations are in the same group. No significant difference was found between preseparation and postseparation hemolysis.

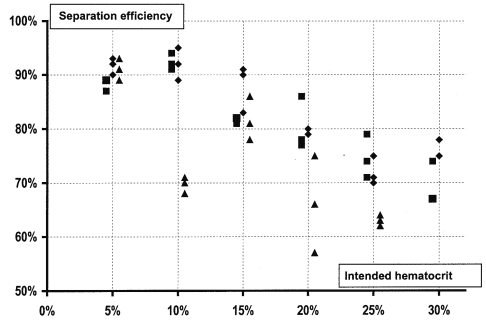

Fig 5. Separation efficiency of red blood cells measured as a function of hematocrit. Samples with 0.5% lipid particles (■), 1% lipid particles (◆), and 2% lipid particles (▲) were compared. Superimposed measurements are indicated by larger symbols.

ocrit (different lipid concentrations were grouped in the same hematocrit group). To test for differences between preseparation and postseparation hemolysis, a sign–rank test was used. Correlations were investigated with univariate analysis, and univariate regression analysis was performed to test dependency. A p value less than 0.05 was considered significant.

Results

Preseparation hematocrits for the different groups were all close to the intended hemoglobin concentrations for the experiments. In addition, hemoconcentration was seen, and hematocrits in blood from the center outlet ranged from 7.9% to 38.1% (Table 1). A low degree of hemolysis was seen in almost all preseparation samples. No change in the degree of hemolysis was seen as a result of the separation (Table 1).

The separation efficiency for erythrocytes, measured as the ratio of the center outlet to the side and center outlets, ranged between 94% and 57% with a mean of 79.8% ± 9.9% (Fig 5). The separation efficiency decreased with increasing hematocrit ($r = 0.70$, $p < 0.0001$).

The separation ratio of lipid particles measured as radioactivity ranged from 66% to 94% with a mean of 81.9% ± 7.6% (Fig 6). In contrast to erythrocytes, the separation ratio for lipids increased with increasing hematocrit in the incoming sample ($r = 0.33$, $p < 0.05$).

A sample of shed blood collected from a patient undergoing cardiac surgery was processed in a separate experiment. From visual examination by macrophotography, we estimated complete removal of all macroscopic lipid microemboli in this model (Fig 1).

Comment

We describe here a novel ultrasound technique with the ability to separate and remove lipid particles from blood. Microembolism has been suggested by many investigators to be the main contributor to the pathogenesis of neurocognitive complications after cardiac surgery [5, 6, 19, 20]. Moody and coworkers [8, 9] showed that there was an increased number of lipid microemboli in brain capillaries after experimental cardiopulmonary bypass, and referred to them as small capillary arteriolar dilatations (SCADS). Brooker and coworkers [10] found that these originated from the pericardial shed blood that is routinely retransfused to the perfusion circuit by means of cardiotomy suction.

During cardiopulmonary bypass the hematocrit is intentionally reduced, as induced hypothermia increases the viscosity of the blood, but it is also done to avoid unnecessary transfusions. A crystalloid priming solution is therefore added to achieve a hematocrit of approximately 20% to 25%. In shed blood, the hematocrit is even lower as it gets mixed with saline solution or other slush fluids used during surgery. The efficiency of the ultrasound separator regarding the removal of lipid particles ranged between 66% and 94% with a mean of 81% at the hematocrit levels investigated. This is much better than that which can be achieved with other methods, such as cell wash by means of centrifugation or filters, currently used in clinical practice.

Saline cell washing, followed by centrifugation (cell-saving device technology), reduced the number of emboli by approximately 50% [12]. However, the method has several drawbacks. The process is intermittent with a need to collect a minimal batch volume (typically 400 to 500 mL) before washing can be initiated, and the devices are large, occupying space in an already crowded environment. Hemolysis is always a side effect, probably as a result of the extreme gravitational force (500 to 2,000 g) exerted on the erythrocytes when the centrifuge reaches the maximum speed.

With filters, an even lower reduction in the number of emboli was achieved. Kincaid and coworkers [12] reported that approximately 30% to 40% was removed, and

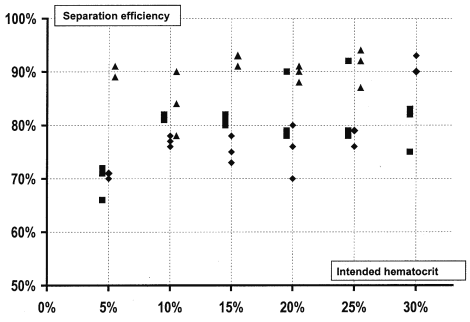

Fig 6. Separation efficiency of lipid particles cells as a function of hematocrit measured by radioactivity. Samples with 0.5% lipid particles (■), 1% lipid particles (◆), and 2% lipid particles (▲) were compared. Superimposed measurements are indicated by larger symbols.

a recent study also showed a 30% reduction [11]. Filters will eventually become saturated, resulting in rapid reduction of filtering capacity [11]. Also, it is generally believed that filters only disperse larger emboli into smaller ones. The typical arterial line filter in use has a pore size of 40 μm, and will still allow lipid particles large enough to wedge in small brain capillaries to pass through.

It might be argued that our test model with very small lipid particles (0.3 μm in diameter) was not optimal, as clinically relevant microemboli must be of a considerably larger size. However, the force exerted by the ultrasound on particles scales with the volume of the particle. A 10-μm particle has a volume 37,000 times larger (the cube of 10/0.3) than that of a 0.3-μm particle. Consequently, the force exerted will be 37,000 times greater. It is therefore reasonable to assume that the separation ratio will increase as the particles become larger. To demonstrate that this method also allows for the removal of larger lipid particles, we tested shed blood from the pericardial cavity of a patient and found by visual inspection that all the lipid droplets had been removed (Fig 1).

Existing methods have a limited efficiency in removing emboli, which may explain why studies of the clinical outcome of emboli removal have shown negative or conflicting results [4, 7]. The present method can cleanse blood of at least 80% of particles. In fact, a separation efficiency greater than 90% was achieved at least once for every sample, and it is reasonable to believe that further improvements and fine tuning of the technique will result in a separation ratio of at least 90% for small particles (diameter less than 1 μm), and probably even higher for larger particles. This will enable us to perform better studies to assess the impact of microemboli removal on the patient's neurocognitive outcome.

The separation rate for erythrocytes ranged between 57% and 95% with a mean of 80%. The test point with low separation ratio could be attributed to artifacts, such as trapping of air bubbles in separation channels, which were not detected by the operator. When these outliers were excluded and relevant hematocrit for the clinical situation chosen ($\leq$20%), the mean recovery rate was 85%. Some erythrocytes were lost to the side outlets, but this can be improved by adjusting the flow velocities in the center and side outlets.

No process-related hemolysis was observed. Ultrasound can, however, be used to achieve hemolysis by inducing shear forces by cavitation [21]. These forces depend on both frequency and intensity, and normally lower frequencies will yield larger forces [22]. On the other hand, low-intensity ultrasound, which is used, for instance, in diagnostic procedures, produces no significant cavitation, and has been proven safe throughout the years [23]. The application of an acoustic standing wave displaces some particles, eg, erythrocytes, to the nodes, and they are thus positioned at a location where no cavitation is present. However, cavitation is present at the antinodes (where lipids are collected), but with the frequency and intensity used in this model, the cavitation forces are weak at the antinodes. For comparison, it can be mentioned that cell-saving device technology displaces erythrocytes to the periphery, where the gravitational force is the highest, which could explain the hemolysis seen after centrifugation [24, 25]. The acoustic separation technique shows no evidence of exposing blood cells to strong shear forces. We found no hemolysis in this study, and the technique seems to be atraumatic to cells, which further adds to the clinical benefit.

Ultrasonic standing-wave techniques, for the purpose of particle separation, have been described earlier [13, 14]. However, these techniques were neither developed for nor tested with blood. Gröschl [13] manufactured a device with a standing wave between two transducers centimeters apart. This device resulted in substantial turbulence, with low efficiency, and only low concentrations of particles could be processed. The technique described in this paper uses the benefits of laminar flow in microfluidic channels. An estimate of the laminar flow index, the Reynolds number, for the flow velocity and channel dimensions used and blood as the fluid yields a value of less than 20 (a Reynolds number of less than 2,000 is considered to indicate laminar flow). Thus, the extremely laminar flow in the channels is another contributing factor to the high separation ratio. Hawkes and Coakley [14], on the other hand, tested single-line separation with low throughput and low precision. The novelty of our technique is the micromechanic fabrication, yielding an extremely high precision, together with a two-dimensional, distribution of channels. The fabrication of a microchannel array (Fig 3) makes it possible to realize parallel channels actuated by a single transducer. Parallel channels are a prerequisite for the scalability and the increased throughput needed to meet clinical demands. The presented device with eight parallel channels can handle 60 mL/h, and at least a 20-fold increase in throughput will be necessary to meet clinical demands. This can be achieved by increasing the number of parallel channels. In addition, the planar technology of channels can also be used to realize serial processes, with improved separation efficiency. For example, two-stage separation could increase the separation efficiency further. If the recovery rate for erythrocytes is 90% in the first step, a second step would yield another 90% recovery of the 10% remaining, resulting in 99% overall recovery.

It was not the aim of this study to investigate the separation efficiency for leukocytes or thrombocytes. However, their physical properties in terms of density and compressibility resemble those of erythrocytes, and, therefore, they will most likely follow erythrocytes to the center outlet. This separation platform can be used in several other fields of particle separation. The physical properties that determine the force exerted on the particles are the density, compressibility, and size. Other biologic particles, such as bacteria, macromolecules, lipoproteins, and viruses, have physical properties that could make separation possible with acoustic technique. We propose the acronym PARSUS (particle separation using ultrasound) be used for this generic separation technique.

In conclusion, a novel technique, using an ultrasound standing wave in a microdomain for the separation of lipid particles in shed blood, is presented. The microembolic load on brain capillaries during cardiac surgery can be abolished or reduced. Whether this, in turn, will lead to an overall improvement in the neurocognitive outcome of individual patients must be assessed in further studies. The generic platform has inherent properties of scalability and design flexibility enabling the implementation of the technique in other types of particle separation.

References

1. Naylor AR, Mehta Z, Rothwell PM, Bell PR. Carotid artery disease and stroke during coronary artery bypass: a critical review of the literature. Eur J Vasc Endovasc Surg 2002;23:283–94.
2. Mahanna EP, Blumenthal JA, White WD, et al. Defining neuropsychological dysfunction after coronary artery bypass grafting. Ann Thorac Surg 1996;61:1342–7.
3. Newman MF, Kirchner JL, Phillips-Bute BRH, et al. Longitudinal assessment of neurocognitive function after coronary-artery bypass surgery. N Engl J Med 2001;344:395–402.
4. Pugsley W, Klinger L, Paschalis C, Treasure T, Harrison M, Newman S. The impact of microemboli during cardiopulmonary bypass on neuropsychological functioning. Stroke 1994;25:1393–9.
5. Stump DA, Rogers AT, Hammon JW, Newman SP. Cerebral emboli and cognitive outcome after cardiac surgery. J Cardiothorac Vasc Anesth 1996;10:113–8.
6. Taggart DP, Westaby S. Neurological and cognitive disorders after coronary artery bypass grafting. Curr Opin Cardiol 2001;16:271–6.
7. Whitaker DC, Newman SP, Stygall J, Hope-Wynne C, Harrison MJ, Walesby RK. The effect of leucocyte-depleting arterial line filters on cerebral microemboli and neuropsychological outcome following coronary artery bypass surgery. Eur J Cardiothorac Surg 2004;25:267–74.
8. Moody DM, Bell MA, Challa VR, Johnston WE, Prough DS. Brain microemboli during cardiac surgery or aortography. Ann Neurol 1990;28:477–86.
9. Moody DM, Brown WR, Challa VR, Stump DA, Reboussin DM, Legault C. Brain microemboli associated with cardiopulmonary bypass: a histologic and magnetic resonance imaging study. Ann Thorac Surg 1995;59:1304–7.
10. Brooker RF, Brown WR, Moody DM, et al. Cardiotomy suction: a major source of brain lipid emboli during cardiopulmonary bypass. Ann Thorac Surg 1998;65:1651–5.
11. de Vries AJ, Gu YJ, Douglas YL, Post WJ, Lip H, van Oeveren W. Clinical evaluation of a new fat removal filter during cardiac surgery. Eur J Cardiothorac Surg 2004;25:261–6.
12. Kincaid EH, Jones TJ, Stump DA, et al. Processing scavenged blood with a cell saver reduces cerebral lipid microembolization. Ann Thorac Surg 2000;70:1296–300.
13. Gröschl M. Ultrasonic separation of suspended particles—part II: design and operation of separation devices. Acust Acta Acust 1998;84:632–42.
14. Hawkes JJ, Coakley WT. Force field particle filter, combining ultrasound standing waves and laminar flow. Sens Actuators B 2001;75:213–22.
15. Nilsson A, Petersson F, Jönsson H, Laurell T. Acoustic control of suspended particles in micro fluidic chips. Lab Chip 2004;4:131–5.
16. Gröschl M. Ultrasonic separation of suspended particles—part I: fundamentals. Acust Acta Acust 1998;85:432–7.
17. Holm C, Österlind T. Lipase and phospholipase protocols. In: Dolittle MH, Reue K, eds. Methods in molecular biology. Totowa, NJ: Humana Press, 1999;109:109–21.
18. Evangelista S, Cochet P, Bromet N, Criscuoli M, Maggi CA. A distribution study with (14)C-otilonium bromide in the rat: evidence for selective tropism for large intestine after oral administration. Drug Metab Dispos 2000;28:643–7.
19. Murkin JM. Etiology and incidence of brain dysfunction after cardiac surgery. J Cardiothorac Vasc Anesth 1999;13(Suppl 1):12–17.
20. Stump DA, Kon NA, Rogers AT, Hammon JW. Emboli, and neuropsychological outcome following cardiopulmonary bypass. Echocardiography 1996;13:555–8.
21. Miller MW, Battaglia LF. The relevance of cell size on ultrasound-induced hemolysis in mouse and human blood in vitro. Ultrasound Med Biol 2003;29:1479–85.
22. Leighton TG. Cavitation in standing-wave fields. In: Leighton TG, ed. The acoustic bubble. San Diego, CA: Academic Press, 1997:495–504.
23. Barnett SB, Ter Haar GR, Ziskin MC, Nyborg WL, Maeda K, Bang J. Current status of research on biophysical effects of ultrasound. Ultrasound Med Biol 1994;20:205–18.
24. Elawad AA, Ohlin AK, Berntorp E, Nilsson IM, Fredin H. Intraoperative autotransfusion in primary hip arthroplasty. A randomized comparison with homologous blood. Acta Orthop Scand 1991;62:557–62.
25. Klodell CT, Richardson JD, Bergamini TM, Spain DA. Does cell-saver blood administration and free hemoglobin load cause renal dysfunction? Am Surg 2001;67:44–7.

INVITED COMMENTARY

Removal of lipid particles has become of interest after the alarming results of Moody and colleagues [1] on lipid embolization in brain arterioles after cardiac surgery. It resulted in various attempts to reduce lipids in retransfusion blood, which would be beneficial after cardiac surgery, but also after orthopedic surgery. Despite the known side effects of retransfusion from the wound area, autologous blood transfusion is increasingly used to reduce the use of allogenic blood. A major problem in justifying the efforts, time, and costs to clear retransfusion blood from lipid particles is to obtain evidence of clinically relevant brain damage and evidence for the dominant role of lipid particles.

First of all, brain damage has been reported with very different significance. A number of studies could not show any deterioration in cognitive functions, whereas biochemical markers of brain damage, such as S100β and enolase, showed in some studies small and transient appearance. Clearly, the specificity of such tests is not sufficient or sensitive enough to demonstrate brain damage. Perhaps new markers, such as carnosinase, may appear relevant for monitoring brain damage.

The second problem is that lipid particles are only one of the suspects of brain damage. Gaseous emboli, macromolecules, inflammatory agents, and leukocyte-platelet aggregates may be involved in occlusion of the small vasculature as well. In their discussion the authors indicated that, eg, macromolecules may also be removed by the current technique of particulate separa-

0003-4975/04/$30.00
doi:10.1016/j.athoracsur.2004.05.043

tion, but other potential sources of embolization possibly remain in retransfusion blood. The combination with other techniques to remove platelets, leukocytes, and products that affect hemostasis or inflammation may be a future option.

Third, the reuse of shed blood is a matter of dispute. It depends on the operation time, preference of surgeons, and need for immediate volume during the procedure. To obtain the technique widely used, it must be simple, fast, and cost effective.

Nevertheless, the PARSUS technique presented here offers new possibilities to improve the quality of retransfusion with high efficacy for removing potential dangerous lipid particles. Hopefully these qualifications will be supported by adequate monitoring instruments. It would be exciting to see the efficacy of a larger scale PARSUS device in clinical practice.

Willem van Oeveren, PhD

Biomedical Engineering
University of Groningen
PO Box 196
Groningen, the Netherlands 9700 AD

e-mail: w.van.oeveren@med.rug.nl

Reference

1. Moody DM, Brown WR, Challa VR, Stump DA, Reboussin DM, Legault C. Brain microemboli associated with cardiopul-monary bypass: a histologic and magnetic resonance imaging study. Ann Thorac Surg 1995;59:1304–7.

Online Discussion Forum

Each month, we select an article from *The Annals of Thoracic Surgery* for discussion within the Surgeon's Forum of the CTSNet Discussion Forum Section. The articles chosen rotate among the six dilemma topics covered under the Surgeon's Forum, which include: General Thoracic Surgery, Adult Cardiac Surgery, Pediatric Cardiac Surgery, Cardiac Transplantation, Lung Transplantation, and Aortic and Vascular Surgery.

Once the article selected for discussion is published in the online version of *The Annals,* we will post a notice on the CTSNet home page **(http://www.ctsnet.org)** with a **FREE LINK** to the full-text article. Readers wishing to comment can post their own commentary in the discussion forum for that article, which will be informally moderated by *The Annals* Internet Editor. We encourage all surgeons to participate in this interesting exchange and to avail themselves of the other valuable features of the CTSNet Discussion Forum and Web site.

For November, the article chosen for discussion under the Adult Cardiac Surgery Dilemma Section of the Discussion Forum is:

Surgical Reconstruction of the Left Main Coronary Artery: Fresh Autologous Pericardium or Saphenous Vein Patch
Ehud Raanani, MD, Alexander Kogan, MD, Yaron Shapira, MD, Alex Sagie, MD, Ran Kornowsky, MD, and Bernardo A. Vidne, MD

Tom R. Karl, MD
The Annals *Internet Editor*
UCSF Children's Hospital
Pediatric Cardiac Surgical Unit
505 Parnassus Ave, Room S-549
San Francisco, CA 94143-0118
Phone: (415) 476-3501
Fax: (212) 202-3622
e-mail: karlt@surgery.ucsf.edu

IV

Acoustic resonances in straight micro channels: Beyond the 1D-approximation

S. M. Hagsäter,[a] A. Lenshof,[b] P. Skafte-Pedersen,[a] J. P. Kutter,[a] T. Laurell[b] and H. Bruus[a]

Received 21st January 2008, Accepted 17th April 2008
First published as an Advance Article on the web 16th May 2008
DOI: 10.1039/b801028e

Acoustic actuation can be used to perform several tasks in microfluidic systems. In this paper, we investigate an acoustic separator through micro-PIV analysis in stop-flow mode and numerical simulations, and a good agreement between the two is found. Moreover, we demonstrate that it is not sufficient only to characterize devices in flow-through mode, since in these systems much different resonant patterns can result in similarly looking band formations. Furthermore, we conclude that extended 1D approximations of the acoustic radiation force are inadvisable, and instead, a 2D model is preferred. The results presented here provide valuable insight into the nature and functionality of acoustic microdevices, and should be useful in the interpretation and understanding of the same.

I. Introduction

Acoustic actuation poses an attractive option for the performance of various relevant microfluidic tasks. Successful demonstrations of acoustic forces used for enrichment,[1,2] mixing,[3,4] cell handling,[5,6] medium exchange,[7] separation,[8–11] sorting[12] and others, have been provided.

However, the evaluation of these devices is mostly limited to quantifying and commenting on the net effect of the acoustic actuation in these systems as a whole, rather than investigating more locally how the desired effects are actually achieved. Moreover, numerical modeling of acoustic formation in the microfluidic designs has not been successfully reported, and, instead, the description of a sphere in a 1D standing wave[13–15] is typically supplied and described as extending uniformly for the whole length of a channel of constant width.[1,2,5,8–10]

In this work, we apply a recently reported method of investigation[16] for the examination of a previously well documented microchip based acoustic separator device.[8] We chose to work with this device as it has a non-complex design, which makes it attractive for both the experimental micro-PIV investigation and the numerical simulations. The device operates in continuous mode and has its function in that it can separate suspended particles from their medium. Moreover, the acoustic separator has seen a large number of successors,[7,9,12,17] intended for various microfluidic scenarios and functionalities, which makes it a suitable representative for a whole range of devices actuated and fabricated in a similar manner.[18] The results presented herein are foremost representative for these devices, but anticipate that similar behavior is to be expected and that the same conclusions are valid for other actuation variants and chip designs as well.

[a]*Department of Micro- and Nanotechnology, Technical University of Denmark, DTU Nanotech Building 345 east, DK-2800, Kongens Lyngby, Denmark*
[b]*Department of Electrical Measurements, Lund University, Box 118, 221 00, Lund, Sweden*

The current investigation has shown that the acoustic resonances are indeed of more complex nature than what is described by an extended 1D approximation. The experimental results were also found to agree with numerical 2D simulations. A discussion on this acoustic separator, and similar devices, is provided.

II. Materials and methods

The investigated acoustic separator was defined in a silicon substrate by the use of UV-lithography and chemical wet etching. After etching, the channel was sealed by a glass lid through anodic bonding, and silicone tubings were glued to the backside of the chip, for easy attachment of fluidic connections. A more detailed description of the fabrication process can be found in Nilsson *et al.*[8] A sketch of the microchannel and the surrounding silicon substrate is seen in Fig. 1.

The device was actuated by a piezo ceramic (Pz26, Ferroperm Piezoceramics, Kvistgard, Denmark), pressed to the backside of the chip and acoustically coupled *via* an ultrasonic gel (Aquasonic Clear, Parker Laboratories Inc., Fairfield, NJ) in between for good acoustic energy transmission. The transducer was biased by a signal generator (33250A, Agilent Technologies Inc., Santa Clara, CA), the effective power measured by a digital power meter (Model 5000-EX, Bird Electronic Corp., Cleveland, Ohio) and the amplitude monitored by an oscilloscope (TDS 210, Tektronix Inc., Beaverton, OR). More information on the experimental details, including piezo-actuation, can also be found in ref. 8.

A progressive scan interline CCD camera (Hisense MkII, Dantec Dynamics, Skovlunde, Denmark), mounted with a 0.63× tv-adapter onto a research microscope (DMLB, Leica Microsystems, Wetzlar, Germany), was used to record multiple sets of image pairs, used for the micro-PIV analysis. For the measurements presented in this paper, a relatively low magnification microscope objective (5×) was chosen, to allow a fairly large part of the microfluidic channel to be recorded in each position. A pulsed blue LED (XLamp XR-E, Cree,

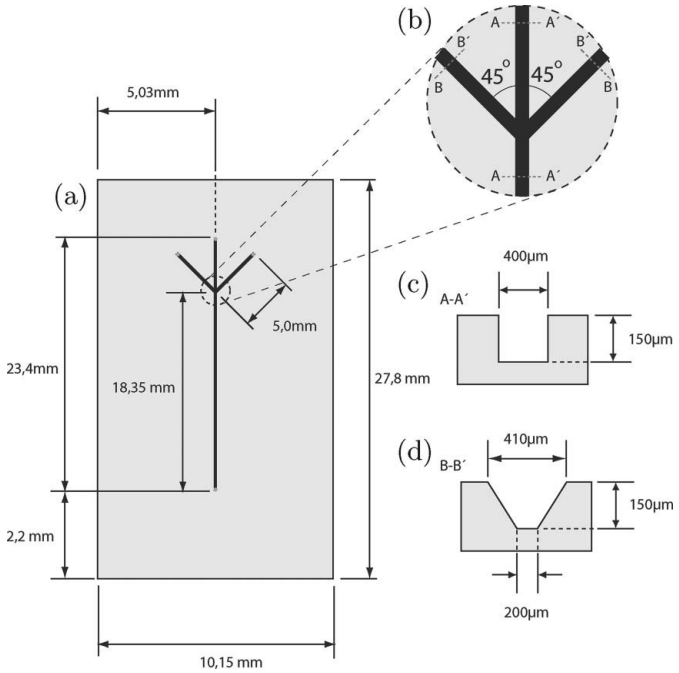

Fig. 1 Sketch with dimensions of the separation chip used in the experiments. (a) Top view of the micro-channel and the surrounding silicon substrate. (b) Close up in junction region. (c) Cross-sectional view of the main channel. (d) Cross-sectional view of the side channels.

Durham, NC), mounted in a front-lit configuration was used to illuminate the sample.[19]

For the separation efficiency measurements, the flow rate was controlled by a syringe pump (WPI SP210iwz, World Precision Instruments, Sarasota, FL), and injection valves (Rheodyne 7000, Cotati, CA) with a fixed loop volume were used to take samples. On the other hand, during the micro-PIV measurements, the same injection valves were used to stop the flow so that only particle motions created by acoustic effects were measured. As the acoustic radiation force scales with the volume of the particle, whereas the acoustic streaming is a motion of the fluid medium, the two respective forces can be distinguished from each other by applying tracer particles of different sizes. That is, the small particles will most likely mainly be affected by the motion of the fluid medium, whilst the primary motion of the larger particles will be from the radiation force. In this study two types of particles were used: 5 µm polyamide micro-beads (Danish Phantom design) and 1 µm fluorescent polystyrene micro-beads (Duke Scientific). The larger particles were also used in the separation efficiency measurements, where the number of particles passing through the middle and the side outlets, respectively, was counted using a Coulter counter (Multisizer 3, Beckman Coulter Inc., Fullerton, CA).

A detailed description of the special adaptations and considerations required when applying micro-PIV for the investigation of acoustic forces in microfluidic systems can be found in ref. 16. In the present work, unless stated otherwise, the same measurement scheme has been applied. Additionally, the 2D chip model, and 2D chamber model simulations, using COMSOL Multiphysics finite element software, have also been performed analogously to Hagsäter *et al.*[16]

III. Results and discussion

A. 1D approximation and 2D simulations

The most dominant acoustic effect for larger particles positioned inside an acoustic standing wave field is the acoustic radiation force.[13–15] For a one-dimensional standing planar acoustic wave, the force $\boldsymbol{F}_r$ on a sphere at the distance x from a pressure node can be described as,[14]

$$\boldsymbol{F}_r = -\left(\frac{\pi p_0^2 V_p \beta_m}{2\lambda}\right)\phi(\beta,\rho)\sin(4\pi x) \quad (1)$$

$$\phi(\beta,\rho) = \frac{5\rho_p - 2\rho_m}{2\rho_p + \rho_m} - \frac{\beta_p}{\beta_m} \quad (2)$$

where λ is the ultrasonic wavelength, p_0 is the pressure amplitude and V_p the volume of the sphere. The factor ϕ defines in which direction the particles will move, either towards or away from the pressure nodes, depending on the relation between the densities and compressibilities of the particle (ρ_p, β_p) and the medium (ρ_m, β_m).

This formula for a 1D wave is often used in the literature to describe the effect of the acoustic radiation force in microfluidic

channels.[1,2,5,7,8,11,12,17,22–25] Typically, the focusing effect is described as a confined extension of the 1D case along the length of the channel of frequency matching width. Acoustic effects are often not ascribed to the parts of the system where there is no frequency matching. The acoustic separator examined in this work described by the extended 1D model, with a channel width of 400 μm and a sound velocity in water of 1483 m s^{-1} (20 °C), yields $\lambda = 800$ μm equivalent to an ideal frequency $f \sim 1.85$ MHz for half a wavelength over the width of the channel. Due to various loss mechanisms, frequency-broadening of the acoustic resonance will occur, but the model only suggests resonant solutions with half a wavelength separation in between.

An improved description of an acoustically actuated microfluidic system can be obtained by finding eigenmode solutions p_n to the Helmholtz eigenvalue equation $\nabla^2 p_n = -(\omega_n^2 / c_i^2) p_n$, where ω_n are the resonance angular frequencies, n is the mode number, and the index i of the sound velocities c_i is referring to the three material domains of silicon, water and glass in the chip.[16] This model of the system including the silicon substrate, water-filled microchannels and glass lid, we denote the 3D model. In the case where the height of the system is less than half of a wavelength, the description can be approximated by a simpler (not least in respect to the requisite of computational power) 2D approach, where the eigenvalue problem is solved only in the center plane of the microchannels and the surrounding silicon substrate. This second model we denote the 2D chip model. A further simplification is obtained by utilizing the large difference in acoustic impedance between water and silicon: the 2D Helmholtz eigenvalue equation is solved only for the fluidic part of the system, while the surrounding chip substrate appears only as a hard wall boundary condition on the walls of the microchannels. This third model we denote the 2D chamber model, and it is valuable, as it gives a more principal representation of the acoustic resonances that can be difficult to detect in the more complete 2D chip model. A justification for the two 2D models, based on the flatness of the system, as well as a more detailed description of how the numerical simulations should be interpreted in relation to experimental results is given in Hagsäter *et al.*[16]

If the Helmholtz eigenvalue equation is solved for the idealized 2D chamber model of the acoustic separator, the result is much different to that suggested by an extended 1D model. Instead of a single solution for one specific frequency, the 2D chamber model suggests several solutions within a rather wide frequency span. More specifically, instead of a uniform pressure amplitude along the length of the channel, the solutions display an increasing number of "pinching regions" along the channel (see Fig. 2). Starting at 1.85 MHz, where we have one full ($n = 1$) pinching region, solutions were identified for all integer values n, up to $n =$ 32 for 2.25 MHz. The frequency shift between the solutions were in the range of 1.5–15 kHz, with a tendency of larger separations for higher frequencies. The calculated eigenfrequencies agree with the observed ones within one percent.

These solutions can be understood by considering that the acoustic eigenmodes in the channel system are dominated by, primarily, a transverse wavelength λ_t and a longitudinal wavelength λ_l contributing to the forming standing wave pattern. As the Helmholtz eigenvalue equation is modeled with a hard wall boundary condition, the resonant wavelengths will be

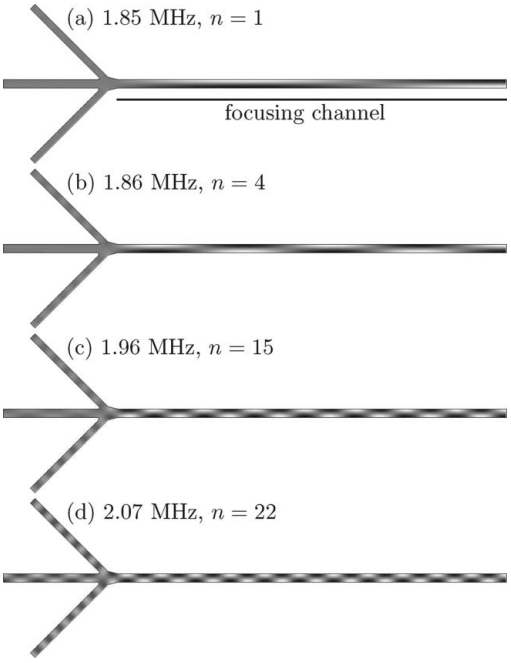

Fig. 2 Gray-scale plots of the pressure eigenmodes p_n for the chamber model at (a) 1.85 MHz, (b) 1.86 MHz, (c) 1.96 MHz and (d) 2.07 MHz. The integer value n is the number of pinching regions in the focusing channel.

fractions of the channel dimensions. The resonance frequencies f can be estimated by

$$f = c_w \sqrt{\lambda_t^{-2} + \lambda_l^{-2}} \tag{3}$$

where c_w is the sound velocity in water. We consider solutions for which there is half a standing wave over the width of the channel, thus $\lambda_t = 2w$ with $w = 400$ μm Similarly, we have $\lambda_l = 2L/n$, where $L = 18.3$ mm is the length of the focusing channel. Since $w \ll L$, f will be dominated by λ_t, and hence, a very small shift in frequency will result in a change of the number of pinching regions n. From this relation we can also conclude that if a microdevice is operated at a fixed frequency, even a small change in the temperature dependent sound velocity will cause a change in the number of pinching regions.

B. Device operated in flow-through mode

As a first investigation of the device, the chip was screened in flow-through mode, with continuous piezo actuation. The frequency of the AC voltage generator was scanned in the interval between 1.8 MHz and 2.2 MHz, while the separation effect was monitored. In the whole of this frequency span, a focusing effect of varying intensity was observed. In Fig. 3 stitched image frames recorded at three local maxima at a flow rate of 0.1 mL min^{-1} are shown. Of these three, the strongest focusing effect was seen at 1.86 MHz, even though the transmitted power was set to a lower value for this frequency

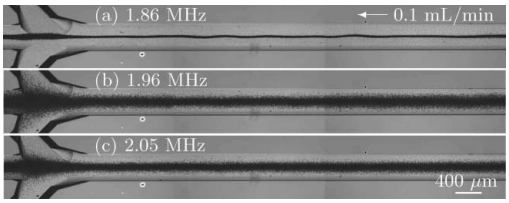

Fig. 3 The final 6 mm of the focusing channel leading up to the separation area of the device operating at frequencies of (a) 1.86 MHz, (b) 1.96 MHz and (c) 2.05 MHz. For comparison the same flow rate 0.1 mL min^{-1} was used in all panels (a)–(c). The transmitted power was set to 0.5 W in (b) and (c), and to 0.2 W in (a), where a much stronger focusing effect was found. The black bands consist of acoustically focused 5 μm beads.

than for the other two. The presence of several local maxima is in agreement with the results of the 2D chamber model simulations. On the other hand, the strong coupling at 1.86 MHz could be interpreted as a support for the extended 1D model, where the local maxima could stem from the impedance of the mounted piezo's frequency dependence, or from the chip favoring coupling of certain frequencies. It is clear that more elaborate measurements are required in order to determine how well the different models agree with real devices.

C. Separation efficiency

The separation efficiency S was quantified at the three previously identified local acoustic maxima. S is defined as $S = P_{center}/P_{tot}$, where the number of particles collected from the center outlet P_{center} is divided by the total number of particles collected from all three outlets $P_{tot} = P_{center} + P_{waste}$. The transmitted power was set to 0.5 W for frequencies 1.96 MHz and 2.05 MHz, and to 0.2 W for 1.86 MHz. For each frequency, six samples were collected at three different flow rates. A more efficient separation was achieved for the frequency of 1.86 MHz than for the other two, see Fig. 4. However, by adjusting the acoustic power and the flow rate, it was possible (at least apparent to visual inspection) to achieve close to complete separation at all frequencies.

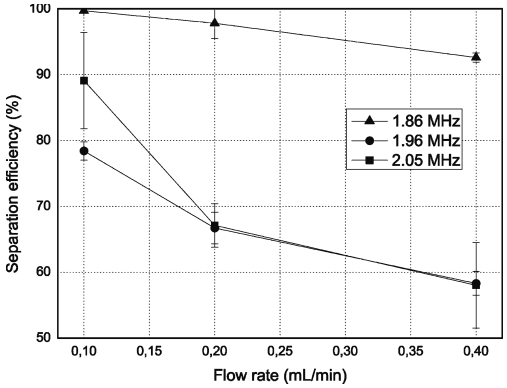

Fig. 4 Separation efficiency ($S = P_{center}/P_{tot}$) *versus* flow rate at three different frequencies.

The difference in separation efficiency between 1.96 MHz and 2.05 MHz at the flow rate of 0.1 mL min^{-1} could be ascribed to a weaker total focusing effect along the separation channel for the lower frequency, even though it is not clearly visible in Fig. 3. Additionally, this deviation could also be explained by the presence of a local focusing asymmetry within the channel junction. For higher flow velocities, the particles are not sufficiently long within this part of the channel system to be notably affected by these forces. This assumption is in agreement with the micro-PIV measurements of the acoustic radiation force presented below (top of Fig. 5).

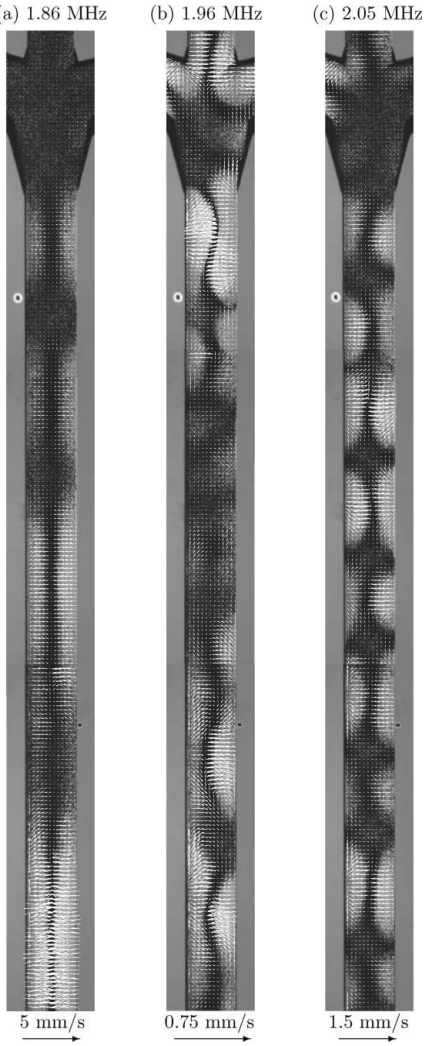

Fig. 5 Velocity vectors for particle displacements in zero flow caused by the acoustic radiation force superimposed on images of transient particle motion. (a) 1.86 MHz, 0.4 s, (b) 1.96 MHz, 2 s and (c) 2.05 MHz, 1 s. The number of pinching regions increases with the frequency. Reference vectors are shown at the bottom of each panel.

D. Measuring the acoustic radiation force with micro-PIV

When the microfluidic device is operated in flow-through mode, it is not possible to determine what the actual focusing patterns look like, since the continuous flow mode yields an image of the integrated acoustic effect along the full length of the separation channel. Therefore, in order to get a better understanding of the function of the device, more qualitative measurements are required. We apply the previously reported micro-PIV investigation approach,[16] where a combination of stop-flow and different sets of particles are used to distinguish and separate the acoustic effects. Furthermore, the identification of acoustic resonant patterns is facilitated if a larger section of the device can be examined. Of course, there is a tradeoff between low and high magnification, as a low magnification has its drawbacks in both reduced in-plane, and in-depth, resolution. Here, images were recorded at three partially overlapping positions, each with a total magnification of 3.15×, starting from the channel junction covering a distance approximately 6 mm upwards in the channel. In Fig. 5 the micro-PIV results of measurements performed with no external flow applied, but with the same frequencies and transmitted powers as were used in the flow-through measurements, are shown. The larger 5 μm particles were used, and thus, the velocity vectors are primarily showing motion of the particles caused by the acoustic radiation force.

Notably, the results are clearly favoring the 2D chamber model solutions compared to the extended 1D model. First of all, the velocity vectors are not all pointing directly towards the middle, and, thus, it is not solely a case of varying intensity along the length of the channel. Instead, the focusing is performed in certain pinching regions, as suggested by the chamber model. Secondly, the number of pinching regions is increasing with the frequency, which was also predicted by the chamber model (see Fig. 2).

From the measurements we can see that even though the 2D chamber model gives valuable and valid information about what the principal focusing pattern will look like, it is far from an exact representation of the actual resonant pattern formed in the system. This is because the acoustic resonances are not confined to the microfludic channels only, but are rather formed over the entire chip. An improved understanding of what the actual resonances may look like, can be given by a 2D chip model.[16] Two such solutions, solved for the measured dimensions of the whole device (Fig. 1), are shown in Fig. 6. These solutions are examples of global resonances that can explain the displacements and intensity irregularities of the patterns seen in the separation channel. However, it is important not to over-interpret the results of the chip model. In the actual situation there are several effects that are not taken into account by the model, such as irregular coupling from the resonator, discrepancies between the measured and actual dimensions of the device, overlapping of resonances, degenerations and 3D effects. In order to obtain a quantitative agreement, a full 3D simulation is required, including exact knowledge of the previously mentioned effects. Therefore, it is futile to search for an exact match between the measured displacements and the resonant patterns given by the 2D chip model. Nonetheless, the chip model has a value in the understanding of the formation of the acoustic resonances, although the principal solutions given by the simpler chamber model can be of larger practical value in a process where a device is designed or characterized. In contrast, an extended 1D model has little practical value, and is often misleading.

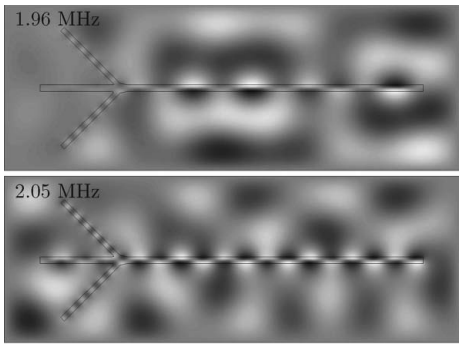

Fig. 6 Chip model simulations shown for two frequencies, supplying an illustration of what the pressure patterns forming over the whole chip may look like. In comparison with the chamber model, the patterns inside the channels are more irregular, which is in agreement with the experimental observations. Note that the model underestimates the number of pinching points in respect to the frequency in the measurements (and in the chamber model).

E. Acoustic streaming results

So far, we have mainly focused on the acoustic radiation force, which is the acoustic effect utilized by the separation device. However, at the length scale of microfluidic devices, the acoustic radiation force is not the only acoustic effect which comes into play—acoustic streaming is also present.[20,21] Compared to the acoustic radiation force, which induces a movement of the particles relative to the medium, the acoustic streaming is a movement of the entire fluid. Since the acoustic radiation force scales with the volume of the particle, the streaming motion can generally be extracted by applying tracer particles of smaller size. In this study, we used 1 μm green fluorescent polystyrene spheres. Apart from the different particles, the streaming measurements were performed under similar conditions as for the micro-PIV measurements of the acoustic radiation force. The results are seen in Fig. 7.

As is evident, the streaming in the system is fairly weak compared to the much stronger acoustic radiation forces, and thus, it has minor influence on the functionality of this particular device. The streaming should, however, not be neglected, and for many micro-devices utilizing acoustic radiation forces, unwanted streaming could clearly pose a limitation to the function and efficiency of the same. For instance, streaming might be the limiting factor for the possibility to separate sub-micrometer particles. Also worth noticing is that there is no direct relation between the acoustic radiation force and the streaming, where in one part of the channel one can be strong whereas the other is not (comparing Fig. 5 and Fig. 7). All in all, it is our recommendation that micro-devices designed to utilize the acoustic radiation force also should be examined for the presence of streaming, especially in the case where the acoustic

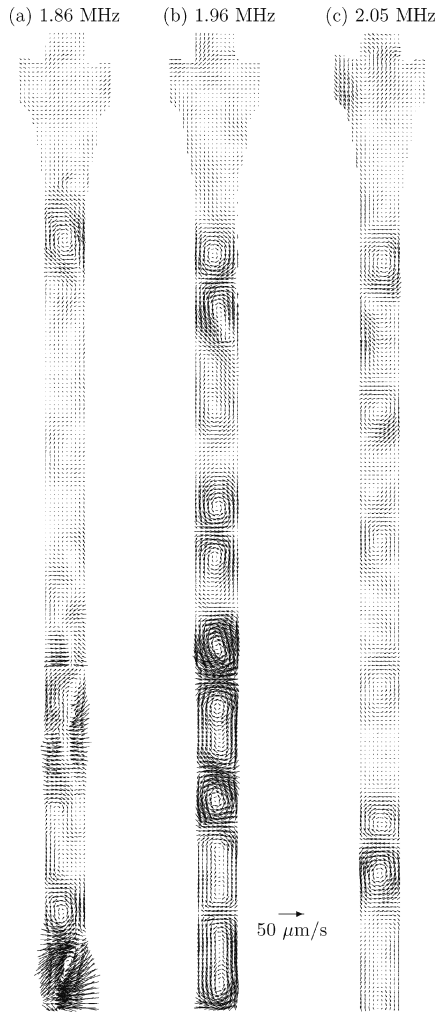

Fig. 7 Velocity vectors of fluid motion caused by acoustic streaming. 1 μm tracer particles were used for recordings at (a) 1.86 MHz, (b) 1.96 MHz and (c) 2.05 MHz. Reference vector is shown for 50 μm s^{-1}.

radiation force magnitude is low and particle translation also is governed by shearing effects, which commonly is the case for particle sizes of 1 μm or smaller.

IV. Conclusion

The function of the chip investigated here is not critically depending upon the exactness of the applied forming acoustic resonances. When operated in flow-through mode, the more refined effects are not directly apparent, which is most likely the reason why they have been overlooked, and not investigated, in previous studies. However, for several proposed micro-devices utilizing acoustic forces (especially for higher order of functionality such as successive separation stages and handling of live cells) the local effects are of great importance to the outcome, and, thus, the overall success of the device. If the local effects are not understood and controlled, these devices have little chance of making it beyond the proof of principle stage in the research lab. Therefore, we suggest that the extended 1D visualizations of acoustic coupling in microfluidic devices should be avoided, since they provide a misleading description of the phenomena in these devices.

Instead, at least a simple 2D model should be considered and included. The reported 2D model provides improved means to understand the acoustic resonance effects obtained in microfluidic acoustic resonators. Yet, further modeling improvements are needed in order to supply an efficient design tool. Furthermore, our results have shown the importance of performing qualitative spatial measurements (such as those provided by the micro-PIV method) of the forming acoustic patterns, since the actual outcome of the acoustic actuation is difficult to predict. This is especially important for devices where the effect is intended to be confined to a much smaller spatial region than what is the case in the acoustic separator device examined here.

Acknowledgements

SMH was supported through Copenhagen Graduate School of Nanoscience and Nanotechnology, in a collaboration between Dantec Dynamics A/S, and DTU Nanotech. AL thanks the Swedish Research Council for financial support.

References

1 K. Yasuda, S. Umemura and K. Takeda, *Jpn. J. Appl. Phys., Part 1*, 1995, **34**, 2715.
2 K. Yasuda, K. Takeda and S. Umemura, *Jpn. J. Appl. Phys., Part 1*, 1996, **35**, 3295.
3 X. Zhu and E. S. Kim, *Sens. Actuators, A*, 1998, **66**, 355.
4 Z. Yang, S. Matsumoto, H. Goto, M. Matsumoto and R. Maeda, *Sens. Actuators, A*, 2001, **93**, 266.
5 M. Saito, N. Kitamura and M. Terauchi, *J. Appl. Phys.*, 2002, **92**, 7581.
6 T. Lilliehorn, U. Simu, M. Nilsson, M. Almqvist, T. Stepinski, T. Laurell, J. Nilsson and S. Johansson, *Ultrasonics*, 2005, **43**, 293.
7 F. Petersson, A. Nilsson, H. Jonsson and T. Laurell, *Anal. Chem.*, 2005, **77**, 1216.
8 A. Nilsson, F. Petersson, H. Jonsson and T. Laurell, *Lab Chip*, 2004, **4**, 131.
9 H. Jonsson, C. Holm, A. Nilsson, F. Petersson, P. Johns-son and T. Laurell, *Ann. Thorac. Surg.*, 2004, **78**, 1572.
10 H. Li and T. Kenny, *Conf. Proc. 26 Ann. Int. Conf. IEEE. Engineering, in Medicne and Biology*, 2004, **3**, 2631, vol. 4.
11 J. J. Hawkes, R. W. Barber, D. R. Emerson and W. T. Coakley, *Lab Chip*, 2004, **4**, 446.
12 F. Petersson, L. Aberg, A.-M. Sward-Nilsson and T. Laurell, *Anal. Chem.*, 2007, **79**, 5117.
13 L. V. King, *Proc. R. Soc. London, Ser. A*, 1934, **147**, 212.
14 K. Yosioka and Y. Kawasima, *Acustica*, 1955, **5**, 167.
15 L. P. Gorkov, *Sov. Phys. Dokl.*, 1962, **6**, 773.
16 S. M. Hagsäter, T. Glasdam Jensen, H. Bruus and J. P. Kutter, *Lab Chip*, 2007, **7**, 1336.
17 F. Petersson, A. Nilsson, C. Holm, H. Jonsson and T. Laurell, *Analyst*, 2004, **129**, 938.
18 T. Laurell, F. Petersson and A. Nilsson, *Chem. Soc. Rev.*, 2007, **36**, 492.

19 S. M. Hagsäter, C. H. Westergaard, H. Bruus and J. P. Kutter, *Exp. Fluids*, 2008, **44**, 211.
20 Lord Rayleigh, *Proc. R. Soc. London*, 1883, **36**, 10.
21 N. Riley, *Annu. Rev. Fluid Mech.*, 2001, **33**, 43.
22 J. F. Spengler, M. Jekel, K. T. Christensen, R. J. Adrian, J. J. Hawkes and W. T. Coakley, *Bioseparation*, 2001, **9**, 329.
23 J. F. Spengler, W. T. Coakley and K. T. Christensen, *AIChE J.*, 2003, **49**, 2773.
24 L. A. Kuznetsova and W. T. Coakley, *J. Acoust. Soc. Am.*, 2004, **116**, 1956.
25 L. A. Kuznetsova, S. Khanna, N. N. Amso and W. T. Coakley, *J. Acoust. Soc. Am.*, 2005, **117**, 104.

V

Anal. Chem. **2008,** *80,* 5178–5185

Acoustophoresis in Wet-Etched Glass Chips

Mikael Evander,* Andreas Lenshof, Thomas Laurell, and Johan Nilsson

The Department of Electrical Measurements, Lund University, P.O. Box 118, 211 00 Lund, Sweden

Acoustophoresis in microfluidic structures has primarily been reported in silicon microfabricated devices. This paper demonstrates, for the first time, acoustophoresis performed in isotropically etched glass chips providing a performance that matches that of the corresponding silicon microdevices. The resonance mode characteristics of the glass chip were equal to those of the silicon chip at its fundamental resonance. At higher order resonance modes the glass chip displays resonances at lower frequencies than the silicon chip. The cross-sectional profiles of acoustically focused particle streams are also reported for the first time, displaying particles confined in a vertical band in the channel center for both glass and silicon chips. A particle extraction efficiency of 98% at flow rates up to 200 μL/min (2% particle concentration) is reported for the glass chip at the fundamental resonance. The glass and silicon chips displayed equal particle extraction performance when tested for increasing particle concentrations of 2−15%, at a flow velocity of 12.9 cm/s for the glass chip and 14.8 cm/s for the silicon chip.

Continuous separation of cells and particles by means of microsystem technology and microfluidics is gaining increased interest in the biomedical and biochemical field. Several techniques are available that either use externally induced forces as the separation mechanism or the geometry of the microfluidic device itself as the separating element. Magnetophoresis[1–3] and dielectrophoresis[4–6] are using magnetic and electric fields, respectively, whereas pinched flow fractionation,[7–9] hydrodynamic filtration,[10–12] and obstacle induced separation[13–15] rely on the combination of laminar flow and the channel geometry. Another alternative for separation with externally induced forces is the use of acoustic forces, acoustophoresis, which is the topic of this paper.

Acoustic forces in microsystems have proven to be a very versatile and gentle tool for on-chip handling of particles and cells. The forces created by standing waves can be used for such diverse tasks as eliminating lipid emboli from shed blood in thoracic surgery,[16,17] blood component fractionation and particle sizing,[18] contaminated blood plasma replacement[19] and buffer media exchange,[20] specific selection of affinity binding phages from bacteriophage libraries,[21] rare event selection,[22] positioning,[23–25] and trapping.[26–28] In addition, several investigations in both macrosystems[29,30] and microsystems[17,26,31,32] have shown that no adverse effects related to the acoustic handling can be seen on cells.

Commonly, the standing wave is formed between two parallel walls, using one wall as an ultrasonic transmitter and the other wall as a reflector. Rectangular geometries with vertical walls have most commonly been used, but systems using focused sound waves have also been reported.[33] The standing wave can be formed either between the bottom and the top of a fluidic channel,

* To whom correspondence should be addressed. Phone: +46-46-222 75 27. Fax: +46-46-222 45 27. E-mail: Mikael.Evander@elmat.lth.se.

(1) Pamme, N.; Manz, A. *Anal. Chem.* **2004**, *76*, 7250–7256.
(2) Pamme, N. *Lab Chip* **2006**, *6*, 24–38.
(3) Han, K. H.; Frazier, A. B. *Lab Chip* **2006**, *6*, 265–273.
(4) Gonzalez, C. F.; Remcho, V. T. *J. Chromatogr., A* **2005**, *1079*, 59–68.
(5) Doh, I.; Cho, Y. H. *Sens. Actuators, A* **2005**, *121*, 59–65.
(6) Hu, X. Y.; Bessette, P. H.; Qian, J. R.; Meinhart, C. D.; Daugherty, P. S.; Soh, H. T. *Proc. Natl. Acad. Sci. U.S.A.* **2005**, *102*, 15757–15761.
(7) Yamada, M.; Nakashima, M.; Seki, M. *Anal. Chem.* **2004**, *76*, 5465–5471.
(8) Takagi, J.; Yamada, M.; Yasuda, M.; Seki, M. *Lab Chip* **2005**, *5*, 778–784.
(9) Zhang, X. L.; Cooper, J. M.; Monaghan, P. B.; Haswell, S. J. *Lab Chip* **2006**, *6*, 561–566.
(10) Yamada, M.; Seki, M. *Lab Chip* **2005**, *5*, 1233–1239.
(11) Yamada, M.; Seki, M. *Anal. Chem.* **2006**, *78*, 1357–1362.
(12) Yang, S.; Undar, A.; Zahn, J. D. *Lab Chip* **2006**, *6*, 871–880.
(13) Huang, L. R.; Cox, E. C.; Austin, R. H.; Sturm, J. C. *Science* **2004**, *304*, 987–990.
(14) Davis, J. A.; Inglis, D. W.; Morton, K. J.; Lawrence, D. A.; Huang, L. R.; Chou, S. Y.; Sturm, J. C.; Austin, R. H. *Proc. Natl. Acad. Sci. U.S.A.* **2006**, *103*, 14779–14784.
(15) Inglis, D. W.; Davis, J. A.; Austin, R. H.; Sturm, J. C. *Lab Chip* **2006**, *6*, 655–658.
(16) Petersson, F.; Nilsson, A.; Holm, C.; Jonsson, H.; Laurell, T. *Analyst* **2004**, *129*, 938–943.
(17) Jönsson, H.; Holm, C.; Nilsson, A.; Petersson, F.; Johnsson, P.; Laurell, T. *Ann. Thorac. Surg.* **2004**, *78*, 1572–1578.
(18) Petersson, F.; Aberg, L.; Sward-Nilsson, A. M.; Laurell, T. *Anal. Chem.* **2007**, *79*, 5117–5123.
(19) Petersson, F.; Nilsson, A.; Jonsson, H.; Laurell, T. *Anal. Chem.* **2005**, *77*, 1216–1221.
(20) Hawkes, J. J.; Barber, R. W.; Emerson, D. R.; Coakley, W. T. *Lab Chip* **2004**, *4*, 446–452.
(21) Augustsson, P.; Persson, J.; Ohlin, M.; Laurell, T. *Proceedings of Micro Total Analysis Systems*, Paris, France, 2007; pp 1813−1815.
(22) Grenvall, C.; Augustsson, P.; Petersson, F.; Laurell, T. *Proceedings of Micro Total Analysis Systems*, Paris, France, 2007; pp 1813−1815.
(23) Neild, A.; Oberti, S.; Beyeler, F.; Dual, J.; Nelson, B. J. *J. Micromech. Microeng.* **2006**, *16*, 1562–1570.
(24) Neild, A.; Oberti, S.; Radziwill, G.; Dual, J. *Biotechnol. Bioeng.* **2007**, *97*, 1335–1339.
(25) Hawkes, J. J.; Long, M. J.; Coakley, W. T.; McDonnell, M. B. *Biosens. Bioelectron.* **2004**, *19*, 1021–1028.
(26) Evander, M.; Johansson, L.; Lilliehorn, T.; Piskur, J.; Lindvall, M.; Johansson, S.; Almqvist, M.; Laurell, T.; Nilsson, J. *Anal. Chem.* **2007**, *79*, 2984–2991.
(27) Spengler, J. F.; Coakley, W. T. *Langmuir* **2003**, *19*, 3635–3642.
(28) Svennebring, J.; Manneberg, O.; Wiklund, M. *J. Micromech. Microeng.* **2007**, 2469.
(29) Pui, P. W. S.; Trampler, F.; Sonderhoff, S. A.; Gröschl, M.; Kilburn, D. G.; Piret, J. M. *Biotechnol. Prog.* **1995**, *11*, 146–152.
(30) Doblhoffdier, O.; Gaida, T.; Katinger, H.; Burger, W.; Groschl, M.; Benes, E. *Biotechnol. Prog.* **1994**, *10*, 428–432.
(31) Hultström, J.; Manneberg, O.; Dopf, K.; Hertz, H. M.; Brismar, H.; Wiklund, M. *Ultrasound Med. Biol.* **2007**, *33*, 145–151.
(32) Bazou, D.; Kuznetsova, L. A.; Coakley, W. T. *Ultrasound Med. Biol.* **2005**, *31*, 423–430.
(33) Wiklund, M.; Toivonen, J.; Tirri, M.; Hanninen, P.; Hertz, H. M. *J. Appl. Phys.* **2004**, *96*, 1242–1248.

10.1021/ac800572n CCC: $40.75
Published on Web 05/20/2008

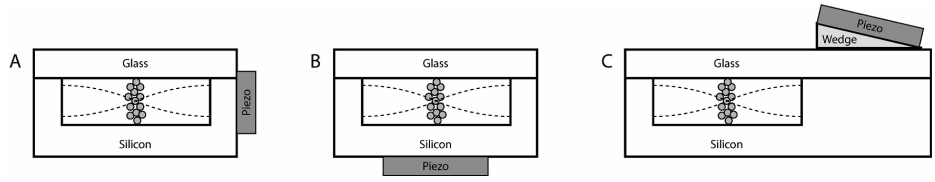

Figure 1. (A) The acoustic standing wave is induced parallel to the wave propagation. (B) The standing wave is induced perpendicular to the primary wave propagation. (C) A wedge is used to couple the waves into the cavity.

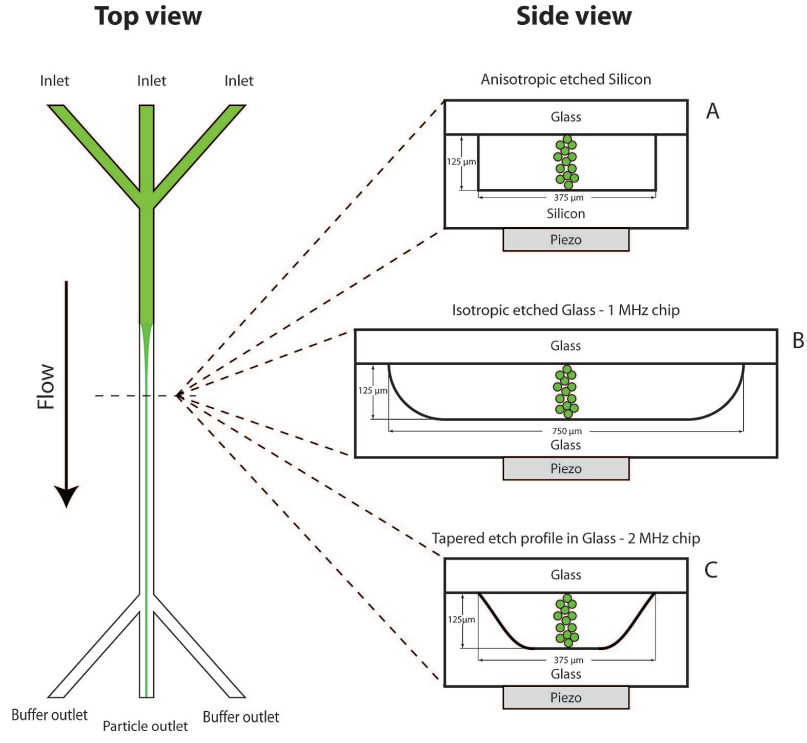

Figure 2. Schematic of the channel design and cross section of the different separation chips investigated. Panel A is the anisotropic silicon chip, panel B the isotropic 1 MHz glass chip, and panel C is the actual shape of the cross section of the 2 MHz glass chip.

between the side walls, or as a combination of both to create a two-dimensional force field.[22,34]

The way of actuation depends both on the chip design and in which direction the force field should be active. The most straightforward approach is to position the ultrasonic transducer with its direction of transmission parallel to the desired force field direction, Figure 1A. It is, however, also possible to create a lateral resonance perpendicular to the direction of transmission,[35] by positioning the transducer as seen in Figure 1B. This can be done with a standard transducer, a shear transducer, or using wedges to increase the amount of shear waves induced,[36] see Figure 1C.

Most devices using lateral resonances are fabricated in silicon using either anisotropic wet etching or deep reactive ion etching (DRIE). As silicon is a relatively expensive material and the fabrication process requires mask aligners for precise pattern transfer, alternative materials with easier fabrication processes are of interest. An alternative way of fabrication is by creating a sandwich structure with different layers defining the dimensions of the channel as well as the chip.[34] The precision in such a method is, however, limited and may cause problems when small tolerances are requested.

Polymers and glass are becoming preferred material bases in chemical and biomedical microdevices as they offer cheaper and less complex fabrication means. Designing polymer-based microdevices for ultrasonic actuation is, however, a nontrivial task due to the large acoustic attenuation. In this perspective, glass has several attractive properties beyond low cost such as optical

(34) Haake, A.; Neild, A.; Kim, D. H.; Ihm, J. E.; Sun, Y.; Dual, J.; Ju, B. K. *Ultrasound Med. Biol.* **2005**, *31*, 857–864.
(35) Nilsson, A.; Petersson, F.; Jonsson, H.; Laurell, T. *Lab Chip* **2004**, *4*, 131–135.
(36) Wiklund, M.; Gunther, C.; Lemor, R.; Jager, M.; Fuhr, G.; Hertz, H. M. *Lab Chip* **2006**, *6*, 1537–1544.

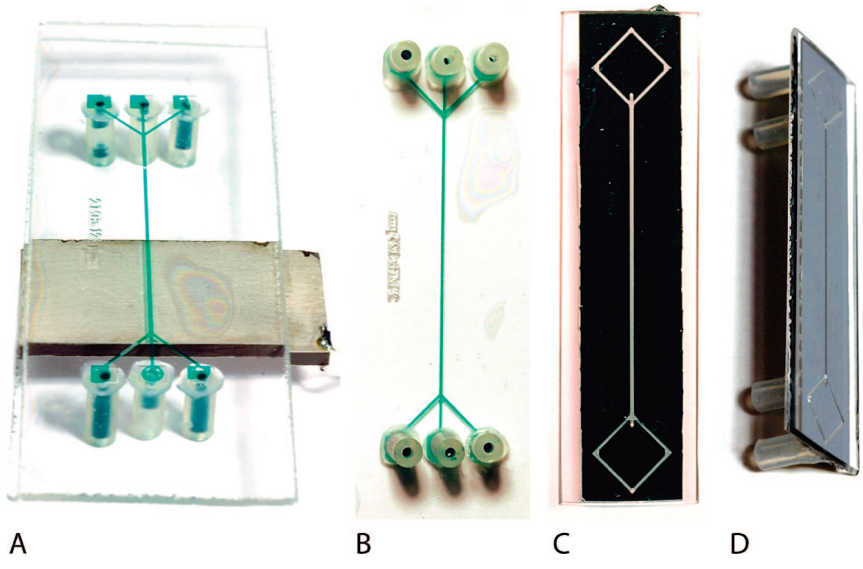

Figure 3. (A) Wet-etched glass chip with the piezoelectric element attached using ultrasonic gel. The back side of the glass chip with silicone tubing (B). The anisotropic silicon chip used for comparison can be seen in (C) and uses the same kind of silicone tubing for fluidic access from the back side (D).

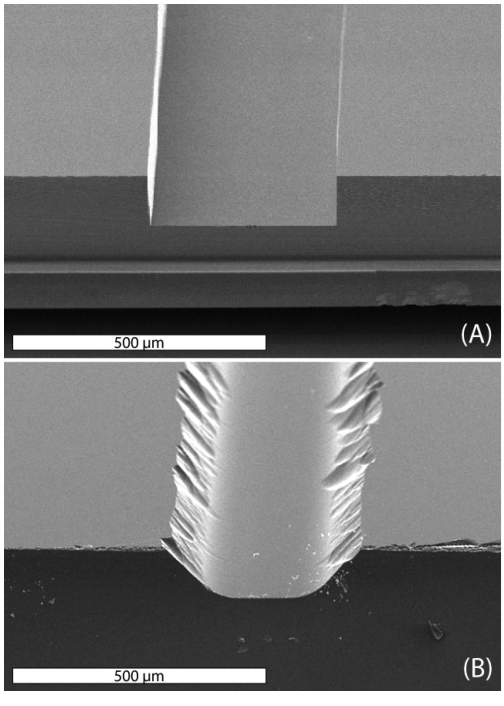

Figure 4. Scanning electron microscopy (SEM) images showing the cross section of the silicon (A) and glass (B) channel.

transparency, hydrophilic surface properties, electrical insulation, and good chemical resistance. Glass also bonds well to silicon and has a very low acoustic attenuation while being amenable to a multitude of micromachining processes. Isotropic wet etching is the most widely used fabrication method offering high performance at low cost. For more complex structures, DRIE[37] and molding/hot embossing[38] are also possible, but both techniques are more laborious and require advanced process equipment. Powder blasting can be employed to manufacture simple structures such as through holes and channels with limited demands in surface smoothness.[39]

The use of glass as the bulk material enables the use of microscopy techniques that have not been possible to use in previously reported acoustic silicon devices. One example is phase contrast imaging, a method commonly used to image cells or other small, transparent objects. Another example is Raman spectroscopy, where recent development projects cancer cell detection in clinical samples.[40] Raman spectroscopy can be anticipated to be combined with acoustic microchip cell handling for label-free on-chip cell sorting. The possibilities in achieving optimal light conditions are also vastly increased when a completely transparent material is used and both reflective and transmission microscopy can be used.

The technique of manipulating cells and particles in the microfluidic domain with acoustic forces relies on an acoustic standing wave generated in an enclosed fluid volume on a chip. The magnitude of the radiation force acting on the particles is strongly dependent on the radius of the particle (to the third

(37) Park, J. H.; Lee, N. E.; Lee, J.; Park, J. S.; Park, H. D. *Microelectron. Eng.* **2005**, *82*, 119–128.
(38) Takahashi, M.; Murakoshi, Y.; Maeda, R.; Hasegawa, K. *Microsyst. Technol.* **2007**, *13*, 379–384.
(39) Pu, Q. S.; Luttge, R.; Gardeniers, H.; van den Berg, A. *Electrophoresis* **2003**, *24*, 162–171.
(40) Chan, J. W.; Taylor, D. S.; Lane, S. M.; Zwerdling, T.; Tuscano, J.; Huser, T. *Anal. Chem.* **2008**, *6*, 2180–2187.

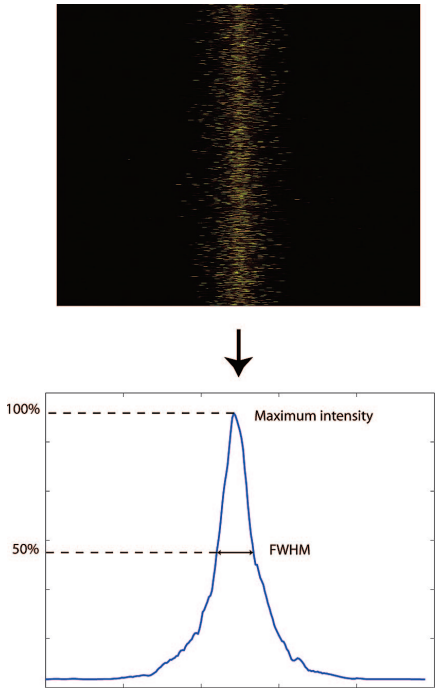

Figure 5. Line scans in the fluorescent image, top image, are averaged to achieve an intensity plot of the lateral particle distribution, lower image. For each confocal depth, the corresponding average full width at half-maximum value (fwhm) is calculated. The fwhm value is used as a representative width of the particle band, intensity-coded using the maximum intensity.

power) and proportional to the acoustic frequency.[41,42] The relationship between the density and compressibility of the particle and the surrounding medium will determine if the particle will move toward a pressure node or an antinode in the standing wave. For instance, a particle suspension flowing through a microchannel with a width of a half-wavelength will experience a radiation force concentrating all particles into a focused band in the center of the channel, see Figure 2. The laminar flow in the microchannel prevents the particles from dispersing again, and if the microchannel ends in a three-way split, the concentrated particles can be collected via the central outlet while the clear medium exits through the side outlets, and a simple separation/concentration step has been achieved.

Our most recent experimental data demonstrate that it is possible to design isotropically wet-etched glass devices that have particle manipulation properties comparable to what previously only has been reported for silicon-based substrates. This paper presents for the first time piezoelectrically actuated particle separation in isotropically etched all-glass microfluidic chips with separation properties matching the performance of silicon-based acoustic separators. The performance of the glass chip is compared to the corresponding anisotropically wet-etched silicon chip in a continuous flow separation application. A continuous medium exchange with live cells using acoustic forces in a glass chip is also presented.

MATERIALS AND METHODS

Design and Fabrication. A basic chip design with three inlets, three outlets, and a separation channel was used to compare the performance between the anisotropic silicon chip and the isotropic glass chip, see Figure 3. The separation performance was measured by focusing and separating 5 μm polyamide microparticles from their suspending medium. The particle suspension was a commercially available blood phantom (Danish Phantom Design, Jyllinge, Denmark) designed to mimic the viscosity, density, and sound velocity of human blood.

The glass and silicon chips were both designed to have a lateral resonance at 2 MHz. In order to achieve a single node at 2 MHz, the channel widths were designed to be 375 μm, i.e., $\lambda/2$ at 2 MHz in water. As the glass chips have an isotropic cross section, the widest part of the channel was designed to be 375 μm. Both chips were etched to a depth of 125 μm and had a 30 mm long separation channel. The glass chip was provided with separate connections, Figure 3B, to the side inlets and outlets, whereas the corresponding inlets and outlets in the silicon chip were united to one single outlet, Figure 3D.

The silicon separator was fabricated by means of double-sided photolithography and anisotropic wet etching using KOH. The chip was sealed by anodic bonding of a glass lid. A more detailed description of the microfabrication of the silicon chip can be found in Nilsson et al.[35] The cross section of the anisotropic separation channel was rectangular with vertical walls, see Figure 4A.

The glass chip was fabricated by wet etching 0.7 mm thick borosilicate chromium blanks (Telic Company, Valencia, CA), precoated with 0.5 μm positive resist, using a $HF/HNO_3/H_2O$ mixture. After etching, fluidic access holes were drilled using a 1 mm diamond glass drill. The etched and drilled chip was then cleaned in KOH in an ultrasonic bath and was thermally bonded to a clean borosilicate glass lid to form a sealed chip. Silicone tubing was glued to the fluidic access holes to hold standard $^1/_{16}$ in. Teflon tubing.

When etching glass in hydrofluoric acid, the resulting shape of the side walls depends on different parameters.[43–45] The adhesion between the masking layer and the glass, the pH or temperature in the etch solution, and the amount and type of stirring used are examples of parameters that can change the shape of the side walls.

The etched 2 MHz glass channel did not have the typical isotropic side-wall geometry, see Figure 4B. This is most likely caused by limited convective exchange of etch components in the zones underetching the mask. A similar channel with a twice as wide mask, with all other parameters unchanged, resulted in a perfect semicircular side wall.

Instrumentation. The chips were actuated using an 11 mm $\times$ 32 mm external PZT piezoelectric transducer (PZ26, Ferroperm Piezoceramics, Kvistgard, Denmark) with a thickness of 1 mm, corresponding to a fundamental resonance of 2 MHz. The

(41) Gorkov, L. P. *Sov. Phys. Dokl.* **1962**, *6*, 773–775.
(42) Laurell, T.; Petersson, F.; Nilsson, A. *Chem. Soc. Rev.* **2007**, *36*, 492–506.
(43) Kal, S.; Haldar, S.; Lahiri, S. K. *Microelectron. Reliab.* **1990**, *30*, 719–722.
(44) Parisi, G. I.; Haszko, S. E.; Rozgonyi, G. A. *J. Electrochem. Soc.* **1977**, *124*, 917–921.
(45) Spierings, G. *J. Mater. Sci.* **1993**, *28*, 6261–6273.

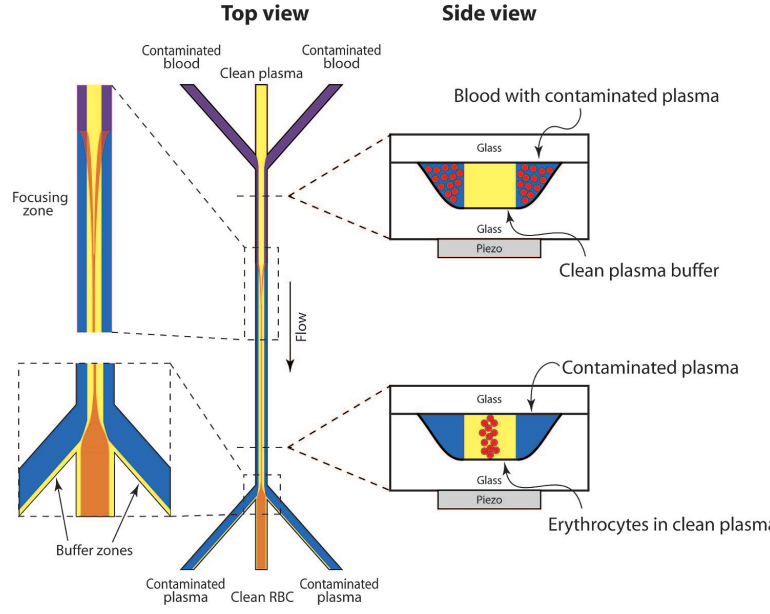

Figure 6. Blood wash and medium exchange principle. Contaminated blood enters from the side inlets, and clean plasma enters through the central inlet. The blood cells are switched over to the clean plasma by the acoustic radiation force and exit through the center outlet while the contaminated medium exits through the side outlets.

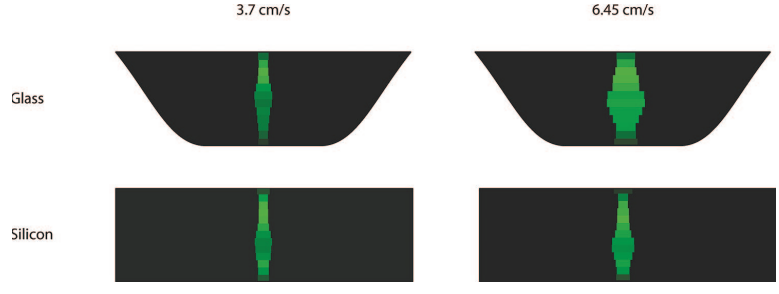

Figure 7. Cross-sectional view of the band formation in the channels based on confocal image data. The width of the particle band is decided by the fwhm value, and the intensity is correlated to the maximum intensity from the averages line scan. The widening of the particle band in the center of the channel is caused by the parabolic flow profile causing the particle in the center to have less time to focus into a narrow band.

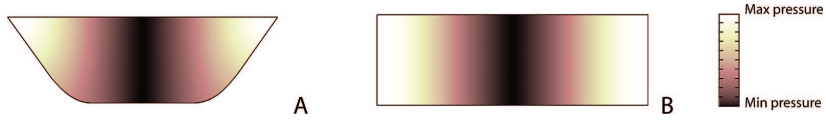

Figure 8. Squared pressure field, proportional to the acoustic force, in the glass cavity (A) and the silicon cavity (B) as simulated in COMSOL Multiphysics using eigen-frequency analysis. The simulation predicts the fundamental frequency to occur at 2.36 MHz for the glass chip and 2.0 MHz for the silicon chip.

transducer was applied to the back side of the chips using ultrasonic gel for good acoustic coupling and clamped in place, see Figure 3A. The transducer was actuated using a Hewlett-Packard 3325B waveform generator and an Amplifier Research 75A250 amplifier. The input power to the transducer was set at 0.5 W for all experiments and monitored using a Bird model 5000-EX digital power meter.

The confocal image data was acquired with an Olympus BX51WI microscope using the Fluoview 300 software. Fluorescent particles with a diameter of 4.1 μm were focused using the acoustic standing waves, and images of the focused particle band were taken at different depth in the channel using a motorized microscope stage and a step size of 10 μm. For each confocal image, the line scans were averaged to obtain the intensity profile

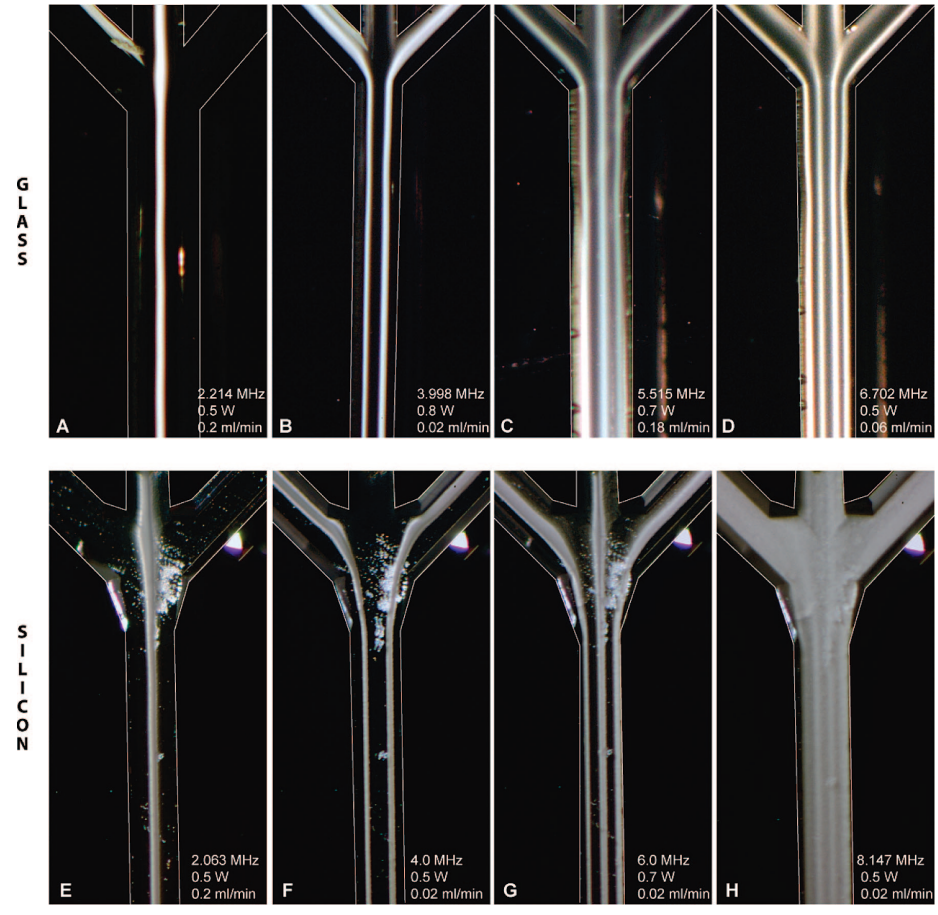

Figure 9. Particle focusing at higher harmonics: the glass chip at the top (A−D) and the silicon chip at the bottom (E−H). The channel walls have been outlined to improve the visibility.

of the lateral particle distribution and the full width at half-maximum (fwhm) and maximum intensity were calculated, see Figure 5. With the use of these data, a corresponding image was created in Adobe Illustrator where the fwhm value was used for the width of the particle band and color intensity of the band was correlated to the maximum intensity value for each confocal depth.

The separation efficiency was measured using a Beckman Coulter Multisizer 3 where the amount of particles in the center outlet was compared to the total amount of particles in all outlets. The samples were collected using 50 μL loops attached to an automated switch valve (Valco Instrument Company Inc.) while running the continuous separation.

Blood Washing and Medium Exchange. A continuous medium exchange with human blood was performed as an alternative mode of performance evaluation.[19] Evans blue (Merck AG, Darmstadt, Germany) was used to simulate a contaminant and was added to human whole blood. The erythrocytes were diluted to a hematocrit of 2% using pure plasma, and 180 μg/mL of Evans blue was added. The contaminated blood was infused through the side inlets at 70 μL/min while clean plasma was infused through the center inlet at 130 μL/min. The acoustic forces moved the erythrocytes from the contaminated plasma into the clean plasma fraction at the center of the channel, Figure 6. An input power of 0.8 W (8 Vpp) was used to ensure a good focusing of cells in the channel center. The erythrocytes transferred to the clean plasma were collected via the center outlet at 70 μL/min while the contaminated plasma continued to the side outlets and was withdrawn with 65 μL/min in each outlet. The different infusion/withdrawal rates ensured that a minor part of the clean buffer zone was directed to the side outlets and reduced the risk of contaminants spilling into the clean center outlet.

The blood washing efficiency was evaluated using a Labsystems Multiskan Multisoft photometric plate reader at an absorption wavelength of 595 nm. The ratio of absorbance in the contaminated media and the washed blood was compared, and an average of six different samples was calculated.

RESULTS AND DISCUSSION

Resonance Mode Characterization. By visual inspection, the best particle focusing for the chips occurred at 2.063 MHz for

the silicon chip and at 2.214 MHz for the glass chip. The particles were focused into the center of the channel with what appeared to be a uniform distribution of particles along the depth of the channel, much like the schematic image shown in Figure 2. To verify the particle distribution, a confocal microscopy scan was performed on fluorescent particles focused at two different flow velocities for each device. The result, seen in Figure 7, shows a slight bulging of the particle band in the center of the channel for both chips. This is most likely explained by the parabolic flow profile, giving a maximal flow velocity in the center of the channel causing particles there to be exposed to and focused by the acoustic standing wave for a shorter time period. The color intensity in the figure is a measure of the particle density, thus being higher in the tightly focused areas as compared to the widened zones.

With the use of COMSOL Multiphysics, an eigen-frequency analysis of the two chips was performed. The simulations predicted a fundamental frequency of 2.36 MHz for the glass chip and 2.0 MHz for the silicon chip. The squared pressure amplitudes, proportional to the acoustic radiation force, show a single pressure node in the center of both channels, see Figure 8. The simulations predicted the harmonics to appear at 4, 6, and 8 MHz for the silicon chip, whereas the glass chip showed a different behavior with harmonics at 4.3, 5.7, and 7.4 MHz.

The glass and silicon chip showed similar behavior in focusing particles when operated at their fundamental frequency, see Figure 9, parts A and E. The particle suspension used was well-focused and exited through the center outlet as expected. The first harmonic, twice the fundamental frequency, was tested to focus the particles into two bands, Figure 9, parts B and F. The glass chip displayed a slightly lower focusing efficiency, with broader particle bands, at this frequency, but the difference between the two materials was marginal.

At the second harmonic a more distinct difference between the chips was seen. The glass chip deviated from the expected frequency of 6.6 MHz and displayed a resonance at 5.515 MHz instead which correlates well with the resonance frequency predicted by the simulations. The focusing was, however, superior to that of the silicon chip where the flow rate had to be lowered to 0.02 mL/min at 0.5 W acoustic input power in order to get a reasonable picture of the band formation, which should be compared to 0.18 mL/min for the glass chip, Figure 9, parts C and G.

The same trend was repeated at the third harmonic where it hardly was possible to achieve a four-band focusing for the silicon chip, whereas the glass chip clearly showed a better focusing, Figure 9, parts D and H. The resonance frequency for the glass chip again differed from the expected 8.8 MHz and was now found at 6.702 MHz.

The reason for the deviation in resonance frequency is not clear but is most likely associated with the tapered shape of the side walls. For a rectangular geometry there is an analytical solution to the different lateral resonances. An isotropic channel is, however, more complex, and the resonances can only be determined by simulations.[46] As a comparison, a wet-etched glass chip with a fundamental resonance at 1.0 MHz, thus with twice the width of the 2 MHz chip, was tested. This chip showed a very nice isotropic cross section as opposed to the 2 MHz chip, see Figure 2B. The 1 MHz chip performed a single-band focusing at 1 MHz and was as expected slightly inferior to the 2 MHz chip in focusing strength due to the lower frequency. However, all of the harmonics for this chip were at the expected multiples of the fundamental frequency: 2.0, 3.0, and 4.0 MHz, respectively. Clearly, more work needs to be done in this area to fully understand how the geometry of the cross section of the chip affects the resonance frequencies.

(46) Townsend, R. J.; Hill, M.; Harris, N. R.; White, N. M. *Ultrasonics* **2006**, *44*, E467−E471.

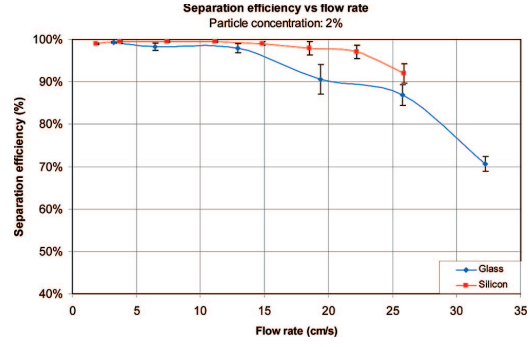

Figure 10. Separation efficiency vs the flow velocity at a particle concentration of 2% and an acoustic power input of 0.5 W. The performance of the two chips is similar although the silicon chip has slightly higher separation efficiency at higher flow velocities. The flow velocities used correspond to volumetric flow rates of 50−700 μL/min.

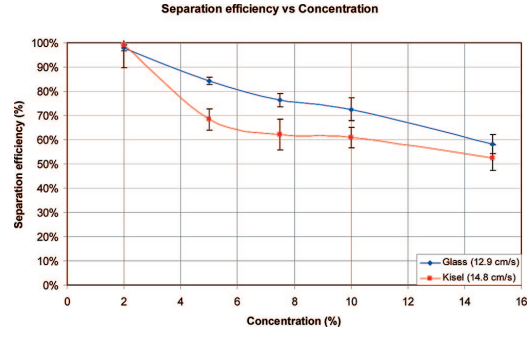

Figure 11. Separation efficiency plotted vs particle concentration. The two chips show a similar behavior although the silicon chip shows slightly lower separation efficiency at a slightly higher flow velocity.

Table 1. Comparison in Contaminant Removal Efficiency between a Glass Chip and a Silicon Chip[a]

	glass	silicon
separation efficiency (%)	92.8 ± 3.9	89.3 ± 5.8
contaminant removal (%)	97.1 ± 1.1	92.3 ± 1.2

[a] An amount of 180 μg/mL of Evan's blue was used as a contaminant, and the blood was diluted with plasma to a hematocrit of 2%.

Particle Focusing Efficiency. The separation efficiency of the particle separation in both glass and silicon chips versus an

increasing flow velocity can be seen in Figure 10. The separation efficiency clearly decreased as the flow velocity increased since the particles spent shorter time in the acoustic force field. At flow velocities up to 10 cm/s, the separation efficiency of the glass and silicon chip was comparable; however, at higher flow velocities the performance of the glass chip decreased as compared to the silicon chip.

While performing the experiments, volumetric flow rates were set on the syringe pumps. Due to the different cross sections of the chips, the flow velocities, and thus the retention times, of the particles will be different in the channels. The corresponding flow velocities were therefore calculated using a three-dimensional COMSOL simulation. For a volumetric flow of 100 μL/min, the glass chip has an average flow velocity of 6.45 cm/s, whereas the silicon chip, with a larger cross section, has an average flow velocity of 3.7 cm/s. Thus, for a given volumetric flow rate, the silicon chip will have a slower velocity and particles will spend more time in the force field.

The volumetric flow rate is many times a crucial factor, and commonly in microfluidic applications a volumetric flow of a few hundred microliters per minute is more than sufficient. If even higher flow rates are needed, several parallel channels actuated by a single transducer can be used.[17] It is also possible to increase the input power and create a stronger force field that will work even for higher flow rates. A higher input power may, however, result in an elevated temperature in the channel due to thermal losses in the transducer. This effect can be counteracted by using heat sinks or Peltier elements and work as a method of controlling the thermal environment on-chip.[26,28]

The separation efficiency for the silicon and glass chip with regards to the inlet sample concentration was compared, see Figure 11. As expected from earlier tests with silicon separation chips,[35] the separation efficiency decreases with particle concentrations ranging from 2−15%. The silicon and the glass chip show almost the same behavior for increasing concentration.

Medium Exchange in Cell Washing. Acoustic manipulation of cells offers a mode of noninvasive and noncontact spatial localization of cells in microfluidic systems. Most importantly, it has been shown in several experiments that acoustic cell manipulation does not induce any traceable adverse reactions to the exposure to an acoustic force field.[17,26,31] This fact opens up for the use of acoustic force manipulation to perform a set of unit operations that can be combined to design relevant bioanalytical sequences, integrated in a single microfluidic device. One such application is the possibility to perform a buffer exchange without having to expose the cells to a mechanically stressing event such as centrifugation. In this case a separation channel operated at its fundamental resonance and supplied with two buffer inlets as outlined in Figure 6 can switch cells from one buffer medium to another by the acoustophoretic process investigated herein.

During the medium exchange, a separation efficiency of 92.8% ± 3.9% was achieved and 97.1% ± 1.1% of the contaminant was removed from the blood using the glass chip, at a blood sample input flow rate of 70 μL/min. This can be compared to a separation efficiency of 89.3% ± 5.8% and a contaminant removal of 92.3% ± 1.2% for the silicon chip, see Table 1. If higher levels of medium exchange are requested it is advised that this process is repeated in a sequential step.

CONCLUSIONS

This paper reports for the first time an all-glass microfabricated chip for acoustic force control of cells and particles in a continuous microfluidic process. Essentially equal performance of the glass chip and its silicon counterpart is reported. The possibility to use acoustic forces in wet-etched glass channels may make microchip-based acoustic cell and particle manipulation widely available to the bioanalytical microfluidics community. The microfabrication of glass is less complicated than the silicon fabrication and also requires fewer and less expensive instruments. Glass is also a cheaper material, and the isotropic nature of the fabrication process allows for a larger degree of freedom in chip design.

The separation efficiency of the glass chips was above 97% for a 2% suspension for flow rates up to 200 μL/min. There are several ways of increasing the throughput in a glass chip while maintaining the high separation efficiency. A rather straightforward approach would be to use several parallel channels, but it is also possible to increase the input power. By increasing the input power the risk of elevating the temperature on-chip is increased, and measures to keep the temperature stable may have to be taken.

The acoustic glass separator has proven to be capable of handling the same tasks as the acoustic silicon separator, including particle separation and continuous medium exchange in human whole blood.

ACKNOWLEDGMENT

The authors thank the Swedish Research Council, the Carl Trygger Foundation, the Swedish Foundation for Strategic Research, the Crafoord Foundation, and the Royal Physiographic Society in Lund for financial support.

SUPPORTING INFORMATION AVAILABLE

A video showing the focusing of a particle suspension in a 2 MHz glass chip. This material is available free of charge via the Internet at http://pubs.acs.org.

Received for review March 19, 2008. Accepted April 14, 2008.

AC800572N

VI

ACOUSTIC WHOLE BLOOD PLASMAPHERESIS CHIP EMPLOYED FOR PSA MICROARRAY DIAGNOSTICS

Andreas Lenshof[1], Asilah Ahmad-Tajudin[1], Kerstin Järås[1,2], Ann-Margret Swärd-Nilsson[3], Lena Åberg[3], György Marko-Varga[1], Johan Malm[2], Hans Lilja[2,4] and Thomas Laurell[1*]

[1]Department of Electrical Measurements, Lund University, Box 118, 221 00 Lund, Sweden
[2]Department of Laboratory Medicine, Division of Clinical Chemistry, Lund University, Malmo¨ University Hospital, Malmö, Sweden
[3]Blood Centre Skane, Lund University Hospital, Lund, Sweden
[4]Departments of Clinical Laboratories, Surgery (Urology), and Medicine (GU-Oncology), Memorial Sloan-Kettering Cancer Center, New York, New York 10021

*Corresponding author. E-mail: thomas.laurell@elmat.lth.se. Phone: +46 (0)46 2227540. Fax: +46 (0)46 2224527.

ABSTRACT

Generating high quality plasma from whole blood is of major interest for many biomedical analysis and clinical diagnostic methods. The handling and processing of fluids with high cell content, like whole blood, in microfluidic separation devices has proven to be a major challenge. An acoustophoresis based separation chip that prepares diagnostic plasma from whole blood and its clinical application are presented. The acoustic separator is able to sequentially remove enriched blood cells in several steps to yield high quality plasma. The generated plasma fulfills the standard requirements of $<6x10^9$ cells/L, suggested by the Council of Europe. The plasmapheresis microchip was also successfully linked to our previously developed porous silicon sandwich antibody microarray chip for Prostate Specific Antigen (PSA) detection. PSA was detectable from the generated plasma via fluorescence readout at clinically significant levels of 0.19-21.8 ng/ml with good linearity ($R^2> 0.99$) without any signal amplification.

INTRODUCTION

The development of micro technology and lab-on-a-chip devices has targeted fast and sample-volume limited operations for the analysis of blood components and blood plasma. Diverse micro-technology techniques have been developed to enable separation and concentration of the different components in whole blood[1]. Several groups have focused on separating red blood cells (RBC) from plasma and red cells from white blood cells (WBC)[2-6]. There have also been extensive efforts on chip integrated plasma generation for subsequent diagnostics.

A common way of separating plasma from blood using micro channels is to create a mesh or a filter with pores too small for cells to enter. It can be either a dead end filtration (weirs[7, 8] or membranes[8, 9]) or cross flow filtration[10, 11] where the plasma exits perpendicular to the main flow channel, a design which is far more preferable since it is much less likely to clog. Another way of separating plasma from cells is to use the plasma skimming[12] where blood cells tend to stick together at low flow rates, thereby creating lower cell concentrations at the walls of the channel where plasma can be removed. The Zwiefach-Fung effect[13, 14], or the bifurcation law, can be used for plasma generations since cells flowing in a channel with higher flow rate than the other in a bifurcation structure stick together and generally flows into that outlet while a small clean plasma fraction leaves the other bifurcation outlet.

Acoustic forces generated in ultrasonic standing waves can also be used to generate clean plasma. The acoustic wave generates a radiation force on the cells moving them into pressure

nodes of the standing wave field. There are basically two different approaches to utilize this phenomenon. The first one uses the acoustic wave to move the cells into larger clusters. When the clusters are sufficiently large they will start to aggregate and sediment, placing all cells at the bottom of the container. This technique can be designed for batch processing[15] or a continuous system where plasma is removed at the top and cell dense medium at the bottom[16]. However, this is a slow process and is not suitable for implementation in microfluidic systems since it is dependant of larger volumes and the sedimentation process will not be very effective in narrow channels where boundary conditions will be dominant.

The other way of using acoustic standing waves for continuous separation is to use a microfluidic channel that is matched to a half wavelength width[17-19]. When a particle suspension flowing through the channel is exposed to the ultrasonic standing wave (USW), the acoustic forces will move all particles to the pressure node located in the center of the channel, figure 1. In a microfluidic device, the USW in combination with the laminar flow will form a band of concentrated particles in the centre of the channel with clean medium at the sides. By terminating the channel outlet in a trifurcation the clean medium will exit through the side outlets while particles enriched in the channel centre will exit through the central outlet. Petersson et al. demonstrated a device where shed blood collected during surgery was separated into a lipid containing fraction and a blood cell fraction[20]. The lipid particles were in that case mixed with the plasma and removed through the side outlets. This configuration can, however, also be used to generate clean plasma if pure blood without lipids is processed.

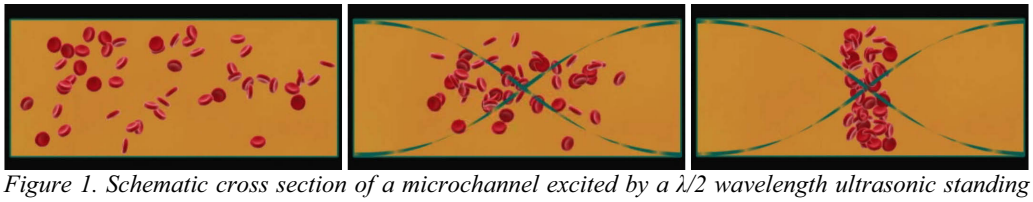

Figure 1. Schematic cross section of a microchannel excited by a λ/2 wavelength ultrasonic standing wave, whereby the erythrocytes sequentially are focused in the channel centre by the primary acoustic radiation force.

Although many of the reported microfluidic devices that handle blood work well for their intended application, most of them suffer from the fact that they require very dilute blood samples for the separation to work. Whole blood has a hematocrit (blood cell concentration) of ~38-54 % [22], which will cause many microfluidics systems to clog or get overloaded. Diluting the sample will however not give a very representative or sometimes not even useful plasma fraction for clinical evaluation. Others chip solutions, which are capable of handling high hematocrit usually have very poor volume throughput (in the nL to µL range per minute).

An obvious outlook for microchip based clinical grade plasmapheresis is the coupling to a chip integrated or microscaled diagnostic readout. The quest for early cancer diagnosis have promoted the exploration of advanced proteomic technologies, where the search and identification of new cancer biomarkers[24] open up for new improved diagnostics. Besides early diagnostics, biomarkers holds promise in providing information about the disease status at any given point in time, making it is possible also to monitor disease progression as well as identifying therapeutic targets [25]. Early detection and determination of cancer therapy is thus anticipated in this emerging era of biomarker research.

Along this line new biochip strategies are being developed for high throughput, parallel protein analysis. Arrays of peptides and proteins for diagnostic and proteomic analyses often involve techniques such as immobilization, assay and detection systems. Protein microarrays are different from DNA microarrays since protein targets are typically heterogenous in their physicochemical properties. The affinity capture reagents are sometimes poorly characterized in which a shortage of sufficiently specific antibodies or other affinity probes makes the analysis results less reliable. This could also be due to the heterogeneity of antibody affinities to their protein targets since antibodies show significant cross-reactivity between target proteins[26]. Parallel multiple affinity arrays may then face problems too, since optimal immobilization as well as assay conditions may be difficult to accomplish. Yet, in the past years dramatic improvements in increasing array sizes for multiplex protein readout has been demonstrated[52] and efforts to move protein microarrays into the clinic is a core area of interest.

Detecting low abundant proteins using antibody microarrays in complex specimens for example in whole blood, plasma or serum samples have successfully been shown by Carlsson et al.[34] and Ingvarsson et al.[35]. However it often requires laborious sample preparation[36] and a reliable microarray platform[37]. Nevertheless, various assay designs[38], labeling strategies[37], signal amplification systems as rolling circle amplication[39-41] or fluorescent nanoparticles[42], as well as different detection modes[43] have shown great improvements in microarray platforms. Improving the sensitivity of antibody microarrays remains a challenge especially with an interest in performing multiplex immunoassays. Although analysis of complex specimens is known to be difficult, several commercially available multiplexed and protein-based diagnostics have already proven that their platforms are reliable enough to enter the market. Triage System (www.biosite.com) and VIDAS (www.biomerieux-usa.com) for example, offer multiplex assays for detection of proteins related to cardiac diseases. Evidence, besides having a platform for cardiac markers detection (www.randox.com) and Luminex bead-based system (www.rulesbasedmedicine.com) offer even wider varieties of multiplex immunoassays for detection of markers related to various other diseases including cancer.

Being the most common male cancer in Western Europe and the United States, prostate cancer is a core area of cancer biomarkers research. Prostate specific antigen (PSA) is a well-known and the most widely used cancer biomarker, measured in serum and plasma of patients for the diagnosis of prostate cancer. However, an elevated value of PSA does not directly indicate prostate cancer since benign prostate hyperplasia cases may exhibit similar outcome. PSA itself is a serine protease[27-29] which is released into seminal plasma upon ejaculation with a concentration of 1g/l whilst its presence in the serum under normal condition is around 0.6ng/ml. The quest for more biomarkers for the detection of cancer leads to extensive worldwide efforts. It is anticipated that the diagnosis in the future would involve screening for more biomarkers in a parallel fashion which then requires a substrate specific for protein microarrays[30].

The potential of using macroporous silicon as a microchip substrate in protein microarray applications has been clearly described by our group as having all the requirements for a good bioassay performance[30, 31]. Porous silicon provides a surface that exhibits a small spot area due to the hydrophobic nature of the micro-/nanomorphology of the chip surface, good spot reproducibility, homogenous spot profiles, low intrinsic fluorescence background, as well as providing an improved limit of detection when compared to other commercially available substrates[32]. It was also demonstrated, that porous silicon is compatible with a dual readout

mode which simultaneously provides both affinity (fluorescence) and mass identity (MALDI-TOF MS) information of the captured protein[33].

This paper presents an ultrasonic standing wave (USW) plasmapheresis microchip, which is capable of processing whole blood and produce plasma fractions for a subsequent standard diagnostic step. The USW separator has increased the separator channel length as compared to our previously reported devices, with outlets along the separation channel, where concentrated cells could be diverted from the main flow without affecting the radiation force, until there is basically only cell free plasma left. Our current results show that 12.5% clean plasma by volume could be extracted from whole blood. The obtained plasma contains less than $6x10^9$ erythrocytes per liter which is in line with the quality specifications for transfusion stated by the Council of Europe[21].

In addition, this paper describes the clinical application of plasmapheresis microchip in an efficient system linking with our previously developed porous silicon sandwich antibody microarray chip for PSA detection[31]. The plasmapheresis microchip successfully generated plasma for a subsequent diagnostic step on porous silicon micro chips for PSA detection by means of fluorescence readout. The sandwich antibody microarray platform utilizes two anti PSA monoclonal antibodies and displays PSA detection at 0.19-21.8ng/ml. By combining USW microfluidics and protein microarray technology, an all microchip based PSA detection from whole blood is obtained in a novel lab-on-a-chip technique.

MATERIALS & METHODS

Plasmapheresis chip fabrication

The plasmapheresis separator was fabricated in silicon through double sided photolithography and chemical anisotropic wet-etching using KOH. The separation channel was designed to have a resonance around 2 MHz and thus the channel width is about 350µm. The channel was sealed with a glass lid using anodic bonding. Silicon tubing was glued to the outlets at the backside to act as docking ports to standard 1/16" Teflon tubing. More detailed information regarding the fabrication process can be found in[17]. The 2 MHz piezoceramic transducer (PZ26, Ferroperm Piezoceramics, Kvistgard, Denmark) was coupled to the chip together via a hydrogel that assured a good acoustic coupling.

Experimental setup

The piezoceramic transducer was actuated using an Agilent 33250A waveform generator and an Amplifier Research 75A250 amplifier. The input power to the transducer was monitored using a Bird model 5000-EX digital power meter. The blood was pumped through the separator using syringe pumps (WPI SP210iwz, World Precision Instruments, Sarasota, FL) and 5 ml Hamilton glass syringes.

Blood samples

Citrate treated blood samples were obtained from deidentified healthy donors. The different hematocrit levels were achieved by diluting the whole blood with centrifuged plasma from the same sample. A Coulter Counter (Beckman Coulter Multisizer 3) was used to determine the separation efficiency and the quality of the generated plasma. The particle sizes counted were in the range of 4-8µm. The diameter of an erythrocyte is about 7µm and leukocytes are generally larger or in the same size[22] which means that they will most certainly be separated even though not counted.

Proteins and Reagents
Prostate Specific Antigen (PSA) from human semen was obtained from Sigma. Monoclonal antibodies 2E9 and H117 were produced and characterized as described[44, 45]. 2E9 was labeled with fluorescein isothiocyanate (FITC) isomer I-celite (Sigma St. Louis, MO) and separated on a PD10 column (Amersham, Uppsala, Sweden).

Human Female Whole Blood Spiked with PSA
Human female blood samples were obtained from healthy donors as described above. The individual blood samples were spiked with PSA to a titration series ranging from 0.3-40ng/ml prior to plasmapheresis.

Porous silicon protein chip
Fabrication of the porous silicon was carried out by anodic dissolution of a p-type monocrystalline silicon wafer (Addison Engineering, Inc. San Jose, CA; resistivity 1.0-10.0 Ohm-cm). In this process, the silicon wafer was placed in between two electrochemical cells filled with electrolyte solution containing a mixture of 1:10 by volume of 40% hydrofluoric acid and 99.8% dimethyl formamide. The electrolyte provides contact to the wafer on both sides. During anodization, the backside of the wafer was illuminated using a 100-W halogen lamp (Osram, Germany), which was placed 10 cm from the window of the chamber. A constant current of 91 mA was passed through the system for 70 minutes, and as this occurs, pore formation was initiated resulting in the formation of porous silicon layer at the anodic side of the wafer. The porosified silicon wafer was further diced into small pieces sized 6 × 6 mm forming the porous silicon chips. A more detailed description on the fabrication setup is described elsewhere[46].

Microarraying using piezoelectric flow-through microdispenser
An in-house developed piezoelectric microdispenser and a software controlled arraying station were used to form microarrays with 600 spots /array of monoclonal mouse anti PSA capture antibody H117. The microdispenser[47-49], which is actuated by a piezoceramic element, is able to generate single 100-pL droplets of antibody to form an array with 150µm distance between each spots. H117 was allowed to bind the surface via physical adsorption.

Sandwich antibody microarray
The porous silicon sandwich antibody microarray protocol[31] was carried out for the detection of PSA in microchip plasmapheresis generated plasma samples. The capture antibody H117 (0.5mg/ml) was arrayed onto the porous silicon chips followed by a 3 time washing step in PBS-tween (0.05% tween 20 in PBS) to remove loosely bound antibodies. Arrayed chips were then blocked with 5% non-fat dry milk in PBS-tween for 30 minutes in order to prevent unspecific binding during the next incubation step. The washing step was repeated before exposing the chips to incubation with 24µl sample solution for 70 minutes. After the incubation, the chips were washed again 3 times. The next step was to incubate the chips with 24µl of FITC-labeled 2E9 monoclonal mouse anti-PSA-antibody. After 1 hour incubation, the chips were washed 3 times in 5-mL of PBS-Tween, quickly dipped in distilled water and dried with pressurized air before confocal microscope detection.

Fluorescence readout and analysis
Fluorescence detection was performed using a confocal microscope setup (Olympus), an oil immersion 20X objective, an ion laser (Melles Griot Laser Group) with excitation wavelength of 488nm and a Fluoview scanner unit (Fluoview, Olympus). Image analysis was carried out

using Fluoview 300 software. The total intensity of each spot was quantified using Fluoview 300 and the circle method. Background total intensity was measured using similar method and was then subtracted from the total intensity of each spot. 9 spots and their backgrounds were measured for each image analysis, thus generating the mean spot intensities presented in the figures.

DELFIA analysis

DELFIA Prostatus PSA Free/Total assay is a quantitative time resolved fluoroimmunoassay developed by Perkin Elmer (Perkin Elmer, Turku, Finland) for simultaneous detection of total PSA and free PSA (uncomplexed PSA) in serum. It is a solid phase immunoassay based on a direct sandwich technique utilizing three monoclonal antibodies. The capture anti total PSA antibody is used to bind both free and complexed PSA to the solid phase. Europium labeled antibodies are directed against the free PSA whereas samarium labeled antibodies are directed against both free and complexed PSA (total PSA). The fluorescence from europium and samarium are detected using time resolved fluorescence and are proportional to the concentrations of free and total PSA in the sample[50]. In this study, DELFIA was used as a reference assay for the chip based total PSA assay.

RESULTS & DISCUSSION

USW plasmapheresis

To separate high particle concentrations based on ultrasonic standing waves, a new acoustophoresis chip design was derived. The goal was to address the limitations of our previously presented microfabricated silicon acoustic separator chips[17, 20], which were not able to process sufficiently high particle concentrations, partly due to the very high acoustic forces required to concentrate particles into a band narrow enough to enable separation. This in turn resulted in high driving voltages to the piezoceramic transducer and a dramatic temperature increase because of power losses in the transducer.

The new separator is a modification of the previously reported designs, in which the separation channel ended in a trifurcation where concentrated blood cells exit through the central outlet and clean plasma exits through the side branches. The new separator was modified in two steps. Firstly, the separation channel was elongated in a meander type of fashion, which enables the blood cells to be affected by the acoustic standing wave for a longer time period. An acoustic force of higher magnitude is thus not necessary, as the radiation force instead acts for a longer duration forcing the cells gently into a focused band. Secondly, several extra outlets were added along the separation channel. These outlets, placed in the middle of the separation channel, allow blood cells already focused to be removed without removing a large part of the blood plasma. This procedure decreases the concentration of blood cells in the separation channel in several consecutive steps by gradually lowering the concentration in the centre of the channel. At the end of the separation channel all remaining cells are packed in a sufficiently narrow band prior to reaching the outlet, enabling a high separation efficiency, see figure 2. Our earlier publication on acoustic particle focusing revealed that the focusing of the cells in the streaming channel occurs throughout the full height of the chip[23], explaining why it is a justified strategy to remove already acoustically focused cells from the centre region of the microchannel as outlined in position A, B and C, figure 2. The design also allow cells to be continuously exposed to the acoustic standing waves during the sequential removal steps since the outlet is placed

perpendicular to the standing waves and no extra diversion of flows with flow splitters is needed.

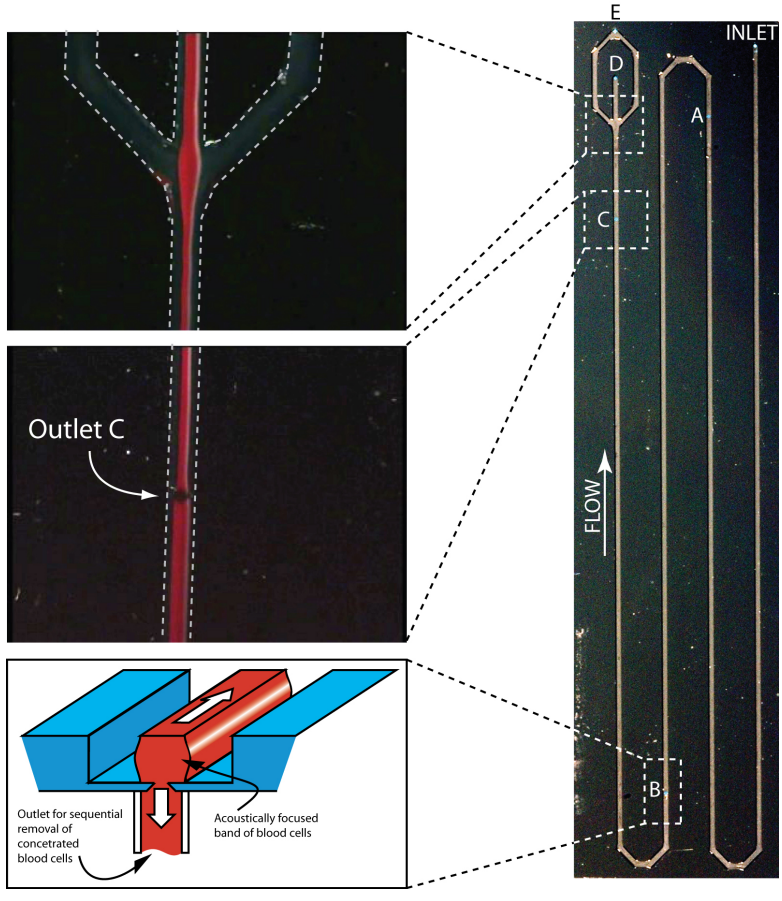

Figure 2. The principle of plasmapheresis. Acoustic standing waves gather blood cells in the pressure node located in the middle of the separation channel. Enriched blood cell fractions are removed through outlets A-C, thus decreasing the hematocrit gradually in the channel. The remaining focused blood cells exit through outlet D while the clean plasma fraction is withdrawn from exit E.

Four different designs with different separation channel length were investigated and all designs have one inlet and five outlets. The basic design was a channel, approximately 56 mm long, with the channel outlets symmetrically placed along the channel. The other designs denoted 2M, 3M and 4M after the number of meanders on the chip had a separation channel length of 108 mm, 166 mm and 224 mm respectively (Figure 3). All separators were actuated with the same transducer at approximately 2.05 MHz, except 1M which had a smaller transducer since the tubing on the backside prevented the use of the larger one. The net input power into the device was however the same in all cases, ~300 mW.

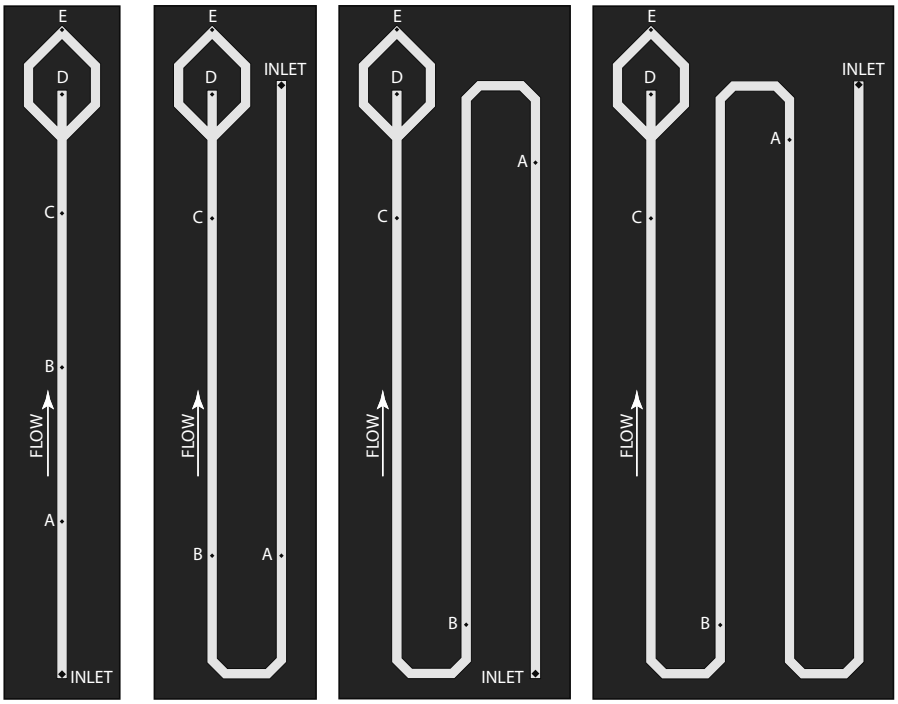

Figure 3. Schematic of the separator designs. They are denoted 1M, 2M, 3M and 4M after the number of meanders present on the chip. The blood enters through the inlet and fractions are removed through outlets A, B, C, D and E. Outputs A-D will contain blood of varying concentration while the clean plasma fraction is taken out from outlet E.

The total flow rate of the plasmapheresis chip was set to 80 µl/min with a flow distribution of the outlets as seen in table 1. These parameters were chosen as it is important to quickly remove the bulk of the focused blood cells in the separation channel in order to lower the concentration so that all remaining cells can be focused before the flow split.

Outlet	A	B	C	D	E
Flow rate (µl/min]	20	20	15	15	10

Table 1. The flow distribution between the different outlets used in the plasmapheresis.

The first tests were made on design 1M, with a suspension comprised of 5µm polyamide particles designed for mimicking blood. 1M consisted of a straight channel with three channel outlets where particles could be removed sequentially before the trifurcation, see figure 3. When tested with higher concentration levels >20%, a plug of stacked particles would build up around outlets A, B or C and occlude the channel. Many different combinations of balancing the flow rates were tested but in the end it was concluded that the outlet itself was too small to handle such high concentrations without being exerted to keystone effects. Instead of being approximately 1/3 of the channel width, the output holes were widened to ~2/3 of the channel width. This of course increased the risk of loosing plasma along the separation when using blood, but as the geometry of the outputs are oriented in a diamond shape in relation to the flow channel, most of the fluid extracted will still be from the central 1/3. Another interesting feature that was noticed during separation, is that the outlets along the

separation channel causes a hydrodynamic focusing effect as particle rich fractions are removed , which actually assists in focusing the remaining particles further by translating them closer to the centre of the separation channel. It should be noted, however, that rigid particles are less flexible than blood cells. Blood with hematocrit of 20% surely behaves differently than a particles suspension of the same concentrations and it is possible that the original sizes of the outlets might have worked out well for blood samples. Blood have been reported to maintain flow as hematocrit reaches as high as 98%[53]. However, the increased size of the outlet holes is still probably beneficial as it applies less shear forces to the cells.

With the fluidic extraction under control, the different designs were tested with blood at the flow rates showed in Table 1. At low hematocrits, ~10 %, all chips performed well but as the concentration was increased the 1M and 2M chips started to loose blood cells in the flow splitter to outlet E. The separation channels were not sufficiently long and thus the duration of the exposure of the cells in the acoustic focusing field to accomplish a complete separation. The tendency of poor separation efficiencies was progressively worse as the concentration increased further. As the hematocrit approached whole blood, i.e. ~40%, the 3M and 4M chips proved to be the only designs capable of handling such high concentrations see figure 4. It should however be noted, that the separation efficiencies are only relative to the total amount of particles processed per minute, which means that there can still be relatively high number of cells present in the plasma fraction even though the separation efficiencies are close to 100%.

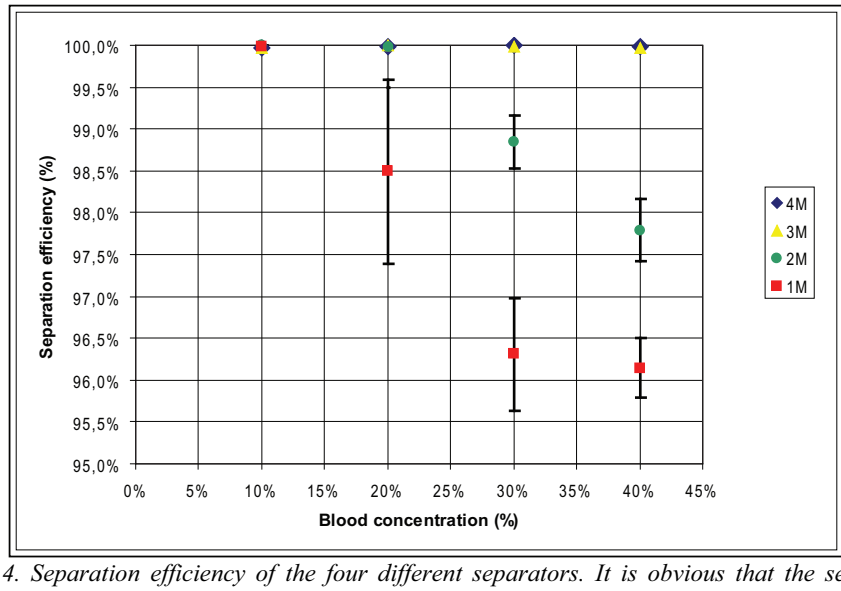

Figure 4. Separation efficiency of the four different separators. It is obvious that the separation efficiency decreases with increased hematocrit for the shorter separation channel designs, 1 M and 2 M, and which are characterized by shorter exposure of the cells to the acoustic force field.

The percentage of cells removed by each outlet at an inlet concentration of 40% is shown in figure 5. The graph demonstrates that most of the cells exit the chip via outlet A and B which can be expected as they have the largest flow rate. But the trend of the height of the stacks shows clearly that the longer the cells are exposed to the field, the larger fraction of the cells can be removed. It also shows that if the cell removal is not effective due to poor particle focusing in the beginning of the separation it will be very difficult to make up for it in the end.

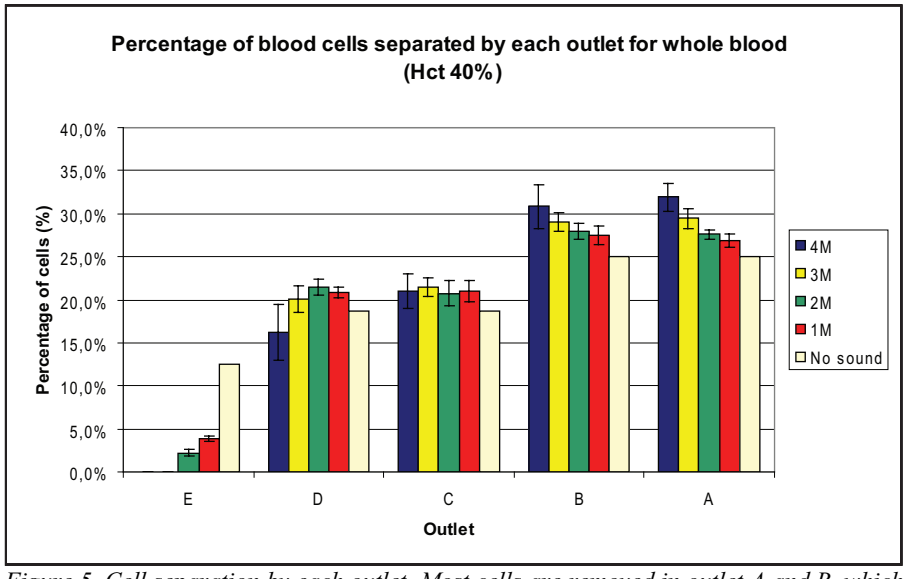

Figure 5. Cell separation by each outlet. Most cells are removed in outlet A and B, which is expected since these also have the highest flow rate. The high percentage of removed cells in A and B for 4M can be explained by the length of the separation channel between the outlets which gives the cells extended time for focusing in the ultrasonic standing wave field.

As mentioned earlier, the separation efficiency is a relative measure which is highly dependent on the total amount of particles separated. Although figure 4 showed 100% separation for design 3M and 4M, they did not show the same result when the absolute number of cells in the plasma fractions were measured. Figure 6 shows the total cell count in the plasma fractions and the dotted green line in the graph represents the number of erythrocytes ($6x10^9$ per liter) below which The Council of Europe recommends plasma for transfusion to be. The number of cells per liter plasma by the 3M design is $8.28x10^9$, which exceed the recommended limit. The 4M design however had a cell count of $3.65x10^9$ per liter which is well below the limit and thus provides approved plasma. It is however unlikely that the separation device could be used for transfusion medicine since the throughput and recovery rate in its current format is not sufficiently high for supporting a full clinical transfusion application. The results however clearly show that the reported plasmapheresis chip can serve as a platform for on-line automated chip based analysis in a clinical setting.

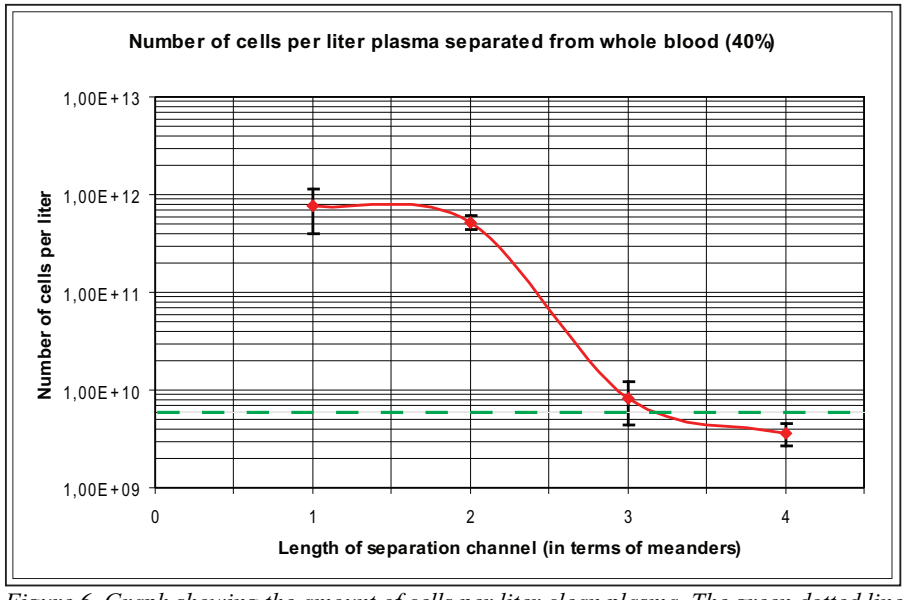

Figure 6. Graph showing the amount of cells per liter clean plasma. The green dotted line show the upper limit of numbers of erythrocytes per liter plasma for transfusion set by the Council of Europe. That limit, which is set to $6x10^9$ erythrocytes per liter, was surpassed by the 4M plasma separator which generated plasma of cell counts of $3.65x10^9$.

PSA microarray detection of whole blood processed by plasmapheresis

In this part of the work proof of principle for the combination of the plasmapheresis microchip and a clinically relevant microarray assay is presented. A system for whole blood analysis was developed in which we successfully linked the acoustic separator with our high performance porous silicon sandwich antibody microarray chip for PSA detection. The system (shown schematically in Figure 7) enables detection of low abundant PSA in whole blood samples. We investigated female whole blood samples spiked with known concentrations of PSA, in the clinically significant range of 0.3-40ng/ml. PSA-spiked whole blood samples were applied to the plasmapheresis microchip and obtained pure plasma fractions were used for the subsequent PSA microarray assay on our porous silicon microchips.

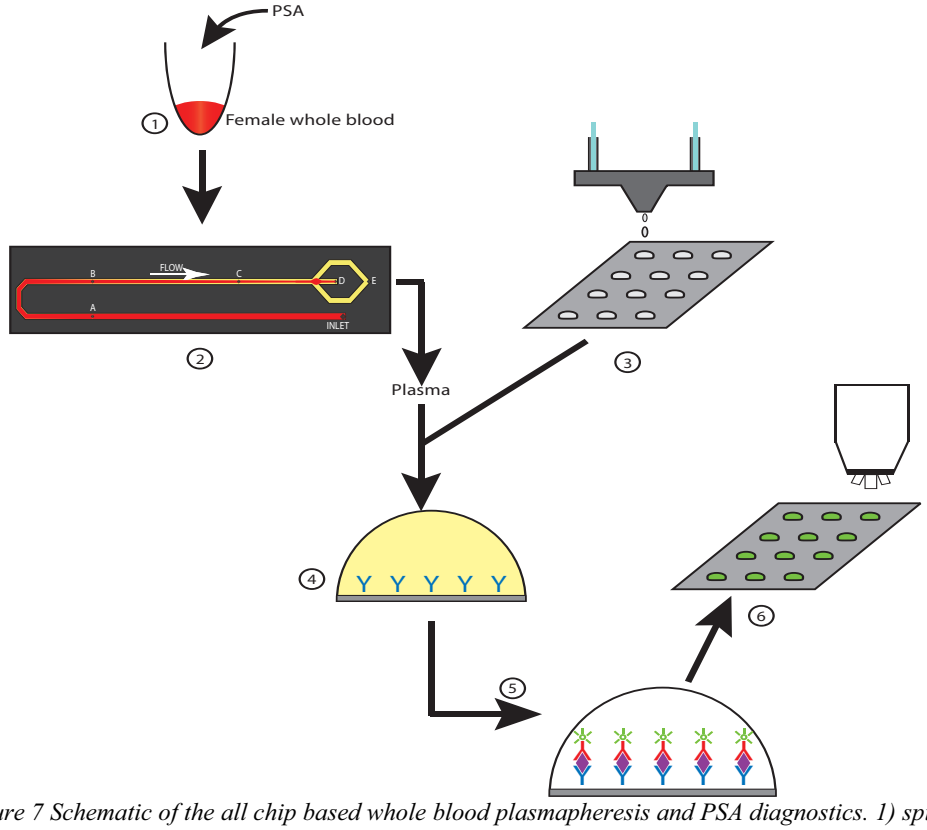

Figure 7 Schematic of the all chip based whole blood plasmapheresis and PSA diagnostics. 1) spiking of PSA in female whole blood, 2) ultrasonic standing wave driven microchip plasmapheresis, 3) Microarraying of PSA antibody, 4) microchip incubation in obtained plasma, 5) sandwich assay, 6) fluorescence readout.

We have earlier shown that our porous silicon sandwich antibody microarray platform is capable of analyzing serum samples for the prostate cancer biomarker PSA[31, 42]. In this sandwich antibody array, the capture antibody H117 is physically absorbed onto the porous silicon surface. As the plasma sample is applied, the PSA is concentrated onto the spots by H117. The captured PSA is subsequently detected with a fluorescently labeled antibody; in this case FITC labeled 2E9. Dynamic range, limit of detection, linearity and assay reproducibility of our sandwich antibody microarray platform have been addressed and described in our earlier publication. No unspecific binding of serum proteins have been found (data not shown), when analyzing crude female serum samples in the assay. A commercially available 96 well based immunoassay (Prostatus PSA Free/Total DELFIA) was used as a reference method to determine the PSA concentration. In this study the DELFIA was used as a reference assay to monitor concentrations of PSA in the spiked whole blood samples and after plasmapheresis.

Our current results, based on duplicate arrays for each concentration of PSA in the titration series, generated high intensity spots (Table 2). The mean spot intensities and CVs of Table 2 were calculated from the spots of the insert images of Figure 8. CVs of around 18 % correlate well with earlier results of the sandwich assay [31]. The graph in Figure 8, showing the mean spot intensity versus PSA concentration, as determined by DELFIA, corresponded to a

coefficient of determination of $R^2 > 0.99$, indicating strong linearity without any signal amplification. The error bars show the standard deviations calculated from the spot intensities.

Concentration ng/mL	Mean spot intensity	Standard deviation (*n*=9)	CV, % (n=9)
0.19	159880.0	40398.03	25.3
2.57	613335.6	108150.7	17.6
3.52	724538.9	155725.1	21.5
5.35	937604.4	130383.3	13.9
21.8	4191924.4	412651.6	9.8

Table 2. PSA concentrations, as measured by DELFIA, mean spot intensities from the sandwich antibody microarray, the corresponding standard deviations and coefficients of variation.

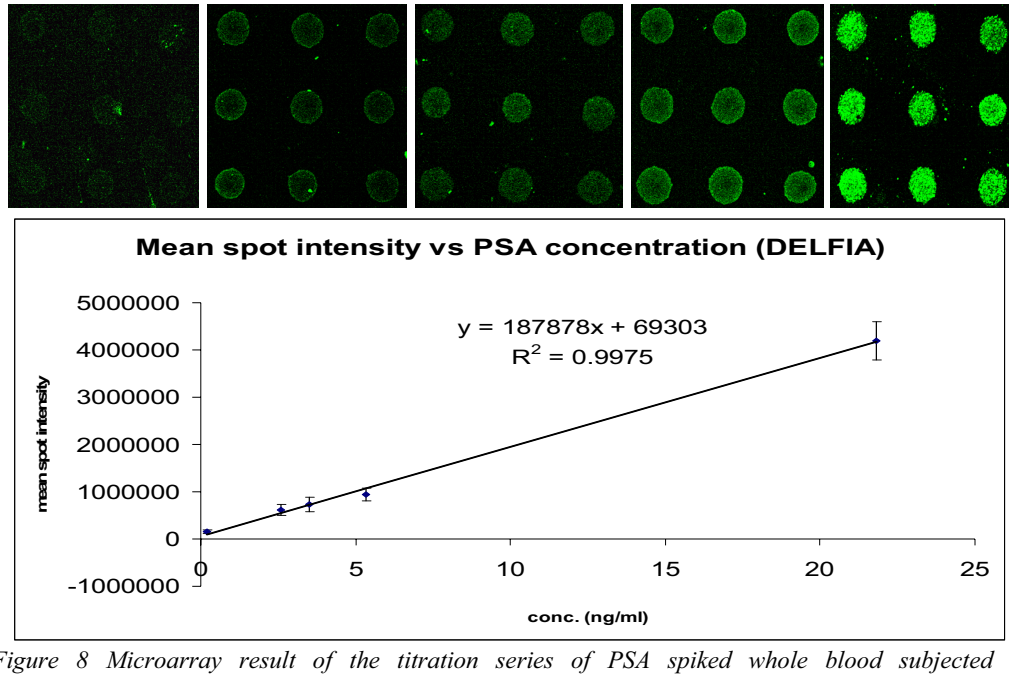

Figure 8 Microarray result of the titration series of PSA spiked whole blood subjected to plasmapheresis. The images shown were obtained from the porous silicon sandwich antibody microarray. Mean spot intensities and standard deviations (error bars) were calculated from the spots in the inset images detected by a 20x lens. The PSA concentrations on the x-axis were obtained by the reference DELFIA assay of the same plasmapheresis treated samples.

It should be noted that the DELFIA analysis showed PSA concentrations in the samples to be 0.57 times lower after plasmapheresis, i.e. upon detection on our sandwich antibody microarray platform, as compared to the PSA concentration in the spiked whole blood samples, Figure 9. It is already known[51] that PSA to some extent bind to α-2 macroglobulin in blood and thus become immunoinaccessible. The decreased PSA concentration in plasma compared to whole blood might also be due to unspecific binding of PSA to blood cells. When the cells are removed upon plasmapheresis the PSA concentration would then also be

decreased. Even so, a linear correlation of PSA concentrations before and after plasmapheresis, as measured by DELFIA, represents systematic loss of PSA in the system (Figure 9). Since the PSA loss is systematic, this artifact does not affect the assay reliability. In addition the DELFIA comparatively stated that PSA at 0.19-21.8ng/ml were detected on our porous silicon via fluorescence readout. The sensitivity of the sandwich assay for PSA presented in this study clearly covered diagnostic cut points of 0.6-4ng/ml that frequently are used for identifying men with elevated risk of malignant or benign prostate disease.

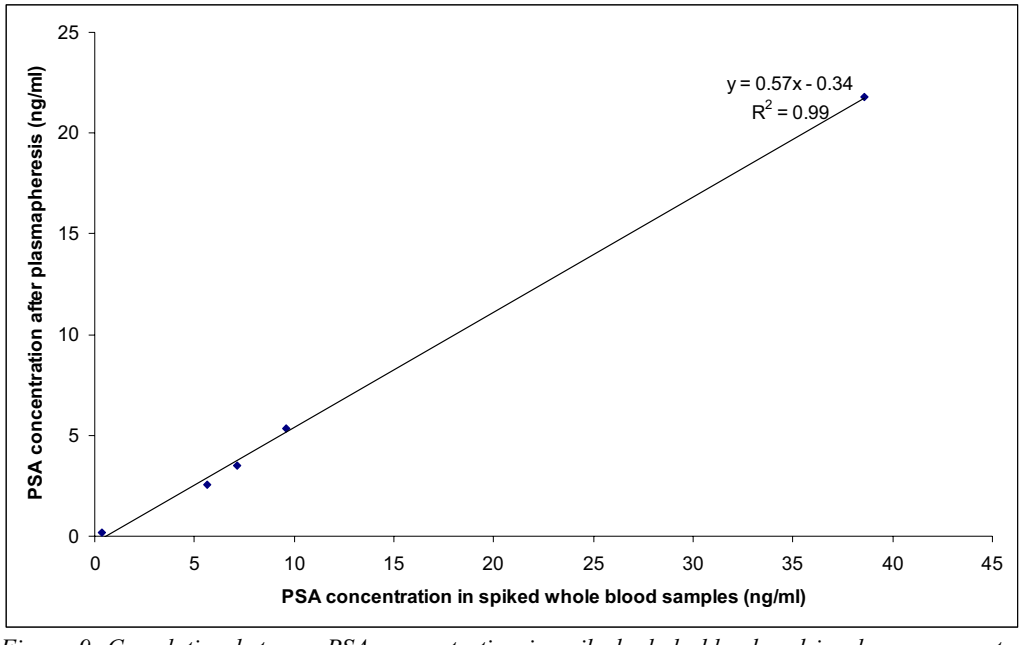

Figure 9. Correlation between PSA concentration in spiked whole blood and in plasma generated after plasmapheresis. The DELFIA assay was used to determine the PSA concentrations.

The developed system, which combines the whole blood acoustic separator (plasmapheresis) microchip and the porous silicon sandwich antibody microarray chip, proved the ability to detect low abundant PSA from whole blood samples. The extended application of this work would be a miniaturized lab-on-a-chip approach, integrating both plasmapheresis and the prostate cancer biomarker assay using minute amounts of patient whole blood.

CONCLUSION

In this work, a novel acoustic chip for plasma extraction from whole blood is presented. The obtained plasma was coupled to microchip based PSA assaying based on nanoporous silicon protein antibody arrays. Obtained PSA microarray data correlated very well with reference measurements by DELFIA.

High hematocrit levels are generally difficult to process by means of acoustophoresis, however, the presented sequential blood cell removal procedure gradually reduced the hematocrit level via a multiple outlet configuration, providing cell free plasma. The quality of the plasma fulfilled the standard set up by The Council of Europe for plasma transfusion.

ACKNOWLEDGEMENTS

The Swedish Research Council, Foundation for Strategic Research, Vinnova, Crafoordstiftelsen, Carl Trygger Foundation, Royal Physiographic Society in Lund, and Knut & Alice Wallenberg Foundation are greatly acknowledged for their financial support.

REFERENCES

(1) Toner, M.; Irimia, D. *Annual Review of Biomedical Engineering* **2005**, *7*, 77-103.
(2) Choi, S.; Park, J. K. *Lab on a Chip* **2007**, *7*, 890-897.
(3) Petersson, F.; Aberg, L.; Sward-Nilsson, A. M.; Laurell, T. *Analytical Chemistry* **2007**, *79*, 5117-5123.
(4) Davis, J. A.; Inglis, D. W.; Morton, K. J.; Lawrence, D. A.; Huang, L. R.; Chou, S. Y.; Sturm, J. C.; Austin, R. H. *Proceedings of the National Academy of Sciences of the United States of America* **2006**, *103*, 14779-14784.
(5) Sethu, P.; Sin, A.; Toner, M. *Lab on a Chip* **2006**, *6*, 83-89.
(6) Yamada, M.; Seki, M. *Lab on a Chip* **2005**, *5*, 1233-1239.
(7) Wilding, P.; Kricka, L. J.; Cheng, J.; Hvichia, G.; Shoffner, M. A.; Fortina, P. *Analytical Biochemistry* **1998**, *257*, 95-100.
(8) Ji, H. M.; Samper, V.; Chen, Y.; Heng, C. K.; Lim, T. M.; Yobas, L. *Biomedical Microdevices* **2008**, *10*, 251-257.
(9) Moorthy, J.; Beebe, D. J. *Lab on a Chip* **2003**, *3*, 62-66.
(10) Crowley, T. A.; Pizziconi, V. *Lab on a Chip* **2005**, *5*, 922-929.
(11) VanDelinder, V.; Groisman, A. *Analytical Chemistry* **2006**, *78*, 3765-3771.
(12) Jaggi, R. D.; Sandoz, R.; Effenhauser, C. S. *Microfluidics and Nanofluidics* **2007**, *3*, 47-53.
(13) Yang, S.; Undar, A.; Zahn, J. D. *Lab on a Chip* **2006**, *6*, 871-880.
(14) Shevkoplyas, S. S.; Yoshida, T.; Munn, L. L.; Bitensky, M. W. *Analytical Chemistry* **2005**, *77*, 933-937.
(15) Cousins, C. M.; Holownia, P.; Hawkes, J. J.; Price, C. P.; Keay, P.; Coakley, W. T. *Ultrasonics* **2000**, *38*, 654-656.
(16) Peterson, S.; Perkins, G.; Baker, C. IEEE/Eighth AnnualConference of the Engineering in Medicine and Biology Society, **1986**; 154-156.
(17) Nilsson, A.; Petersson, F.; Jonsson, H.; Laurell, T. *Lab on a Chip* **2004**, *4*, 131-135.
(18) Harris, N. R.; Hill, M.; Beeby, S.; Shen, Y.; White, N. M.; Hawkes, J. J.; Coakley, W. T. *Sensors and Actuators B: Chemical* **2003**, *95*, 425-434.
(19) Hawkes, J. J.; Barber, R. W.; Emerson, D. R.; Coakley, W. T. *Lab on a Chip* **2004**, *4*, 446-452.
(20) Petersson, F.; Nilsson, A.; Holm, C.; Jonsson, H.; Laurell, T. *The Analyst* **2004**, *129*, 938-943.
(21) *Guide to the preparation, use and quality assurance of blood components*, 12th ed.; Council of Europe Publishing, Strasbourg, **2006**
(22) Dailey, J.F. *Dailey's notes on blood, Fourth Ed.*, Medical Consulting Group, Arlington, MA, USA **2002**
(23) Evander M., Lenshof A., Nilsson J. and Laurell T., *Analytical Chemistry*, **2008**, *80* (13), 5178–5185.
(24) Srinivas, P.R.; Srivastava, S.; Hanash, S. and Wright Jr, G.L. *Clinical Chemistry,* **2001**, 47 (10), 1901-1911.
(25) Anderson, J.E.; Hansen, L.L.; Mooren, F.C.; Post, M.; Hug, H.; Zuse, A. and Los, M. *Drug Resistance Updates*, **2006**, doi:10.1016/j.drup.2006.08.001.

(26) Poetz, O.; Ostendorp, R.; Brocks, B.; Schwenk, J.M.; Stoll, D.; Joos, T.O. and Templin, M.F. P*roteomics*, **2005**, 5, 2402-2411.
(27) Lilja, H.; Oldbring, J.; Rannevik, G.; Laurell, C. B. *J.Clin.Invest.* 1**987**, 80, 281-285.
(28) Lilja, H.; Abrahamsson, P.A.; Lundwall, A. *J. Biol. Chem.* **1989**, 264, 1894-1900.
(29) Lilja, H.; Lundwall, A. *Proc. Natl. Acad. Sci. U.S.A,* **1992**, 89, 4559-4563.
(30) Ressine, A.; Ekstrom, S.; Marko-Varga, G. and Laurell, T. *Anal. Chem.* **2003**, 75, 6968-6974.
(31) Jaras, K.; Ressine, A.; Nilsson, E.; Malm, J.; Marko-Varga, G.; Lilja, H and Laurell, T. *Anal.Chem*. **2007**, 79, 5817-5825.
(32) Steinhauer, C.; Ressine, A.; Marko-Varga, G.; Laurell, T.; Borrebaeck, C. A. and Wingren, C. *Anal.Biochem*, **2005**, 341, 204-213.
(33) Finnskog, D.; Ressine, A.; Laurell, T.; Marko-Varga, G. *J. Proteome Res.* **2004**, 3, 988-994.
(34) Carlsson, A.; Wingren, C.; Ingvarsson, J.; Ellmark, P.; Baldertorp, B.; Fernö, M.; Olsson, H.;, Borrebaeck, C. A.; *Eur J Cancer*. **2008**, 44(3):472-80.
(35) Ingvarsson, J.; Wingren, C.; Carlsson, A.; Ellmark, P.; Wahren, B.; Engström, G.; Harmenberg, U.; Krogh, M.; Peterson, C.; Borrebaeck, C. A. *Proteomics*. **2008**, 8(11):2211-9.
(36) Ingvarsson, J.; Lindstedt, M.; Borrebaeck, C. A.; Wingren, C. *J Proteome Res.* **2006**, 5(1):170-6.
(37) Kusnezow, W.; Banzon, V.; Schroder, C.; Schaal, R.; Hoheisel, J.D.; Ruffer, S.; Luft, P.; Duschl, A. and Syagailo, Y.V. *Proteomics*, **2007**, 7, 1786-1799.
(38) Ingvarsson, J.; Larsson, A.; Sjoholm, A. G.; Truedsson, L.; Jansson, B.; Borrebaeck, C.A. and Wingren, C. *J.Proteome Res.*, **2007**, 6, 3527-3536.
(39) Jarvius, M.; Paulsson, J.; Weibrecht, I.; Leuchowius, K. J.; Andersson, A. C.; Wahlby, C.; Gullberg, M.; Botling, J.; Sjoblom, T.; Markova, B.; Ostman, A.; Landegren, U. and Soderberg, O. *Proteomics*, **2007**, 6, 1500-1509.
(40) Zhou, H.; Bouwman, K.; Schotanus, M.; Verweij, C.; Marrero, J. A.; Dillon, D.; Costa, J.; Lizardi, P.; Haab, B. B. *GenomeBiology*, **2004**, 5 (4), R28.
(41) Schweitzer, B.; Wiltshire, S.; Lambert, J.; O'Malley, S.; Kukankis, K.; Zhu, Z.; Kingsmore, S. F.; Lizardi, P. M. and Ward, D. C. *Proc. Natl. Acad. Sci, U.S.A.*, **2000**, 97 (18), 10113-10119.
(42) Jaras, K.; Ahmad Tajudin, A.; Ressine, A.; Soukka, T.; Marko-Varga, G.; Bjartell, A.; Malm, J.; Laurell, T. and Lilja, H. *J. Proteome Res*. **2008**, 7 (3), 1308-1314.
(43) Rai, A.J.; Gelfand, C. A.; Haywood, B. C.; Warunek, D. J. *Proteomics*, **2005**, 5, 3262-3277.
(44) Lilja, H.; Christensson, A.; Dahlen, U.; Matikainen, M. T.; Nilsson, O.; Pettersson, K. and Lovgren, T. *Clinical Chemistry*, 1**991**, 37, 1618-1625.
(45) Pettersson, K.; Vehnianen, M.; Viloma, S.; Makinen, M. L.; Manstala, P. and Lovgren, T. *Clinical Chemistry*, **1995**, 41, S81-S81.
(46) Drott, J.; Lindstrom, K.; Rosengren, L. and Laurell, T. *J. Micromech. Microeng*. **1997**, 7, 14-23.
(47) Laurell, T.; Wallman, L. and Nilsson, J. *J. Micromech. Microeng.* **1999**, 9, 369-376.
(48) Miliotis, T.; Kjellstrom, S.; Nilsson, J.; Laurell, T. *J. Mass Spectrom*. **2000**, 35, 369-377.
(49) Onnerfjord, P.; Nilsson, J.; Wallman, L. and Laurell, T. *Anal. Chem*. **1998**, 70, 4755-4760.
(50) Mitrunen, K.; Pettersson, K.; Piironen, T.; Bjork, T.; Lilja, H. and Lovgren, T. *Clinical Chemistry*, **1995**, 41, 1115-1120
(51) Christenssen, A.; Laurell, C. B. and Lilja, H. *Eur. J. Biochem*. **1990**, 194, 755-763.

(52) Hartmann, M.; Roeraade, J.; Stoll, D.; Templin, M. F. and Joos, T. O. *Anal. Bioanal. Chem*, **2008**, DOI 10.1007/s00216-008-2379-z.
(53) Bitsch, L.; Master thesis c960370, MIC, Technical University of Denmark, **2002**